Experimental investigation of microscopic CO_2 injection for enhanced oil recovery in tight reservoirs

Alkharraa, H.S.H.

DOI
10.4233/uuid:69412fde-347d-45d0-87d1-5a56ee7668ac

Publication date
2024

Document Version
Final published version

Citation (APA)
Alkharraa, H. S. H. (2024). *Experimental investigation of microscopic CO_2 injection for enhanced oil recovery in tight reservoirs*. [Dissertation (TU Delft), Delft University of Technology]. https://doi.org/10.4233/uuid:69412fde-347d-45d0-87d1-5a56ee7668ac

Important note
To cite this publication, please use the final published version (if applicable).
Please check the document version above.

EXPERIMENTAL INVESTIGATION OF MICROSCOPIC CO_2 INJECTION FOR ENHANCED OIL RECOVERY IN TIGHT RESERVOIRS

Doctor of Philosophy

HAMAD SALMAN HAMAD ALKHARRAA

2024

EXPERIMENTAL INVESTIGATION OF MICROSCOPIC CO_2 INJECTION FOR ENHANCED OIL RECOVERY IN TIGHT RESERVOIRS

Hamad Salman Hamad ALKHARRAA

EXPERIMENTAL INVESTIGATION OF MICROSCOPIC CO_2 INJECTION FOR ENHANCED OIL RECOVERY IN TIGHT RESERVOIRS

Dissertation

for the purpose of obtaining the degree of doctor at Delft University of Technology
by the authority of the Rector Magnificus prof.dr.ir. T.H.J.J. van der Hagen
chair of the Board for Doctorates to be defended publicly on
Wednesday 17 April 2024 at 10:00 o'clock

by

Hamad Salman Hamad ALKHARRAA

Master of Science in Petroleum Engineering
King Fahd University of Petroleum & Minerals, Dhahran, Kingdom of Saudi Arabia
born in Al-Khobar, Kingdom of Saudi Arabia

This dissertation has been approved by the promotors.

Composition of the doctoral committee:

Rector Magnificus,	chairperson
Prof. dr. ir. P.L.J. Zitha	Delft University of Technology, promotor
Dr. K-H.A.A.Wolf	Delft University of Technology, promotor

Independent members:

Prof. dr. ir. R.A.W.M. Henkes	Delft University of Technology
Prof. dr. ir. S. Geiger	Delft University of Technology
Prof. dr. ir. M. Mahmoud	King Fahd University of Petroleum and Minerals, KSA
Dr. ir. A.A.M. Dieudonné	Delft University of Technology
Dr. M. Al Duhailan	Saudi Aramco, KSA

Prof. dr. ir. J.D. Jansen	Delft University of Technology, reserve member

Keywords: Green transition, global energy demand, climate change, CO_2 underground storage, microscopic CO_2 injection, pore-fluid distribution, low-permeability micropore system, clay minerals

Printed by: Proefschriftspecialist.nl

ISBN 978-94-6384-551-9

An electronic version of this dissertation is available at
http://repository.tudelft.nl/.

To:

My dear parents

Salman Hamad Al-Kharra'a

Mona Abdullah Al-Hammad

My dear grandparents

Abdullah Abdulrahman Al-Hammad

Hussah Abdulaziz Al-Khaldi

In memory of my dear Professor

Pacelli Lidio Jose Zitha

and my beloved grandparents

Hamad Abdullah Al-Kharra'a

Mneera Salman Al-Subug

"The path to development passes first through education, secondly through education, and thirdly through education. Education, in short, is the first and last word in the epic of development."

Ghazi Al-Gosaibi

CONTENTS

1. INTRODUCTION

Despite the push for the transition to renewable energy, hydrocarbons remain the world's primary energy source, accounting for 82% of all global energy sources. Hydrocarbons' combustion is carbon intensive, markedly adding to global greenhouse gas (GHGs) emissions. This study focuses on experimental carbon dioxide–enhanced oil recovery (CO_2–EOR) in tight reservoirs, which provides both benefits for increasing oil recovery and reducing CO_2 emissions by CO_2 storage. This chapter presents the CO_2 emission projections and discusses the methods utilized for reducing atmospheric CO_2 levels. An overview of CO_2–EOR's history, major field projects, CO_2 injection mechanisms and their challenges are presented. Finally, the importance of microscopic CO_2–EOR of tight rocks to exploit unconventional resources and meet the rising global energy demand is highlighted and thesis's objectives and outline are presented.

1.1. GLOBAL ENERGY CONSUMPTION AND POPULATION GROWTH

Population growth drives the global energy demand for human activities [1]. As of August 2023, the world's population increased by nearly 0.8% compared to 2022, bringing the global primary energy consumption to 604 exajoules (EJ), 2.8% higher than that consumed in 2019 [2]. The global population is estimated to increase by 25% in the next 30 years and meeting this growing energy demand will require massive expansion of primary energy resources, including nuclear, hydrocarbon, and renewable energies [3]. Despite the global shift toward renewable energy, consumption remained to be low at approximately 14% in 2022, showing no change from the previous year [1]. One reason for restrained renewable energy use is referred to changing weather conditions [4]. Moreover, installing renewable energy infrastructure requires huge investments, especially for developing countries with limited financial resources [5]. Such challenges explain the current high hydrocarbons consumption, particularly oil, which represents 32% of the world's 2022 energy consumption and is expected to increase by approximately 6% in 2028 owing to continuously rising energy consumption worldwide [6]. To the contrary, the Stated Policies Scenario indicates that the share of fossil fuels in global energy demand is projected to decrease to 73% by 2030. This projection aligns with most of the world government policies, directed toward green energy transition by improving non-fossil fuel energy sources. For instance, China, one of the largest consumer of primary energy, has experienced substantial increase in oil and natural gas consumption over the past decade. Nevertheless, by 2028 China's energy consumption is anticipated to shift as clean energy sources become increasingly prevalent, reducing reliance on hydrocarbons by 100% [7].

1.2. GREENHOUSE GAS EFFECT AND GLOBAL WARMING HISTORY

Oil is highly carbon intensive releasing nearly 32% of global CO_2 emissions leading to increasing greenhouse gas (GHG) emissions, rising planet temperature, and instigating climate change [8,9]. Before the mid-20th century, CO_2 emissions were below 5 billion tons (Gt) with atmospheric

average CO_2 concentration at 300 parts per million (ppm). Consequently, earth's temperature rise was below 0.5°C [10,11]. Global CO_2 emissions increased to 35.1 Gt in 2022 due to growing reliance on hydrocarbons as the primary energy source [12]. Subsequently, atmospheric CO_2 level increased over 40% compared to that in 1900s, increasing the earth's temperature approximately 0.91°C in 2022 [13].

Radiative forcing is a term used to measure climate change caused by imbalanced incoming solar and outgoing reflected radiation due to GHG. Radiative forcing is expressed in watts per square meter (W/m^2) [14]. The Intergovernmental Panel on Climate Change (IPCC) used Radiative forcing to choose four representative concentration pathways (RCPs) for climate change forecast [15]. Models RCP2.6, RCP4.5, RCP6, and RCP8.5 correspond to 2.6, 4.5, 6, and 8.5 W/m^2 of radiative forcing [16]. RCP2.6 shows the most optimistic scenario projecting CO_2 concentrations near current levels (approximately 400 ppm) throughout the century, leading to global net zero emission by the century's end. RCP8.5, the worst-case scenario, predicts three times more CO_2 concentration compared to current levels, increasing the global temperature by 4°C by the century's end [17]. The Organization for Economic Co-operation and Development links gross domestic product (GDP) to climate change and they forecast that rising global temperatures may reduce the global GDP by 10% in 2100 if RCP8.5 scenario is adapted [18]. Therefore, reducing CO_2 emissions and keeping the average global temperature below 1.5 °C as recommended by IPCC [19] without scarifying the global energy demand is essential.

1.3. CO_2 EMISSIONS MITIGATION APPROACHES

Various methods can be implemented to mitigate rising atmospheric CO_2 concentration. These are listed as follows:

- Straightforward reduction of fossil fuels consumption, but this is considered to be challenging, given the increasing demand and population growth.
- Use of forests as natural carbon sinks. As of March 2023, the European Parliament, and the European Council approved rules to expand European Union forests by around 15% to remove 310 million tons (Mt) of carbon dioxide equivalent annually by 2030 [20].
- Implementation of a carbon tax. Industries in the Netherlands were subject to a carbon tax of €30 per ton of CO_2 emission in 2021, which will ultimately escalate to €125 per ton in 2030 [21]. Canada also proposed a carbon tax of C$30 per ton of CO_2 in 2018 [22]. However, we believe this approach will suppress the energy supply, especially with limited use of renewable energy.
- CO_2 geological storage. This process involves capturing and storing CO_2 in depleted reservoirs and geological structures, including coal beds, geothermal sites, and saline

aquifers [23,24]. Saline aquifers are the most widely used storage sites worldwide due to their storage capacities ranging from 400 to 10,000 Gt [25,26].

- CO_2–EOR as a dually beneficial process. Use of this process will aid in reducing CO_2 emissions and increasing oil recovery. Nevertheless, many argue that CO_2–EOR only serves the latter purpose, since it emits CO_2 during the production life cycle making it incapable of reducing emissions [27]. It is reported that United States (U.S.) CO_2–EOR usage ranges from 300 to 600 kilograms (kg) of gas per oil barrel produced, while an average oil barrel releases about 500 kg of CO_2 during production, processing, transportation, and combustion [28]. However, CO_2–EOR is a closed-loop process in which part of the injected CO_2 remains in the reservoir and the released CO_2 through production is separated and reinjected, leading to permanent storage [29,30]. Therefore, CO_2–EOR can be considered carbon–negative throughout its operational lifespan. In contradiction, Farajzadeh et al. [31], concluded in their study of several pilot field examples to examine whether CO_2 can be stored efficiently by using CO_2–EOR, that CO_2–EOR with a storage option is unsustainable as the process consumed more energy, hence, emitting more CO_2 during the capturing and injection processes. They also stated that a combination of CO_2–EOR and storage yields 30–40% less exergy compared to a CO_2–EOR option that receives CO2 from a natural source.

1.4. OIL RECOVERY METHODS

Oil field production involves three recovery stages namely primary, secondary, and tertiary [32]. During primary recovery, oil flows naturally from the reservoir to the surface due to several drive mechanisms, including the gas cap drive, water drive, solution gas drive, rock and fluid expansion, and gravity drainage [33]. Oil recovery at this stage varies according to the reservoir's characteristics and, on average, amounts to around 10% of the original oil in place (OOIP) [34]. As reservoir pressure declines, the energy in the reservoir is insufficient to drive fluids to the surface; hence, secondary recovery methods are implemented. Secondary stage includes the injection of water or gas into the pressure-depleted formation to increase reservoir pressure and, ultimately, enhance oil production [35]. Nevertheless, oil remaining after primary and secondary methods is quite high amounting to 60% to 80% of the OOIP due to poor volumetric (E_V) and microscopic displacement efficiencies (E_D) [36].

Tertiary recovery or EOR methods are implemented at later stage to maximize recovery efficiency (E_R) by improving E_V and E_D, targeting the oil remaining after the first two recovery stages [37]. It is worth mentioning that E_V measures fluid vertical and areal sweeps while E_D evaluates oil mobilization at the pore scale [38]. EOR methods are classified into thermal methods, such as

steam injection and in-situ combustion; chemical methods, such as surfactant, polymer flooding or combination of both; and miscible or immiscible gas injection modes using natural gas, CO_2 or nitrogen [39]. The choice of the injection mode or gas type is based on availability and economic feasibility, in-situ oil properties, and reservoir conditions [40].

Several factors are considered when EOR process is to be implemented. Mobility ratio (M), a dimensionless number that relates the mobility of the injected fluid to the mobility of in-situ fluid, is a crucial factor to be considered in evaluating the success of displacement efficiency or EOR methods implemented. Favorable displacement occurs when $M \leq 1$, indicating that the displacing fluid has less mobility than the in-situ fluid [41]. Conversely, unfavorable displacement occurs when $M > 1$, indicating that the displacing fluid moves faster than the in-situ fluid, resulting in poor displacement due to viscous fingering [42]. Another factor is the capillary effect that may entrap the residual oil and needs to be reduced. Chemical or thermal EOR can be implemented to overcome these challenges by lowering the oil viscosity to provide favorable displacement, reducing oil-water interfacial tension and altering rock wettability to overcome the capillary entrapment [43]. Gravity override is another unfavorable displacement phenomenon occurs during gas injection when less-dense fluid such as the injected gas flows at the top of the reservoir bypassing the in-situ fluid at the bottom [44]. To mitigate this challenge, water alternating gas (WAG) injection or foam is implemented to improve the sweep efficiency [45]. Gas injection can be efficient in low permeability reservoirs because of its high microscopic displacement efficiency at the pore level. This work investigates the microscopic displacement efficiency of tight sandstone reservoirs using CO_2–EOR process.

1.5. CO_2 INJECTION MECHANISM

CO_2–EOR is a win-win approach in which concentrated CO_2 is separated from industrial and natural point sources and injected into the depleted oil fields to increase oil recovery and reduce CO_2 emissions through underground CO_2 entrapment. Knowledge of CO_2 properties is essential to understand the CO_2 injection mechanism. Under ambient conditions, CO_2 is approximately 1.5 times heavier than air and its critical pressure and the temperature at which its gaseous and liquid forms coexist are 1,070.6 psi (73.8 bar) and 300.25°K (31.1°C). Above these values, CO_2 becomes supercritical maintaining its viscosity but with increased density [46].

CO_2–EOR is conducted in miscible or immiscible modes depending on the in-situ fluid properties and reservoir characteristics [47]. In both modes, CO_2 injection provides a good displacement by swelling the in-situ oil, reducing its viscosity, and lowering the interfacial tension between CO_2 and the in-situ oil [48]. In miscible injection, the interfacial tension between the injected CO_2 and the in-situ oil vanishes and forms a single phase [49]. Therefore, miscible CO_2–EOR has higher

incremental oil recovery ranging from 75% to 90% OOIP, compared to 30% to 40% OOIP for immiscible CO_2 injection mode [50]. CO_2–oil miscibility can result in first-contact or multi-contact [51].

Incremental oil recovery during CO_2–EOR varies depending on factors such as channeling, viscous fingering, and gravity override [52]. Channeling occurs when the injected CO_2 flows through highly permeable streaks or natural fractures [53] leading to early CO_2 breakthrough and low oil recovery. Viscous fingering refers to viscosity difference of the injected CO_2 compared to the in-situ oil, resulting in low oil recovery due to unfavorable mobility ratios [54]. Gravity override may occur during CO_2 injection, especially during the immiscible injection process, due to density difference between the injected CO_2 and the in-situ oil [55]. Given these challenges, selecting the optimal CO_2 injection method is essential for maximizing oil recovery. Therefore, various injection schemes are performed in both miscible and immiscible CO_2 injections [56–60]. These are listed as:

- Continuous secondary injection referring to direct CO_2 injection at initial oil saturation.
- Continuous tertiary injection involving CO_2 injection at residual oil saturation following secondary waterflooding.
- WAG injection in which gas and water are injected at different WAG ratios and slug sizes. This scheme is implemented to mitigate mobility problems.
- Gas assisted gravity drainage (GAGD) where gas is injected above the target formation to sweep in situ oil downward towards horizontal production wells using gravity.
- Carbonated water injection (CWI) in which CO_2-enriched brine is injected to improve oil mobilization by increasing the density and viscosity of injected fluid thereby reducing the channeling and gravity segregation.
- CO_2 foam injection conducted by mixing gas, surfactant, and water to create a series of dispersed CO_2 droplets separated by surfactant-stabilized lamellae forming a foam slug ahead of the injected gas for stable gas displacement.

This work aims to investigate the efficiency of the first two schemes in both miscible and immiscible injection modes.

1.6. CO_2–EOR IN TIGHT RESERVOIRS

The petroleum industry has successfully applied CO_2–EOR for almost fifty years [61,62]. After Whorton et al.'s patent in 1952 [63], the first pilot field test of CO_2 and carbonated water injection was performed in 1964 in the Mead–Strawn Oilfield, U.S.A., resulting in oil recovery ranging between 53% to 82% OOIP [64]. The first commercial CO_2–EOR project was started in 1972 at the Scurry Area Canyon Reef Operator's Committee unit of Kelly–Snyder Field, Texas producing

over 28,000 barrels of oil daily (bbl/d) [65,66]. These successful stories promoted the U.S. CO_2–EOR projects to 142 in 2021, with an incremental oil production of approximately 273,000 bbl/d and an approximate total CO_2 storage of 1.6 billion cubic feet daily [67].

Globally, over 166 CO_2–EOR projects exist and they are producing an estimated 500,000 bbl/d, estimated to supply 375 billion barrels of oil and geo-storing approximately 360 Gt in the next 50 years [68,69]. Famous world CO_2–EOR projects are the Weyburn-Midale project in Canada, Petrobras Lula oil offshore field in Rio de Janeiro, Brazil, and Croatia Ivanić and Žutica oil fields [70].

Low-permeability tight oil reservoirs have become a significant source of U.S. oil, with an estimated recoverable reserve of 195 billion barrels [71]. The U.S. tight oil production increased from about 0.5 million bbl/d in 2010 to over 7 million bbl/d in 2022, almost 66% of the U.S.'s total crude oil production [72]. This success triggered the global interest in unconventional oil and gas resources to meet the rising energy demand. It has been agreed that unconventional (tight) reservoirs are those of permeability value (k) < 0.1 mD [73]. Such cut-off value could affect the understanding of flow behavior in tight reservoirs due to their heterogeneous pore systems, presence of various clay minerals, and high capillary forces [74]. Pore systems are classified into macro-, meso- and micro pores [75]. Macropores are mostly voids between detrital grains that form during the depositional process while micropores are those formed before and during the burial process and commonly found between detrital grains, authigenic clay minerals, and weathered mineral products [76]. Cementing materials presence can obstruct fluid transport by bridging and clogging pore networks and reducing porosity and permeability [77,78].

It is noteworthy that capillary force is inversely related to pore throat size [79]. Following Nelson's pore system classification, pore bodies under 10 microns and throats with diameters under 1 micron are microporous and characterized by bound fluid due to high capillary pressure [80]. Macro- and mesopore systems are characterized by pore bodies exceeding 30 microns and throat diameters over 1 micron where fluids move freely in large pores due to low capillary pressure.

One applied completion technique in tight reservoirs is horizontal multistage fracturing (MSF) [81]. The average oil recovery of MSF is under 10% of the OOIP [82]. Consequently, different recovery methods can be implemented to recover the significant quantity of oil remaining. Waterflooding is unsuitable for tight reservoirs due to its low injectivity and unfavorable E_D [83]. Additionally, clay's expansion during waterflooding can lessen permeability by blocking pore throats and preventing water movement within rock pores [84]. In addition, narrow pore-throats and high interfacial tension between the displacing and the displaced fluids tend to increase the

capillary forces, leading to significant residual oil entrapment due to the high capillary forces [85,86] especially in water-wet systems [87]. The capillary forces effect can be characterized by the dimensionless capillary number (*Nc*); which relates viscous to capillary forces. High *Nc* leads to high E_D for a given recovery method [88].

Tight reservoirs have low petrophysical properties and complex pore structures and gas flooding is believed to be effective in increasing the capillary number and ultimately improving the oil recovery of these reservoirs. CO_2 injection is usually used due to its low cost compared to other gases, high injectivity compared to waterflood, and the need to mitigate atmospheric GHGs via underground CO_2 storage [89]. CO_2 displacement mechanism in tight reservoirs is negatively affected by CO_2 early breakthrough and water-blocking [90]. CO_2 early breakthrough occurs when the injected CO_2 favors the macro-pore system characterized by less-resistant paths failing to reach the oil in the micropore system due to the high capillary pressure, resulting in low oil recovery. After waterflooding, the injected brine surrounds the remaining oil in large pores, resulting in a phenomenon called water-blocking, where water prevents the injected CO_2 from interacting with the in-situ oil due to the high capillary forces between brine and CO_2 resulting in poor displacement efficiency [91]. The high capillary pressure can also hinder CO_2 displacement in small pores. In a study conducted on tight sandstone of Chang-8 formation, China the micro-residual oil during WAG flooding was investigated using Micro-computed tomography (Micro-CT) and digital core technology. Results indicate a higher oil displacement from larger pores. The oil remaining exists in discontinuous form mainly dispersed or as thin films within large pores in addition to continuous oil trapped by the tight throat of the small and medium-sized pores [92].

The efficiency of implementing CO_2–EOR process in tight reservoirs and its ability to meet the ever-growing energy demand and control of CO_2 emission is still at its early stage. Therefore, there is a need for further investigation to shed light on pore fluid distribution and fluid mobilization during CO_2 displacement in different complex pore systems. In this work, different modes and schemes of CO_2–EOR were conducted, and Nuclear Magnetic Resonance (NMR) tool was utilized to assess the contribution of both macro and micro pore systems in overall oil displacement and CO_2 entrapment.

1.7. THESIS OBJECTIVES

CO_2–EOR proved to be effective in conventional reservoirs; however, the main challenge in tight reservoirs is the complex nature of pore systems and the contribution of micropores in overall fluid displacement so the question underlying this work is: *Can CO_2–EOR be effective in tight rocks?*

This research work intends to investigate oil mobilization in micropore systems during CO_2 injection and to identify the optimal injection mode and schemes for better recovery in tight reservoirs. The findings will contribute to the broader understanding of CO_2–EOR and CO_2 geological sequestration in tight rocks in addition to their use as input parameters for future lab- and field-scale flow modeling. The following are the main objectives listed for this work:

- Determine the pore framework of multiple tight sandstones to be subjected for microscopic CO_2 injection using the mineralogical, elemental, petrographic and petrophysical measurements utilizing X-ray Diffraction (XRD), X-ray Fluorescence (XRF), thin section, Scan Electron Microscopy (SEM), Micro-CT, NMR, and Mercury Injection Capillary Pressure (MICP) to answer the following questions: *What are the pore size distributions of the investigated tested tight sandstones?* and *how clay content, type and size affect these micro-pore bodies and throats*?
- Assess pore fluids distribution (PFD) using centrifuge displacement and NMR measurements to answer the following questions: *What are the contributions of micro and macro pores in overall fluids displacement?* and *what are the criteria to be used to determine the best tight sandstone candidate for CO_2 injection?*
- Evaluate the effectiveness of different miscible and immiscible CO_2 injection schemes to displace oil from tight sandstones using flooding runs and NMR to answer the following questions: *Can injected CO_2 mobilize the micropore oil? Do results differ using the tested flooding schemes? If so, why? and what injection scheme is more efficient in displacing the resident oil?*

1.8. THESIS OUTLINE

This dissertation is based on three journal articles and one conference presentation. The document is divided into five chapters. **Chapter 1**, the introduction, discusses the dual benefits of using CO_2–EOR to meet energy demands and reduce CO_2 emissions. It highlights the importance of exploiting tight reservoirs to meet rising energy demands and surveys CO_2–EOR's challenges in tight reservoirs. **Chapter 2** presents mineralogical and petrophysical investigations of three tight outcrop sandstones (Bandera, Kentucky, and Scioto) to determine the most suitable one for microscopic CO_2 injections in tight sandstones. This includes determination of pore framework of the three sandstones, clay minerals' (content and type) impact on rock's micro- and macropore systems and evaluate the proportion of micro and macropores to overall pore system of each sandstone. **Chapter 3** covers the tight sandstones pore–fluid distribution to determine the CO_2 storativity and confinement within the various pore systems and the contribution of micropore system in overall fluid displacement. Based on chapters 2 and 3, Scioto sandstone was selected

for CO_2–EOR and **Chapter 4** was devoted to assessing the oil recovery of miscible and immiscible secondary and tertiary CO_2 injection schemes to evaluate their microscopic displacement efficiency. Finally, **Chapter 5** summarizes the conclusions obtained and recommends possible future work.

REFERENCES

1. Energy Institute, 2023. Statistical review of world energy.
2. Citaristi, I., 2022. United Nations Population Fund—UNFPA. In the Europa directory of international organizations 2022 (pp. 293–296). Routledge.
3. Cashin, P., Mohaddes, K., Raissi, M., and Raissi, M., 2014. The differential effects of oil demand and supply shocks on the global economy. Energy Economics, 44, pp.113–134.
4. Chen, H., Shi, Y., and Zhao, X., 2022. Investment in renewable energy resources, sustainable financial inclusion, and energy efficiency: A case of US economy. Resources Policy, 77, 102680.
5. Suberu, M.Y., Mustafa, M.W., and Bashir, N., 2014. Energy storage systems for renewable energy power sector integration and mitigation of intermittency. Renewable and Sustainable Energy Reviews, 35, pp.499–514.
6. International Energy Agency, 2023. Oil market report—July 2023, IEA. https://www.iea.org/reports/oil-market-report-july-2023.
7. IEA, 2023. World Energy Outlook. https://www.iea.org/reports/world-energy-outlook-2023.
8. Kweku, D.W., Bismark, O., Maxwell, A., Desmond, K.A., Danso, K.B., Oti-Mensah, E.A., Quachie, A.T., and Adormaa, B.B., 2018. Greenhouse effect: Greenhouse gases and their impact on global warming. Journal of Scientific Research and Reports, 17(6), pp.1–9.
9. EIA, 2022. Greenhouse gas emissions and atmospheric concentrations have increased over the past 150 years. https://www.eia.gov/energyexplained/energy-and-the-environment/greenhouse-gases-and-the-climate.php.
10. NOAA, 2023. NOAA updates its Global surface temperature dataset. https://www.ncei.noaa.gov/news/noaa-updates-its-global-surface-temperature-dataset.
11. Friedlingstein, P., Jones, M.W., O'Sullivan, M., Andrew, R.M., Bakker, D.C., Hauck, J., Le Quéré, C., Peters, G.P., Peters, W., Pongratz, J., and Sitch, S., 2022. Global carbon budget 2021. Earth System Science Data, 14(4), pp.1917–2005.
12. National Research Council and Climate Research Committee, 2005. Radiative forcing of climate change: Expanding the concept and addressing uncertainties. National Academies Press.

13. Giorgi, F., and Mearns, L.O., 1991. Approaches to the simulation of regional climate change: Reviews of Geophysics, 29(2), pp.191–216.
14. Baek, H.J., Lee, J., Lee, H.S., Hyun, Y.K., Cho, C., Kwon, W.T., Marzin, C., Gan, S.Y., Kim, M.J., Choi, D.H., and Lee, J., 2013. Climate change in the 21st century simulated by HadGEM2-AO under representative concentration pathways. Asia–Pacific Journal of Atmospheric Sciences, 49, pp.603–618.
15. Schulz, M., Textor, C., Kinne, S., Balkanski, Y., Bauer, S., Berntsen, T., Berglen, T., Boucher, O., Dentener, F., Guibert, S., and Isaksen, I.S.A., 2006. Radiative forcing by aerosols as derived from the AeroCom present-day and pre-industrial simulations. Atmospheric Chemistry and Physics, 6(12), pp.5225–5246.
16. Van Vuuren, D.P., Edmonds, J., Kainuma, M., Riahi, K., Thomson, A., Hibbard, K., Hurtt, G.C., Kram, T., Krey, V., Lamarque, J.F., and Masui, T., 2011. The representative concentration pathways: An overview. Climatic Change, 109, pp.5–31.
17. Akhmat, G., Zaman, K., Shukui, T., and Sajjad, F., 2014. Does energy consumption contribute to climate change? Evidence from major regions of the world. Renewable and sustainable energy reviews, 36, pp.123–134.
18. Papell, D.H., and Prodan, R., 2012. The statistical behavior of GDP after financial crises and severe recessions. The B.E. Journal of Macroeconomics, 12(3).
19. Metz, B., Davidson, O., De Coninck, H.C., Loos, M., and Meyer, L., 2005. IPCC special report on carbon dioxide capture and storage. Cambridge University Press, Cambridge, UK, 442 pp
20. Mann, C., Loft, L., and Hernández–Morcillo, M., 2021. Assessing forest governance innovations in Europe: Needs, challenges, and ways forward for sustainable forest ecosystem service provision. Ecosystem Services, 52, 101384.
21. Jansen, P., Beeston, S.J., and Van Acker, L., 2022. The sustainability guidelines of the Netherlands Authority for Consumers and Markets: An impetus for a modern EU approach to sustainability and competition policy reflecting the principle that the polluter pays? European Competition Journal, 18(2), pp.287-327.
22. Taft, K., 2019. The politics of Alberta's carbon tax. In Orange Chinook: Politics in the New Alberta (p.173). University of Calgary Press.
23. He, X., Zhu, W., AlSinan, M., Kwak, H., and Hoteit, H., 2022, February. CO_2 storage capacity prediction in deep saline aquifers: Uncertainty and global sensitivity analysis. In International Petroleum Technology Conference (p. D021S044R003). IPTC.
24. Warwick, P.D., Blondes, M.S., Brennan, S.T., Corum, M.D., and Merrill, M.D., 2013. US

geological survey geologic CO_2 storage resource assessment of the United States. Energy Procedia, 37, pp.5275–5279.

25. Luo, A., Li, Y., Chen, X., Zhu, Z., and Peng, Y., 2022. Review of CO_2 sequestration mechanism in saline aquifers. Natural Gas Industry B, 9(4), pp.383–393.
26. Ismail, I., and Gaganis, V., 2023. Carbon capture, utilization, and storage in saline aquifers: Subsurface policies, development plans, well control strategies, and optimization approaches—a review. Clean Technol., 5(2), pp.1–29.
27. Núñez-López, V., Gil-Egui, R., and Hosseini, S.A., 2019. Environmental and operational performance of CO_2-EOR as a CCUS technology: A Cranfield example with dynamic LCA considerations. Energies, 12(3), p.448.
28. Núñez-López, V., and Moskal, E., 2019. Potential of CO_2–EOR for near-term decarbonization. Frontiers in Climate, 1, p.5.
29. Sandrea, I., and Sandrea, R., 2007. Recovery factors leave vast target for EOR technologies. Oil & Gas Journal, 105(41), pp.44–47.
30. McGlade, C., 2019. Can CO_2–EOR really provide carbon-negative oil? Viewed 15 April 2021, https://www.iea.org/commentaries/can-co$_2$-eor-really-provide-carbon-negative-oil.
31. Farajzadeh, R., Eftekhari, A., Dafnomilis, G., Lake, L. and Bruining, J., 2020. On the sustainability of CO_2 storage through CO_2–Enhanced oil recovery. Applied Energy, 261, p.114467.
32. Morrow, N., and Buckley, J., 2011. Improved oil recovery by low-salinity waterflooding. Journal of Petroleum Technology, 63(5), pp.106–112.
33. Thomas, S., 2008. Enhanced oil recovery—an overview. Oil & Gas Science and Technology—Revue de l'IFP, 63(1), pp.9–19.
34. Dake, L.P., 2001. The practice of reservoir engineering (revised edition). Elsevier.
35. Bahadori, A., 2018. Fundamentals of enhanced oil and gas recovery from conventional and unconventional reservoirs. Gulf Professional Publishing.
36. Green, D.W., and Willhite, G.P., 1998. Enhanced oil recovery (Vol. 6, pp. 143–154). Richardson, TX: Henry L. Doherty Memorial Fund of AIME, Society of Petroleum Engineers.
37. Janssen, M.T., Pilus, R.M., and Zitha, P.L., 2020. A comparative study of gas flooding and foam-assisted chemical flooding in Bentheimer sandstones. Transport in Porous Media, 131, pp.101–134.
38. Al Adasani, A. and Bai, B., 2011. Analysis of EOR projects and updated screening criteria. Journal of Petroleum Science and Engineering, 79(1-2), pp.10-24.

39. Farajzadeh, R., Andrianov, A., and Zitha, P.L.J., 2010. Investigation of immiscible and miscible foam for enhancing oil recovery. Industrial & Engineering Chemistry Research, 49(4), pp.1910–1919.
40. Van Poollen, H.K., 1980. Fundamentals of enhanced oil recovery. Pennwell Books, Tulsa, Oklahoma, 1980, pp. 58–113.
41. Homsy, G.M., 1987. Viscous fingering in porous media. Annu. Rev. Fluid. Mech. 19(1), 271–311.
42. Wang, Y., Liu, H., Zhang, Q., Chen, Z., Wang, J., Dong, X. and Chen, F., 2020. Pore-scale experimental study on EOR mechanisms of combining thermal and chemical flooding in heavy oil reservoirs. Journal of Petroleum Science and Engineering, 185, p.106649.
43. Druetta, P., Raffa, P. and Picchioni, F., 2019. Chemical enhanced oil recovery and the role of chemical product design. Applied energy, 252, p.113480.
44. Talebian, S.H., Masoudi, R., Tan, I.M. and Zitha, P.L.J., 2014. Foam assisted CO_2-EOR: A review of concept, challenges, and future prospects. Journal of Petroleum Science and Engineering, 120, pp.202-215.
45. Bennion, B., and Bachu, S., 2006, April. The impact of interfacial tension and pore-size distribution/capillary pressure character on CO_2 relative permeability at reservoir conditions in CO_2-brine systems. In SPE/DOE Symposium on Improved Oil Recovery. SPE-99325-MS. https://doi.org/10.2118/99325-MS.
46. Iota, V. and Yoo, C.S., 2001. Phase diagram of carbon dioxide: Evidence for a new associated phase. Physical Review Letters, 86(26), 5922.
47. Tan, Y., Li, Q., Xu, L., Ghaffar, A., Zhou, X. and Li, P., 2022. A critical review of carbon dioxide enhanced oil recovery in carbonate reservoirs. Fuel, 328, p.125256.
48. Kumar, N., Sampaio, M.A., Ojha, K., Hoteit, H. and Mandal, A., 2022. Fundamental aspects, mechanisms and emerging possibilities of CO_2 miscible flooding in enhanced oil recovery: A review. Fuel, 330, p.125633.
49. Bikkina, P., Wan, J., Kim, Y., Kneafsey, T.J. and Tokunaga, T.K., 2016. Influence of wettability and permeability heterogeneity on miscible CO_2 flooding efficiency. Fuel, 166, pp.219-226.
50. Johns, R.T., and Orr, F.M., 1996. Miscible gas displacement of multicomponent oils. SPE Journal, 1(1), pp.39–50.
51. Holm, L.W., and Josendal, V.A., 1982. Effect of oil composition on miscible-type displacement by carbon dioxide. SPE Journal, 22(1), pp.87–98.
52. Shaw, J. and Bachu, S., 2002. Screening, evaluation, and ranking of oil reservoirs suitable for

CO_2-flood EOR and carbon dioxide sequestration. Journal of Canadian Petroleum Technology, 41(09). http://dx.doi.org/10.2118/02-09-05.

53. Martin, D.F., and Taber, J.J., 1992. Carbon dioxide flooding. Journal of Petroleum Technology, 44(4), pp.396–400.
54. Juanes, R., and Blunt., M.J. (2007). Impact of viscous fingering on the prediction of optimum WAG ratio. Soc. Pet. Eng. J. 12, 486–495. doi: 10.2118/99721-PA.
55. Han, J., Lee, M., Lee, W., Lee, Y., and Sung, W., 2016. Effect of gravity segregation on CO_2 sequestration and oil production during CO_2 flooding. Applied Energy, 161, pp.85-91.
56. Wang, G.C., 1982. Microscopic investigation of CO_2 flooding process. Journal of Petroleum Technology, 34(8), pp.1789–1797.
57. Rao, D.N., Ayirala, S.C., Kulkarni, M.M., Paidin, W.R., Mahmoud, T.N., Sequeira, D.S., and Sharma, A.P., 2006. Development and optimization of gas-assisted gravity drainage (GAGD) process for improved light oil recovery. Louisiana State Univ., Baton Rouge, LA (United States).
58. Christensen, J.R., Stenby, E.H., and Skauge, A., 2001. Review of WAG field experience. SPE Reservoir Evaluation & Engineering, 4(2), pp.97–106.
59. Stalkup Jr., F.I., 1983. Status of miscible displacement. Journal of Petroleum Technology, 35(4), pp.815–826.
60. Esene, C., Rezaei, N., Aborig, A., and Zendehboudi, S., 2019. Comprehensive review of carbonated water injection for enhanced oil recovery. Fuel, 237, pp.1086–1107.
61. Ettehadtavakkol, A., Lake, L.W., and Bryant, S.L., 2014. CO_2–EOR and storage design optimization. International Journal of Greenhouse Gas Control, 25, pp.79–92.
62. Melzer, L.S., 2012. Carbon dioxide enhanced oil recovery (CO_2–EOR): Factors involved in adding carbon capture, utilization, and storage (CCUS) to enhanced oil recovery. Centre for Climate and Energy Solutions, pp.1–17.
63. Whorton, L.P., Brownscombe, E.R., and Dyes, A.B., Atlantic Refining Co., 1952. Method for producing oil by means of carbon dioxide. U.S. Patent 2,623,596.
64. Vikara, D., Wendt, A., Marquis, M., Grant, T., Rassipour, R., Eppink, J., Heidrick, T.L., Alvarado, R., Guinan, A., Shih, C.Y., and Lin, S., 2019. CO_2 leakage during EOR operations—analogy studies to geologic storage of CO_2 (Report No. DOE/NETL-2017/1865). National Energy Technology Laboratory.
65. White, D., 2009. Monitoring CO_2 storage during EOR at the Weyburn–Midale Field. The Leading Edge, 28(7), pp.838–842.
66. Advanced Resources Intl. (ARI), 2021. U.S. CO_2 Enhanced Oil Recovery Survey 2021

Update. https://www.eoriwyoming.org/projects-resources/publications/eori-library/co2-eor-survey-update-2021.

67. Li, X., Xue, J., Wang, Y., Yang, W., and Lu, J., 2022. Experimental study of oil recovery from pore of different sizes in tight sandstone reservoirs during CO_2 flooding. Journal of Petroleum Science and Engineering, 208, 109740.
68. Gould, T., and McGlade, C., 2019. Could tight oil go global? Paris: International Energy Agency, https://www.iea.org/newsroom/news/2019/january/couldtight-oil-go-global.html.
69. Muther, T., Qureshi, H.A., Syed, F.I., Aziz, H., Siyal, A., Dahaghi, A.K., and Negahban, S., 2022. Unconventional hydrocarbon resources: Geological statistics, petrophysical characterization, and field development strategies. Journal of Petroleum Exploration and Production Technology, 12(6), pp.1463–1488.
70. Veerabhadra, D., and Ganesh, T., 2021. Carbon capture and CO_2-EOR/storage—a game changer CCUS technology. The Way Ahead. https://jpt.spe.org/twa/carbon capture and-CO2 EOR storage game changer CCUS technology.
71. EIA, 2022. Tight oil production estimates by play. EIA. https://www.eia.gov/tools/faqs/faq.php?id=847&t=6.
72. EIA, 2022. Cost and performance characteristics of new generating technologies, Annual Energy Outlook 2021. EIA.
73. Holditch, S.A., 2006. Tight gas sands. Journal of Petroleum Technology, 58(6), pp.86–93.
74. Nabawy, B.S., Khalil, H.M., Fathy, M.S., and Ali, F., 2020. Impacts of microfacies type on reservoir quality and pore fabric anisotropy of the Nubia sandstone in the central Eastern Desert, Egypt. Geological Journal, 55(6), pp.4507–4524.
75. Worden, R.H., and Burley, S.D., 2003. Sandstone diagenesis: The evolution of sand to stone. Sandstone diagenesis: Recent and ancient, pp.1–44.
76. Kaneko, K., 1994. Determination of pore size and pore size distribution: 1. Adsorbents and catalysts. Journal of membrane science, 96(1-2), pp.59-89.
77. Tong, M., Li, L., Wang, W., and Jiang, Y., 2006. Determining capillary-pressure curve, pore-size distribution, and permeability from induced polarization of shaley sand. Geophysics, 71(3), pp.33–N40.
78. Diamond, S., 1970. Pore size distributions in clays. Clays and clay minerals, 18, pp.7–23.
79. Larson, R.G. and Morrow, N.R., 1981. Effects of sample size on capillary pressures in porous media. Powder technology, 30(2), pp.123-138.
80. Nelson, P.H., 2009. Pore-throat sizes in sandstones, tight sandstones, and shales. AAPG Bulletin, 93(3), pp.329–340.

81. Barati, R., and Liang, J.T., 2014. A review of fracturing fluid systems used for hydraulic fracturing of oil and gas wells. Journal of Applied Polymer Science, 131(16). http://dx.doi.org/10.1002/app.40735.
82. Nasralla, R.A., and Nasr-El-Din, H.A., 2014. Double-layer expansion: Is it a primary mechanism of improved oil recovery by low-salinity waterflooding? SPE Reservoir Evaluation & Engineering, 17(1), pp.49–59.
83. Pu, W., Gao, H., Zhao, S. and Gao, X., 2022. Microscopic oil displacement mechanism of CO_2 in low-permeability heterogeneous Glutenite reservoirs in the Junggar Basin. ACS omega, 7(5), pp.4420-4428.
84. Barnaji, M.J., Pourafshary, P. and Rasaie, M.R., 2016. Visual investigation of the effects of clay minerals on enhancement of oil recovery by low salinity water flooding. Fuel, 184, pp.826-835.
85. Bello, A., Ivanova, A. and Cheremisin, A., 2023. Foam EOR as an optimization technique for Gas EOR: A Comprehensive Review of Laboratory and Field implementations. Energies, 16(2), p.972.
86. Bondor, P.L., 1992. Applications of carbon dioxide in enhanced oil recovery. Energy Conversion and Management, 33(5-8), pp.579-586.
87. Arab, D., Bryant, S.L., Torsaeter, O. and Kantzas, A., 2022. Water flooding of sandstone oil reservoirs: Underlying mechanisms in imbibition vs. drainage displacement. Journal of Petroleum Science and Engineering, 213, p.110379.
88. Bikkina, P., Wan, J., Kim, Y., Kneafsey, T.J. and Tokunaga, T.K., 2016. Influence of wettability and permeability heterogeneity on miscible CO_2 flooding efficiency. Fuel, 166, pp.219-226.
89. Chen, M., Dai, J., Liu, X., Kuang, Y., Wang, Z., Gou, S., Qin, M. and Li, M., 2020. Effect of displacement rates on fluid distributions and dynamics during water flooding in tight oil sandstone cores from nuclear magnetic resonance (NMR). Journal of Petroleum Science and Engineering, 184, p.106588.
90. Wang, T., Wang, W., Liu, W., Zhang, H., Fang, W. and Liu, B., 2023. Oscillating electric field-induced water blocking breakthrough to facilitate CO_2 miscible flooding. Molecular Physics, p.e2241933.
91. Song, Z., Li, Y., Song, Y., Bai, B., Hou, J., Song, K., Jiang, A., and Su, S., 2020, October. A critical review of CO_2 enhanced oil recovery in tight oil reservoirs of North America and China. In SPE Asia Pacific Oil & Gas Conference and Exhibition. SPE-196548-MS. https://doi.org/10.2118/196548-MS.

92. Yue, P., Liu, F., Yang, K., Han, C., Ren, C., Zhou, J., Wang, X., Fang, Q., Li, X. and Dou, L., 2022. Micro-displacement and storage mechanism of CO_2 in tight sandstone reservoirs based on CT scanning. Energies, 15(17), p.6201.

2. PETROGRAPHIC AND PETROPHYSICAL CHARACTERIZATION

Previously we highlighted the significance of using CO_2–EOR in conventional oil reservoirs to fulfill energy requirements and reduce CO_2 emissions. However, the question arises, can this method be effective in tight reservoirs? To answer this, a set of mineralogical, elemental and petrophysical rock analyses is crucial in understanding the pore systems, which further helps in evaluating the effectiveness of CO_2 injection in tight rocks. This chapter investigates the impact of clay minerals on the pore framework of tight sandstone in order to relate that to the CO_2 displacement efficiency in tight reservoirs. several experimental techniques were used, including routine core analysis, XRD, XRF, thin sections petrography, SEM and capillarity/pore size distributions using MICP, NMR, and Micro-CT. Three tight sandstones have been investigated, and results indicate that presence of clay in form of fibrous illite, acting as pore bridging in Bandera and Kentucky sandstones, have blocked the overall micro-pore throats. On the other hand, absence of fibrous illite and the presence of illite platelets in Scioto sandstone preserved the sample's micro-pore throat system. Dimensionless micro-pore throat modality, defined as the ratio of micro-throat size to macro-pore throat size, was developed and it shows the highest value of 1.44 for Scioto sandstone indicating the contribution of both macro- and micro-pore systems to fluids flow. Therefore, the mitigation of oil bypass from smaller pores is the key criterion in selecting the proper recovery method. Results show the effect of clay mineralogy on pore system considering a part of the physical and spatial properties the pore/grain framework of the tight sandstones.

The content of this chapter is based on the below publications:

Al-Kharra'a, H.S., Wolf, K.H.A., AlQuraishi, A.A., Mahmoud, M.A., Deshenenkov, I., AlDuhailan, M.A., Alarifi, S.A., AlQahtani, N.B., Kwak, H.T. and Zitha, P.L.J., 2023. Impact of clay mineralogy on the petrophysical properties of tight sandstones. Geoenergy Science and Engineering, 227, p.211883.

AlKharra'a, H.S., Wolf, K.H.A., Kwak, H.T., Deshenenkov, I.S., AlDuhailan, M.A., Mahmoud, M.A., Arifi, S.A., AlQahtani, N.B., AlQuraishi, A.A. and Zitha, P.L.J., 2023, January. A Characterization of Tight Sandstone: Effect of Clay Mineralogy on Pore-Framework. Paper presented at The SPE Reservoir Characterization and Simulation Conference and Exhibition, Abu Dhabi, UAE.

2.1. INTRODUCTION

Tight reservoirs are one of the main types of unconventional resources. They are categorized as shale, sandstone, or carbonate rocks with low permeability and porosity [1]. In the 1970's, the U.S government classified tight reservoirs as those with permeability values less than 0.1 mD. This was considered in order to make well development eligible for federal-state tax relief [2]. The National Resources of Canada (NRC) defined tight oil reservoirs as petroleum resources producing economically via hydraulic fracturing techniques regardless of the type of lithology [3]. Several researchers used porosity (ϕ) and permeability (k) as threshold cut-off to characterize tight reservoirs and they classify tight as reservoirs characterized with $\phi < 10\%$ and $k < 0.1$ mD [4,5].

Flow behavior in tight reservoirs is complicated because of their pore system (bodies and throats) heterogeneity formed during depositional and diagenetic processes [6]. Geological and petrophysical rock characterization can help understand the pore systems and thus enable a better description of the flow processes involved in the production operations [7]. Although many industry professionals and researchers classify tight reservoirs based on a permeability threshold of 0.1 mD, investigating the complex pore size distribution should be considered as an essential key in tight reservoirs classification. Spatial correlations of pore throats and bodies are most relevant parameters for permeability in tight rock characterization. Smaller throat sizes lead to higher capillary pressures obstructing the fluid mobilization [8,9]. The knowledge of the pore throats and bodies systems (structure, distribution, etc.) is of crucial importance for the exploration and development of tight hydrocarbon reservoirs. For this reason, various techniques such as MICP, Micro-CT scan, and NMR are commonly used in petrophysical analysis to examine the pore system of reservoir rocks with varied limitations for each technique when applied to tight rocks.

Micro-CT scanning is a non-destructive method utilized to characterize and determine high-resolution images of pore systems. Nevertheless, small sample sizes are be used to obtain higher resolution [10]. Several studies reported Micro-CT scanning of tight rocks with resolutions ranging from 5 to 8 microns, which enabled smaller grains and micro-pores to be recognized [11,12]. MICP technique is commonly used to obtain the distribution of pore-throat size of rock specimens. It estimates the distribution of pore volume by injecting mercury under elevated pressure. MICP works well in tight rocks as it is capable of measuring pore-throat size down to around 0.003 microns [13]. It is noteworthy that MICP is a destructive technique with both environmental and health concerns that need to be properly addressed [14]. It is worth mentioning that both Micro-CT and MICP techniques are at laboratory scale, while NMR method is applied

at both field and laboratory scales [15]. The NMR method characterizes the distribution of pore size and estimate the porosity of rock saturated with water or oil [16]. The relaxation time (T_2) is generated by NMR measurements and proportional to pore size, where larger pores depict longer T_2 values, and small pores show shorter T_2 values. The NMR porosity represents the area under the NMR T_2 spectrum [17,18]. Estimated NMR porosity in rocks of various permeability values ranging between 0.07 and 4,450 mD are in good agreement with that measured by helium porosimeter [19].

Centrifuge and NMR techniques were utilized to estimate the connate water and pore fluid distributions for the Middle Bakken formation [20]. It was observed that oil tend to occupy larger pores while water resides in smaller pores. NMR measurements can determine fluid volumes of core samples by knowing the T_2 cut-off value. In order to estimate the T_2 cut-off for given sample, T_2 relaxation is measured before and after the drainage displacement process. T_2 cut-off value is related to rock mineralogy [21,22]. Many studies recommended using the standard cut-off value of 33 ms for sandstone samples; however, the mineral composition of sandstone can vary significantly. Thus, using the standard cut-off value can result in pore volumes misinterpretation [23]. Therefore, mineralogical composition has a vital role in the determination of a sandstone fluid distribution and hence pore framework.

In one study the quartz overgrowth affected the petrophysical properties of Fontainebleau sandstone by reducing both porosity and permeability [24]. Other minerals present such as accessory oxides, clays and feldspar were mostly included in the quartz overgrowth. Various types and abundances of clay material can bridge and even clog the pore networks preventing the fluid transport. In addition, distribution of the clays varies from reservoir to reservoir that makes 2D and 3D microscopy analysis of the core material a key factor for both successful oil and gas exploration and development campaigns [25].

The presence of clay minerals lowers the rock quality in sandstones [26]. Porosity and permeability reveal an inverse relationship with the total clay content [27,28]. Presence of fibrous illite in Rotliegend sandstone contributes negatively to permeability [29]. On the other hand, kaolinite clay minerals reduce porosity in sandstone while it has less effect on permeability [30]. Previous works investigated the impact of clay minerals on pore structure in sandstone rocks [31,32], nevertheless, detailed analyses of the effect of clay contents (type and size) on the micro-pore bodies and throats and relating them to the microscopic displacement efficiency of the micropore system in tight sandstone rocks are still not fully discussed.

In this work, three representative tight sandstone namely, Scioto, Bandera and Kentucky were characterized. Measurements and quantifications of the mineralogy accessory of the three

outcrops samples were conducted utilizing several imaging techniques (Micro-CT, XRD, SEM and petrographic thin sections). This multiple approach allows us to acquire mineral type and content at different resolutions. A set of experimental tests was performed by using a helium porosimeter, gas permeameter, MICP, NMR, and Micro-CT imaging, to determine key petrophysical parameters of the three sandstone samples and to establish the effect of clay mineralogy and contents on the pore framework of tight sandstone reservoirs. A new dimensionless number is established to characterize pore throat's heterogeneity and their control on fluids flow at different pore levels during the recovery processes in tight sandstones helping in better planning of such processes.

2.2. MATERIALS AND METHODOLOGY

2.2.1. CORE SAMPLES

Three outcrop sandstone samples, namely Bandera, Kentucky, and Scioto were obtained from different quarries by Kocurek Industries company™, Caldwell, TX, US. Figure 2.1 is maps of the area where samples were collected. It is important to state that these outcrops are not representative of any hydrocarbon reservoir and the rocks of such outcrops are usually applied in petroleum engineering labs for research purposes due to their homogeneous clean nature [33–37]. All samples are originated during the Carboniferous period in a fluvial depositional system and characterized with low porosity impacted by their burial history.

Bandera sandstone, located in Southeastern Kansas, is a member of Bandera shale formation that was deposited during the Desmoinesian age of the middle Pennsylvanian subsystem (323-299 Ma) [38,39]. It is a brown, thin-bedded sandstone with outcrop thickness of 0 – 10 m. The original fluvial depositional environment is fine-grained, and poorly-sorted [40–42]. Kentucky sandstone is light grey excavated from the western portion of the Kentucky Coal Field. It belongs to the Caseyville formation that was deposited during lower Pennsylvanian time [44–48].

Finally, Scioto sandstone samples were acquired from the Buena Vista member near McDermott, southern Scioto County, Ohio. This member is part of the lower Mississippian Cuyahoga formation covering the western part of Appalachian basin and has been deposited as deltaic turbidite deposits [49–51]. Scioto sandstone is blue grey, consisting of mostly coarse silt or fine sand and generally characterizes as well-sorted [52]. Stratigraphic columns of the tested sandstones are presented in Figure 2.2.

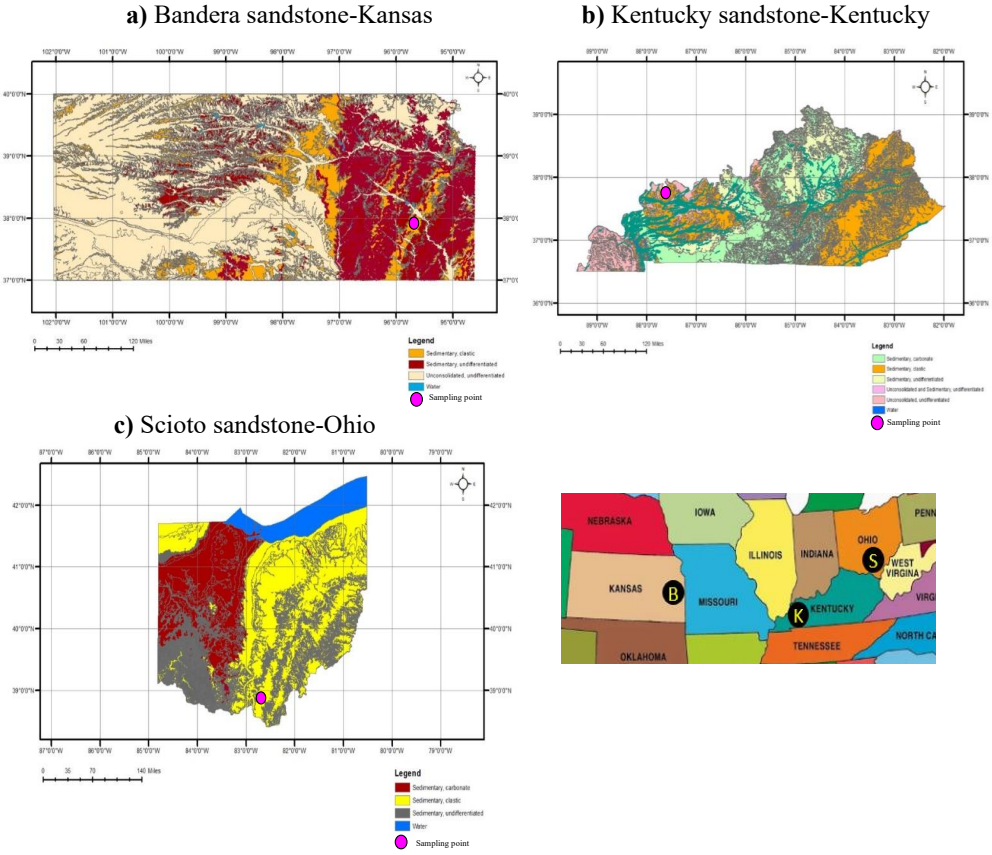

Figure 2.1. Location of the sandstone samples of **(a)** Bandera, **(b)** Kentucky, and **(c)** Scioto [43].

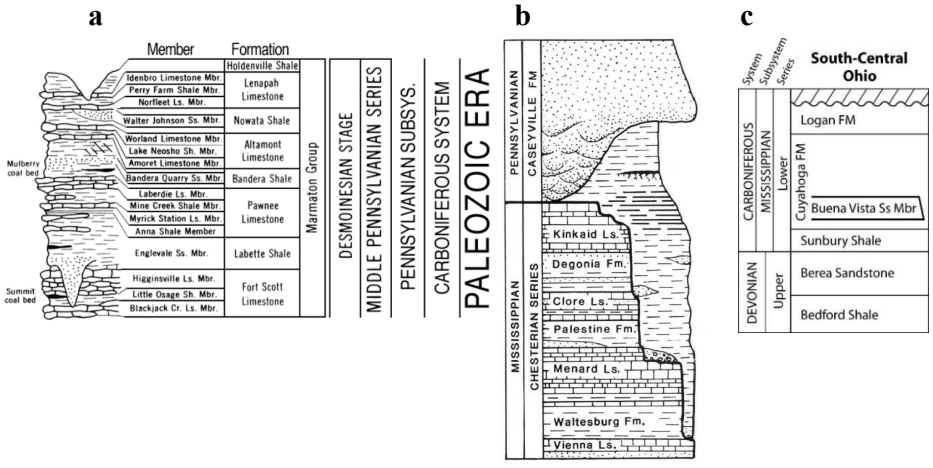

Figure 2.2. Stratigraphic divisions of outcrop sections of **(a)** Bandera [53], **(b)** Kentucky [54], and **(c)** Scioto [55].

2.2.2. EXPERIMENTAL DATA COLLECTION AND PROCESSING

Dry samples with radius of 3.8 cm and length of 4 cm were vacuumed for two days at 75°C and samples effective porosity was measured at 20°C using helium porosimeter. Permeability was determined using gas permeameter corrected to Klinkenberg liquid permeability. Petrographical and morphological analysis of the investigated samples were conducted using Micro CT, SEM, and thin-section imaging. Thin sections of ca. 3 cm^2 area were prepared from the end trim of the three sandstone plugs by using polarization microscopy. Image analysis program (Image J) was applied to analyze and quantify the characteristics of the 2D images to evaluate the mineralogy, mineral distribution, textures, and porosity with resolution down to 1 micron [56–60]. A thin disk of circa 5 mm in thickness and a volume of ca. 10 mm^3 solid rock volume was then prepared to provide a sub- nano-meter range resolution image using TESCAN™ SEM/EDX (model MIRA3). This helps in distinguishing the growth and interaction in and between mineral grains in addition to pore morphology [61,62].

For spatial 3D texture quantification, Micro-CT scanning with a 3D X-ray Microscope Zeiss™ Xradia Versa-620 was used on cylindrical plugs. The measurements were carried out by using a 100 kV/7 W X-ray source, providing 5001 slices. The resolution of the Micro-CT depends on sample shape and volume; therefore, different size cylindrical plugs were prepared to obtain a 5-micron voxel size. Samples size is listed in Table 2.1. Pore structure characterization was performed using the maximum ball method [63,64].

Table 2.1. List of plug samples with corresponding dimensions and Micro-CT scan voxel size.

Sample	**Resolution** (µm/voxel)	**NY** (voxel)	**NX** (voxel)	**NZ** (voxel)	**Length size** (mm)	**Diameter size** (mm)
Bandera	5	761	828	836	3.81	4.14
Kentucky	5	709	717	715	3.55	3.59
Scioto	5	709	717	715	3.55	3.59

Elemental and mineralogical analyses (XRF and XRD measurements) were performed on grinded samples. XRF measurements were conducted using Rigaku™ NEX CG instrument with a maximum voltage of 40 kV and current of 1 mA. Data acquisition and elements evaluation was completed with QuantEZ software. XRD measurements were obtained with a Rigaku™ ULTIMA IV powder X-Ray diffractometer using a Cukα source at 40 kV and 40 mA with a 2θ-range of 3°–100° at 0.02° step size within 8 minutes.

NMR measurements were conducted using a 2 MHz Oxford™ Instruments GeoSpec 2-75 equipped with Green Imaging Technologies (v6.1) software. The NMR measurements were done by the Carr-Purcell-Meiboom-Gill (CPMG) pulse [65]. The main acquisition parameters used in these experiments are listed in Table 2.2. Three vacuumed samples were saturated with 3% Potassium chloride (KCL) brine and subjected to NMR measurements. KCL was used in this work to mitigate any damage to rocks samples [66]. A Centrifuge at 4,000 revolutions per minute (rpm) was then used to desaturate the samples with air as the displacing phase and another NMR measurements was conducted to determine the movable and immovable fluid volume.

Table 2.2. Main parameters of NMR acquisition.

Parameter	Value
Echo spacing time	0.11ms
Signal to Noise Ratio	150
Total number of scans	32
Number of Echoes	27,272
Maximum T_2	300 ms

Micrometrics Auto Pore V 9600 was used for MICP analysis. The experiments were conducted to estimate the distribution of throat size distribution through drainage capillary pressure measurement. The instrument measures pore throat diameters between 0.003 to 500 microns by incremental injection pressures up to 4,137 bar (60,000 psia). In order to preserve the clay structure, the test was conducted on dry cylindrical 1.27 x 1.27 cm plugs.

2.3. RESULTS

2.3.1. POROSITY AND PERMEABILITY

The estimated permeability and porosity of investigated samples are listed in Table 2.3.

The results indicate that Scioto and Kentucky have close petrophysical properties. Bandera on the other hand shows a better reservoir quality with higher porosity and permeability.

Table 2.3. Porosity and permeability values of core samples. All core samples have diameter of 3.8 ± 0.1 cm and length of 3.9 ± 0.1 cm.

Sample	Porosity (vol.%)	Permeability (mD)
Bandera	24.4 ± 0.2	24.12 ± 1.5
Kentucky	15.0 ± 0.1	0.98 ± 0.1
Scioto	17.5 ± 0.1	1.21 ± 0.1

2.3.2. PETROGRAPHY AND MINERALOGY

Petrographic and mineralogical analyses were determined with thin-sections (Polarization microscopy), SEM and XRD techniques. SEM and thin-section results show moderately well sorted grains of medium silt to fine sand sizes of 30 to 120 microns (on average, 110 microns) for Scioto sandstone. The grain shape is subangular to subrounded with predominantly point to face grains contact. Based on point counting, Scioto sandstone shows a visible intergranular porosity of 24% (Figure 2.3a).

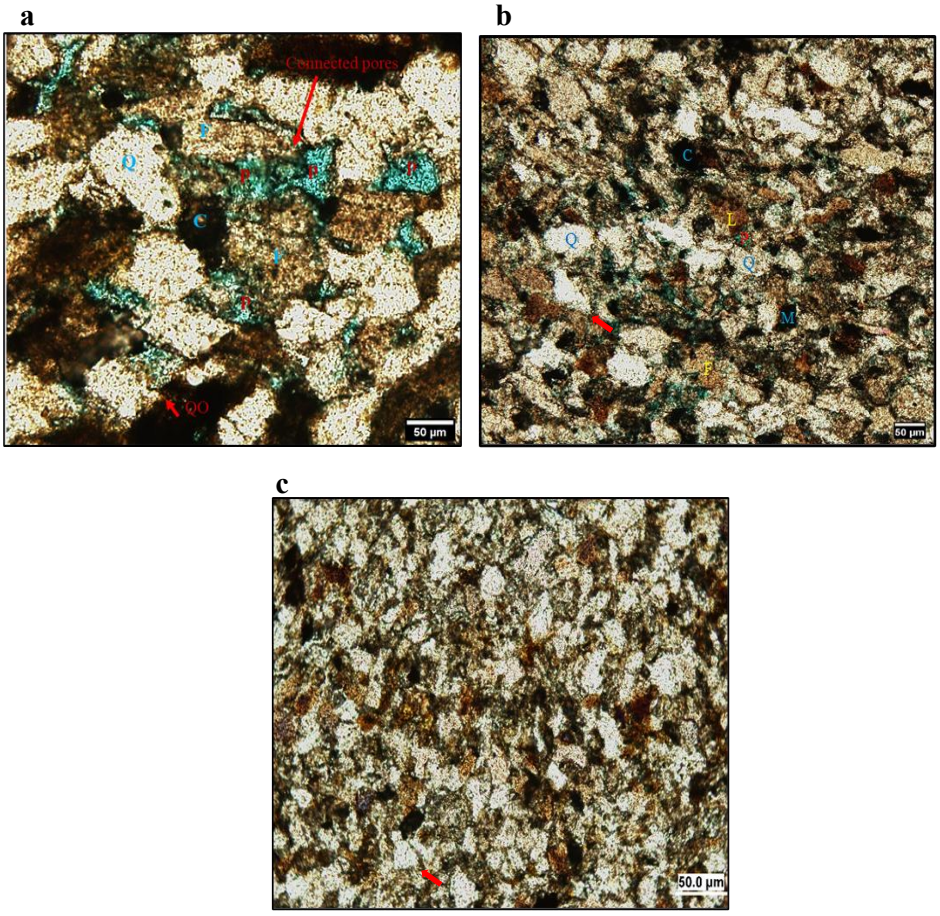

Figure 2.3. Thin-sections showing the textural properties of **(a)** Scioto exhibiting coarse silt to fine-sized grains. Lithics (L) exists and illustrated as dirty brown colors. Straight edges are seen as a result of quartz overgrowths (QO) around elongated quartz grains (Q). Feldspar weathering is shown as (F). Dark color indicates sample matrix (M) and moderately visible pores are denoted as (P), **(b)** Bandera showing angular to sub-rounded, well sorted fine grains with QO around the original grains. Visible primary pore spaces are clearly recognizable, **(c)** Kentucky showing poorly sorted, medium to coarse silt size sediments. Some QO around grains are seen but no visible pores exist.

SEM micrographs of Scioto revealed a pore-lining illite platelets coating the quartz grains (Figure 2.4a). Point counting (300 points) shows grain framework composed of circa 44 % quartz, 14 % lithics, and < 1% feldspar, where the rock fragments are composed of metamorphic and sedimentary rocks, with a minor amount of volcanic rock fragments.

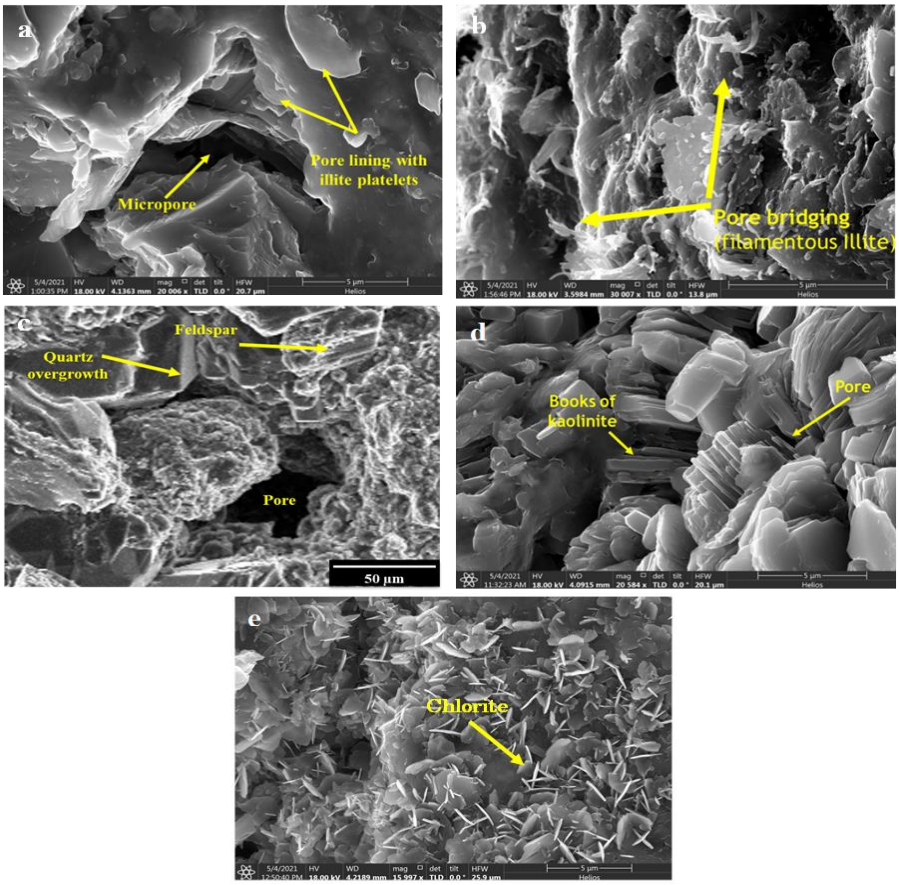

Figure 2.4. SEM images representing: **(a)** Scioto showing pore-lining with illite platelets and visible micro-pores, **(b)** Kentucky showing pore bridging with filamentous illite, **(c)** Bandera showing sharp surface as a result of the quartz overgrowths and visible pores between elongated grains, and top partly weathered feldspar with clays, **(d)** Kentucky showing books of kaolinite occluding pores, and **(e)** Bandera showing circular chlorite filling micropores.

Based on the textural maturity classification by Folk [67], Scioto's grains are subrounded and moderately sorted with low amount of clay content. Therefore, the sandstone can be classified as submature sublitharenite (Figure 2.5) [68,69]. Bandera sandstone has a grain framework comprising of 64% quartz, 2% feldspars and 1% lithic fragments, classifying the sandstone as quartzarenite, according to the triangle of Folk [69].

The rock fragments of Bandera sandstone include metamorphic, sedimentary, and minor volcanic fragments. The existing mica consists of 8 % muscovite (with an average of 2.8%) and trace amount (<1%) of biotite. Particle size revealed fine to very fine-grained, between 30 and 180 microns (average size of 87 microns), moderately to well sorted.

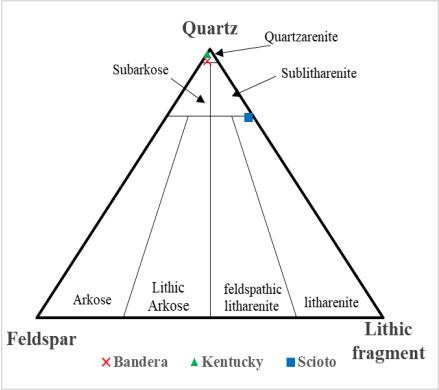

Figure 2.5. Classification of sandstone after Folk criterion, where Bandera and Kentucky sandstones could be classified as quartzarenite, while Scioto sandstone can be classified as Sublitharenite [69].

Grains are mainly sub-angular to angular exhibiting long grain contacts (Figure 2.3b). Booklets of Kaolinite were recognized by SEM images with ranges of 5 microns to 10 microns in size (Figure 2.4d). Such booklets can partially or completely reduce porosity in general and micro-porosity in specific. Additionally, SEM images shows clear kaolinite 'books' and filamentous illite overlying the quartz and preventing its overgrowth (Figure 2.4c). Visible pores between grains were clearly observed in thin-sections and SEM images shown in Figures 2.3b and 2.4c, respectively.

Kentucky sandstone shows moderately to poorly sorted coarse silt-size grains of 55 microns on average. The grains are largely subangular to angular in shape with clay minerals filling the spaces between grains indicating that the sample has a matrix supported fabric (Figure 2.3c). SEM images demonstrate the existence of fibrous illite acting as pore bridging (average 0.25 micron wide). Fibrous illite tend to reduce the sandstone permeability due to the partial pore throats blockage (Figure 2.4b). Mineralogically, Kentucky consists of 58% quartz, 1% feldspars, 1% lithic fragments, and 20% mica. The grains contacts are long to concave-convex contact planes. Thin-section images show intergranular porosity of 14% with unclearly observed micro-pores.

XRD and XRF results are summarized in Tables 2.4 and 2.5, respectively. The results show high percentages of quartz, 89.2, 77.1, and 64.2% for the Scioto, Kentucky, and Bandera sandstones, respectively. Bandera sandstone has a total clay content of 14.3% comprised of illite, kaolinite, and chlorite. Total clay contents of Kentucky and Scioto sandstones are 3.6 and 4.1%, respectively. Illite is the prevailed clay mineral in the three sandstones investigated measuring 6.4%, 3.6% and 2.2% for Bandera, Kentucky, and Scioto, respectively (Figure 2.6).

Table 2.4. Mineralogical Compositions of the tested sandstone samples (wt%).

Mineral	Bandera	Kentucky	Scioto
Quartz	64.4	77.1	89.2
Plagioclase	12	10.2	2.1
Illite	6.4	3.6	2.2
Kaolinite	4.5	0	1
Chlorite	3.4	0	0.9
Anhydrite	3	3.6	3
Halite	1.4	0.8	0.2
Hematite	1.2	0.3	0.5
Orthoclase	1	2.8	0.7
Ilmenite	1	0	0
Pyrite	0.8	0	0
Siderite	0.5	0.7	0.2
Dolomite	0.4	0.9	0

Table 2.5. Elemental compositions of Bandera, Kentucky, and Scioto sandstone samples (wt%).

Sample	Al_2O_3	SiO_2	TiO_2	Fe_2O_3	MnO	MgO	CaO	Na_2O	K_2O	P_2O_5	SO_3
Bandera	4.93	79.90	0.49	3.02	0.86	1.16	1.50	0.92	0.71	0.12	1.87
Kentucky	2.88	88.25	0.59	0.81	0.13	0.31	1.91	0.76	0.83	0.05	1.81
Scioto	1.20	93.21	0.50	0.81	0.10	0.30	1.28	0.38	0.31	0.1	1.20

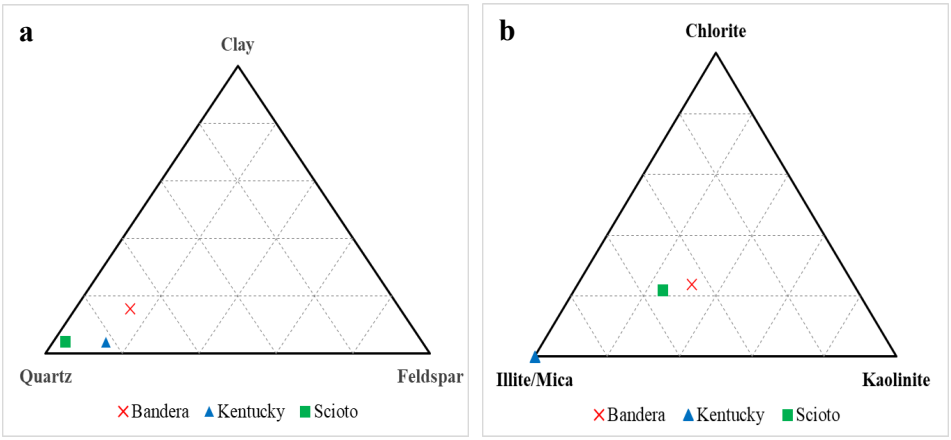

Figure 2.6. Ternary diagrams of the tested sandstone samples representing: **(a)** minerals content and **(b)** clay minerals content.

2.3.3. PETROPHYSICAL MEASUREMENT

MICP, Micro-CT, and NMR were conducted to investigate the impact of clay minerals on micro-pore bodies and throats. According to Nelson's pore system size distribution, micro-porosity is assigned to pore bodies smaller than 10 microns, and micro-pore throats have throat diameters smaller than 1 micron. However, the macro-, and meso-pore systems are applied to pore bodies exceeding 30 microns and a throat diameter larger than 1 micron [70]. Micro-CT scan results were utilized for the three sandstones (Figure 2.7a). All sandstone samples show broader pore size spectrum with Bandera displaying relatively dispersed pore body distribution between 5 to 50 microns (averaging 24.4 microns). Kentucky and Scioto exhibit almost similar pore body size distribution with 5 to 28 microns (averaging 16.8 microns) for Kentucky, and 5 to 30 microns (averaging 18 microns) for Scioto.

MICP measurements were conducted to determine the pore throat distributions of the investigated sandstones and results are demonstrated in Figure 2.7b. Bandera shows clear macro- and meso-pore throat systems with an average pore throat diameter of circa 6 microns. Kentucky and Scioto show narrower average throat sizes of approximately 1.8 microns. Based on the micro-pore system criterion by Nelson [70], Scioto show the highest micro-pore throat and the second highest micro-pore body contribution to the total pore system with 59.1 vol.% and 23 vol.%, respectively. Kentucky sandstone follows with a micro-pore throat and body contribution of 50.9 vol.% and 29.5 vol.%, respectively. Bandera sandstone micro-pore throat and micro-pore body show the lowest contribution with 36 vol.%, and 10.6 vol.%, respectively (Figure 2.7).

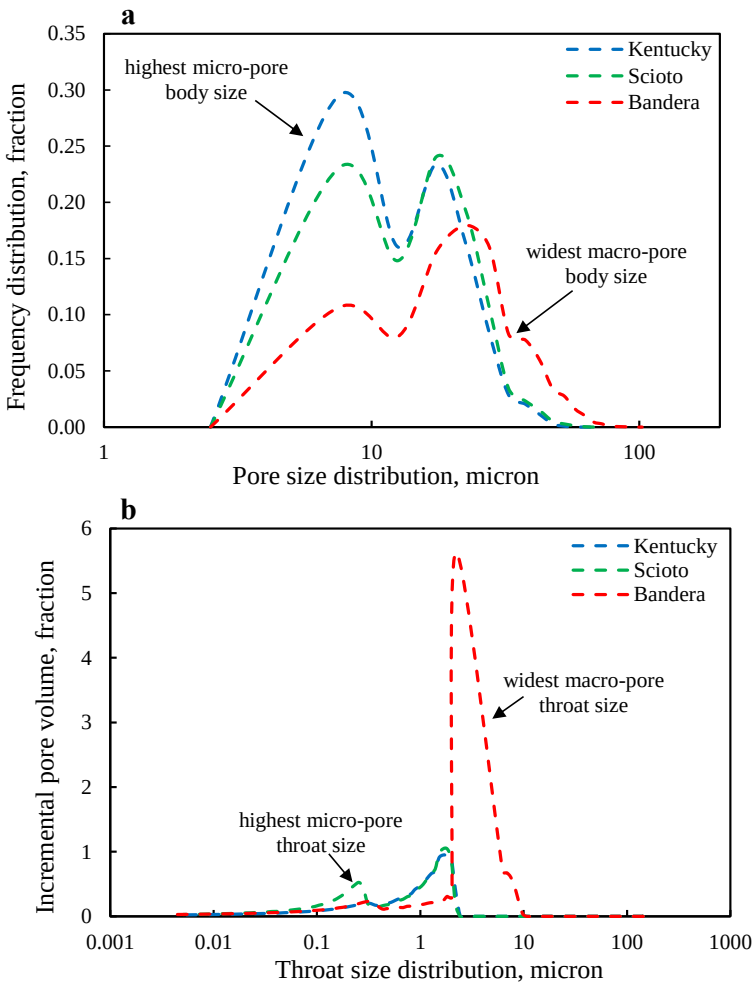

Figure 2.7. Pore and throat size and distributions of Bandera, Kentucky, and Scioto sandstones, where **(a)** shows pore-body diameter distributions obtained by Micro-CT scan and **(b)** represents pore-throat diameter distributions obtained with MICP.

To further investigate the pore systems, NMR T_2 measurements were conducted pre and post centrifuge displacement runs. T_2 cut-off values of tested sandstones were determined to be 17.8, 12.2, and 24.6ms for Bandera, Kentucky, and Scioto, respectively. Subsequently, these values were utilized to estimate the bound volume index (BVI) and Free fluid index (FFI) of all pore frameworks. BVI is the cumulative NMR-porosity after centrifuge test, while FFI is fully saturated cumulative NMR-porosity minus BVI. Results show that Scioto has the highest bound fluid with almost 9% of the total porosity, while Kentucky shows the lowest bound fluid value of 7.5% of the total porosity. Bandera sandstone exhibits the highest movable fluid among the three sandstones with 14.3% of the total porosity (Figure 2.8).

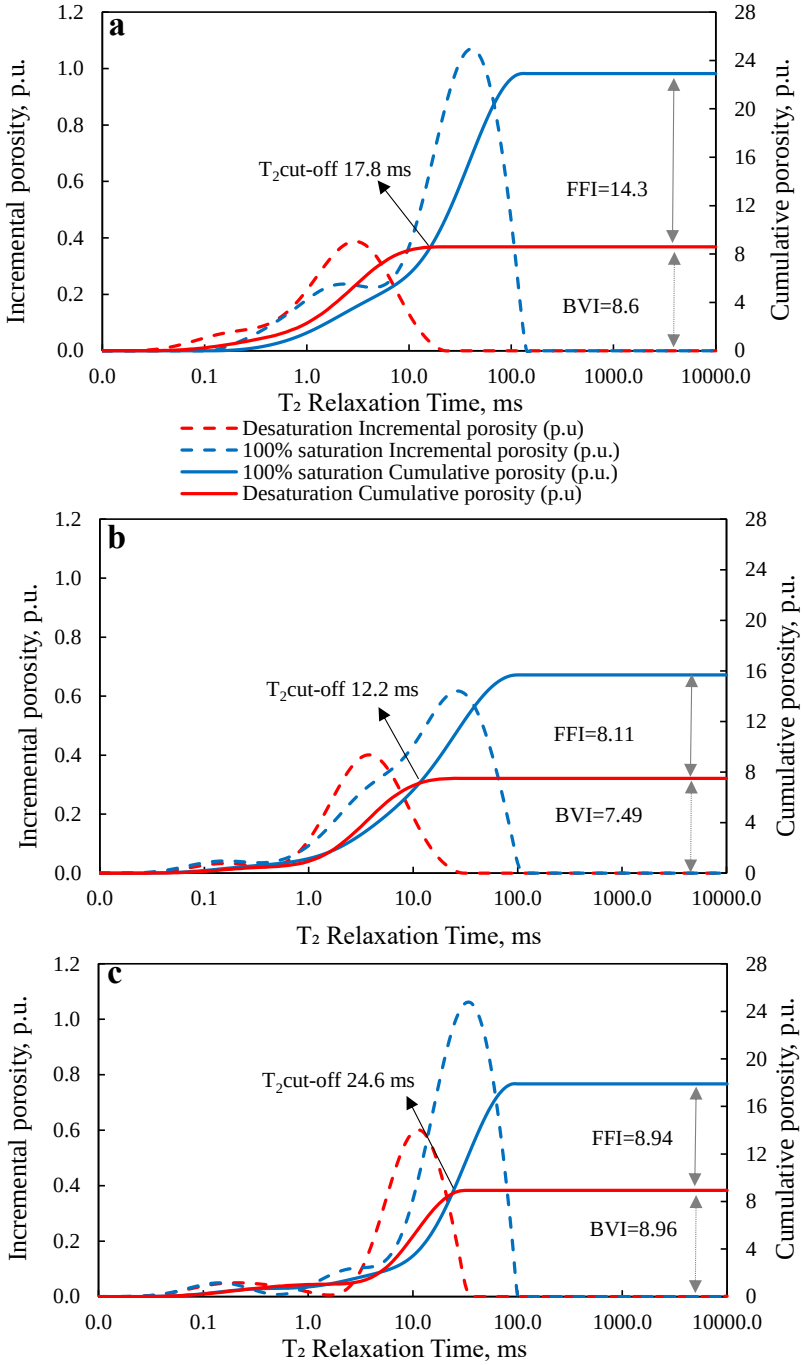

Figure 2.8. T_2 relaxation measurements of fully brine saturated and desaturated plugs for: **(a)** Bandera, **(b)** Kentucky, and **(c)** Scioto where dark blue solid line denotes cumulative porosity at fully brine saturation, dark blue dashed line denotes incremental porosity at fully brine saturation, red solid line denotes cumulative porosity post drainage with air, and red dashed line denotes incremental porosity post drainage with air. BVI is the cumulative porosity after centrifuge test and FFI is fully saturated cumulative porosity minus BVI.

2.4. DISCUSSION

The primary goal of this study was to investigate the impact of clay minerals on the pore framework of tight sandstone samples and to relate that to the displacement efficiency. At the outset of this study, we hypothesized that illite clay, acting as pore bridging, could reduce the micro-throat system. Furthermore, we have argued that pore-filling kaolinite booklets could reduce micro-pore body system in tight sandstone. Finally, we have also proposed that the distribution of throats and bodies plays a significant role in the hydraulic properties of tight sandstone.

Table 2.6. Summary of the grain size, Micro-pore bodies and throats proportions, micropore system, and MTMR of three sandstones samples.

Sample	**Average grain size** (μm)	**Micro-pore proportion** (μCT) (%)	**Micro-throat proportion** (MICP) (%)	**Micropore system proportion** (NMR) (%)	**Micro-throat modality ratio (MTMR)** (v/v)
Bandera	87	10.6	36	38	0.56
Kentucky	55	29.5	50.9	48	1.03
Scioto	59	23	59.1	50	1.44

The multi-techniques analysis clearly supports the above hypotheses on how clay minerals affect pore structure, but needs to be placed in the context of the existing study. For the tight sandstones analyzed, porosity and permeability increase with the total clay content (Figure 2.9a–b), and this is consistent with the literature findings [71,72]. To gain a deeper insight into the relationship of porosity, permeability, and clay minerals, it is more convenient to focus on the effect of clay contents on pore bodies and throats. Our study shows wider pore-throat size distribution for Bandera characterized with porosity and permeability of 24.4% and 24.11 mD and the highest total clay content of 14.3%. The pore throats system covers micro-, meso-, and macro-pore throats; however, macro-pore throat system has the most significant contribution to fluid flow comprising to 64% (Table 2.6).

This macro-pore throat system accesses only the dominant macro-pore body system (89.4% pore body system proportion) as yielded from digital rock analysis. This is in contradiction previous study, stating that the lower the clay content, the larger are the pores and the more the movable fluid in the larger pore throats [73]. In contrast, this study displayed that the marked presence of the macro-pore system in Bandera, when compared to the other sandstones, can be ascribed to the absence of quartz overgrowth due to the clay coating effect, and the relatively larger grain size (average of 87 microns). Such finding aligns well with the observation of Al Saadi et al. [24].

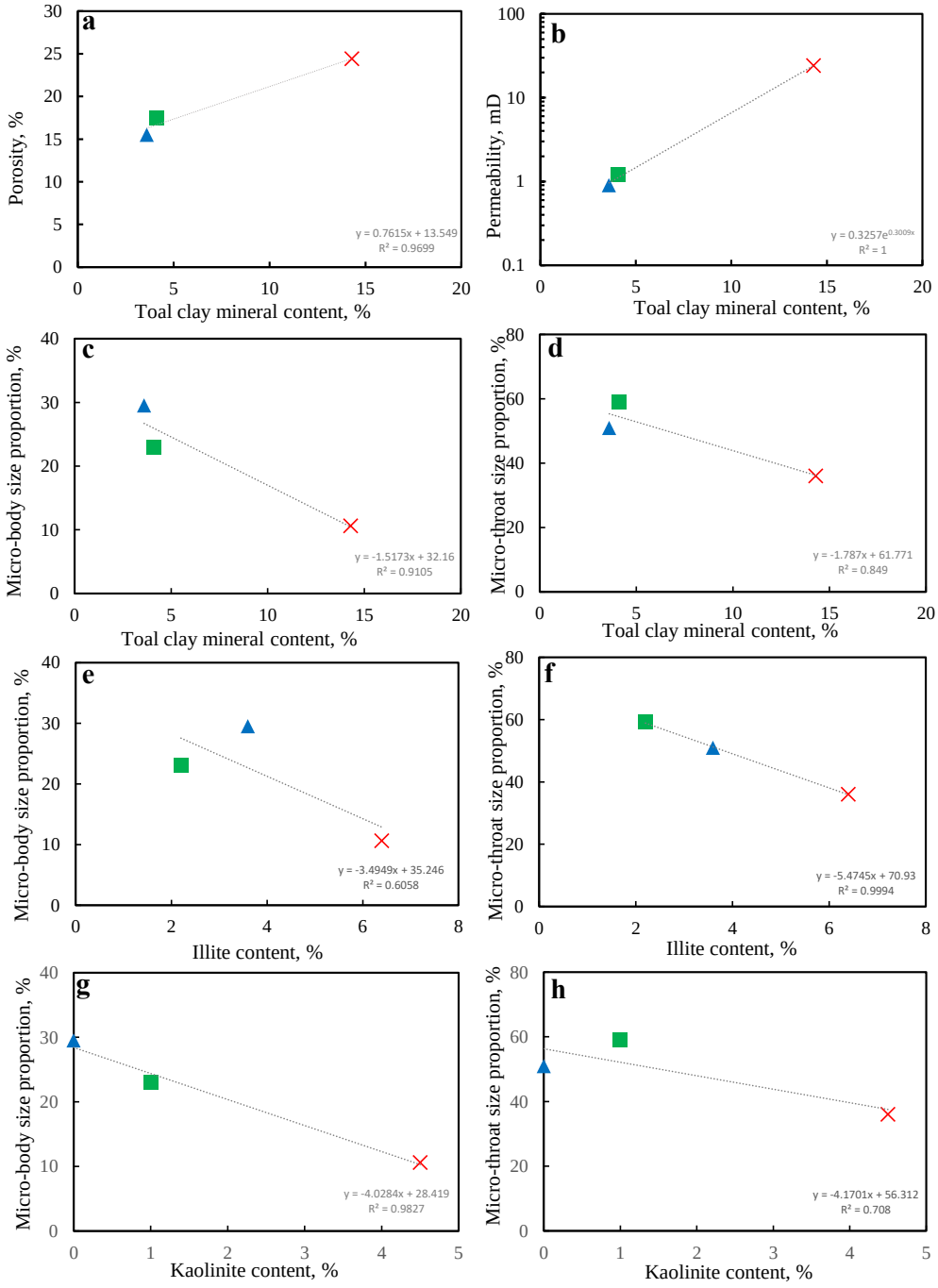

Figure 2.9. Cross-plots of **(a)** porosity versus total clay mineral content, **(b)** permeability versus total clay mineral content, **(c)** micro-pore body size proportion versus total clay mineral content, **(d)** micro-pore throat size proportion versus total clay mineral content, **(e)** the cross plots between illite content and micro-pore body size proportion, **(f)** micro-pore throat size proportion versus illite content, **(g)** micro-pore body size proportion versus kaolinite content, **(h)** micro-pore throat size proportion versus kaolinite content. (*Note the trendlines show the relation between measurements*).

The low contribution of the macro-pore system in Kentucky and Scioto is attributed to the smaller pore size characterizing these rocks (average of 16 microns for Kentucky and 18 microns for Scioto) and finer grain size (average of 55 microns for Kentucky and 59 microns for Scioto) compared to Bandera characterized with relatively higher pore and grain sizes of 24 microns and 87 microns, respectively (Figure 2.10a). Therefore, a higher macro-body size proportion contributes to higher porosity (Figure 2.10b).

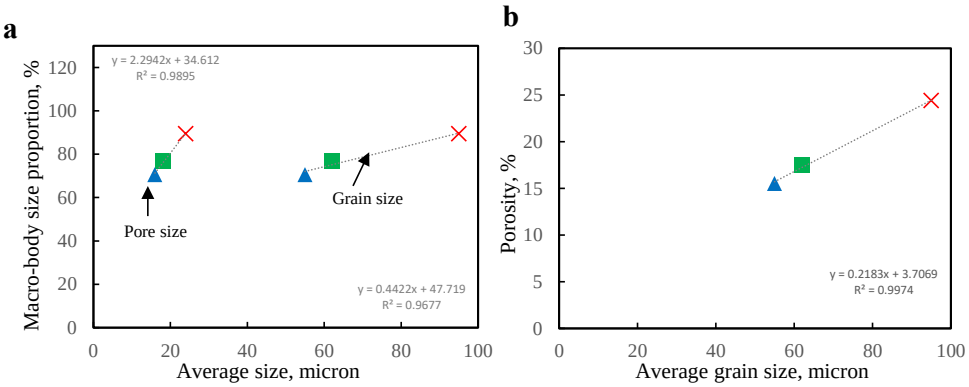

Figure 2.10. Cross-plots showing: **(a)** macro-body proportion versus grain size and pore body size and **(b)** porosity versus grain size. (*Note the trendlines show the relation between measurements*).

This work shows that micro-pore body proportion (Figure 2.9c) and micro-throat proportion (Figure 2.9d) increase with the drop of the total clay content for all tested samples. This is in good agreement with Wang et al. (2020) [72]; where they showed that the increasing percentage of clay minerals clearly decreases the pore throat distribution, porosity, and permeability of tight sandstone. However, we specifically showed that fibrous illite clay acting as pore bridging in sandstone tends to block the existing micro-throat system, affecting the flow displacement efficiency. Illite content and micro-throat size proportion are strongly correlated (R^2 = 0.9994, Figure 2.9f). This confirms that the low contribution of micro-throat system is attributed to illite-chocking and that validates the stated hypothesis of this study.

In contrast, there is a weak correlation between illite content and micro-pore body proportion, revealing less influence on micro-pore body proportion (R^2 = 0.6058, Figure 2.9e). The micro-pore body system of Bandera is measured to be the least among the sandstones tested representing 10.6% of the total pore system. This is attributed to the presence of Kaolinite as pore filling (average size of 5.2 microns), which tends to fill the micro-pores and hence reduces their contribution in overall porosity. On the contrary, micro-pore systems of Kentucky and Scioto show higher values with 50.1% and 59 %, respectively. The kaolinite content and micro-pore body proportions show a strong correlation (R^2 = 0.9827, Figure 2.9g).

However, kaolinite and micro-throat size proportions relation reveals a relatively weaker correlation ($R^2 = 0.708$, Figure 2.9h), indicating that the kaolinite has little effect on micro-throat radius in tight sandstones.

The above experimental outcomes are consistent with the micro-pore system contribution obtained from NMR results. It indicates that Scioto has the highest micro-pore system contribution comprising almost 50% of the total porosity. Kentucky follows with 48% and Bandera has the least micro-pore system contribution of 38%, as shown in Table 2.6. Furthermore, NMR measurements show the dominance of the macro-pore system in Bandera comprising 62%, which are in agreement with high percentage of intergranular pores observed with thin sections for this sandstone (Figure 2.3b).

In addition, Micro-CT and MICP results confirm that Banderas' macro-pore body and throat system proportions are the highest among the tested samples with 89.4% and 64%, respectively. The difference of micro-pore bodies and throats proportions is related to the limitation of each technique, which should be a subjected to further future studies. It is worth noting that those rocks are considered to be water wet as examined by (Alotaibi et al., 2011 and Mahmoud, 2018) [73,74]. Moreover, due to the significant complication of the pore-throat systems in tight rocks, most of displacing fluid during the injection process will favor the least resistant paths (macro-pore throat) (Figure 2.11). As a result, lower microscopic displacement efficiency of the injection process is faced due to channeling effect [75–77].

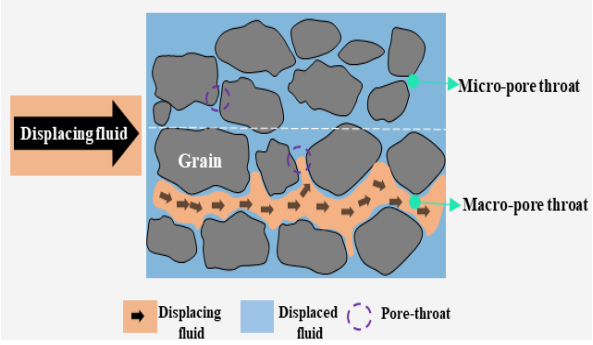

Figure 2.11. Schematic showing the flow of displacing fluid through the least resistance path (macro-pore throat) bypassing the micro-pore throat area due to capillary effect.

Micro-pore throat modality ratio (*MTMR*), a dimensionless number that relates the abundance size of the micro-pore throat to the macro-pore throat, can be considered for describing the microscopic displacement efficiency of improved and enhanced oil recovery (IOR/EOR) processes.

$$MTMR = \frac{Micro - throat\ proportion}{Macro - throat\ proportion}$$

A large MTMR value demonstrates that most of the displacing fluid will flow mainly through the macro-pore throat. As a result, poor microscopic displacement efficiency occurs due to the inability of injected fluid to access the micro-pore system mobilizing the displaced fluid [78,79]. Kaolinite has little effect on MTMR, while illite reveals a strong negative correlation with MTMR for the tested sandstones as demonstrated in Figure 2.12. Such relationship will negatively affect the microscopic displacement efficiency of tight sandstone.

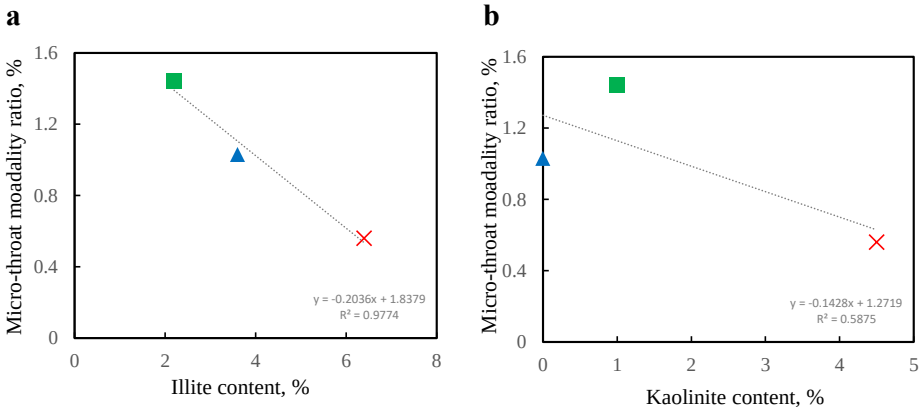

Figure 2.12. Cross-plots showing. **(a)** MTMR versus illite content and **(b)** MTMR versus kaolinite content. (*Note the trendlines show the relation between measurements*).

High values of MTMR are needed to divert the displacing fluid and this can be conducted using, polymer or foam to reach out the oil residing in smaller pores and hence improving the microscopic displacement efficiency [80,81]. This novel micro-pore throat modality ratio is believed to be a key criterion in selecting the most efficient EOR methods in tight formations. Larger dataset would offer further insight this can be a potential for future work.

2.5. CONCLUSIONS

Different tight sandstones were analysed to define their petrography, mineralogy and petrophysical properties. Petrographic thin-sections, XRD, XRF and SEM were used to determine the mineralogical and elemental composition. MICP was used to define pore throat size

distributions and NMR and Micro-CT were utilized to determine the pore size distributions. Based on the multiple measurements conducted, the following can be concluded:

- Illite clay acting as pore bridging tends to reduce the micro-throat system. A strong correlation was obtained between illite content and micro-pore throat proportion in tested sandstone samples implying that the higher the illite content, the lower the micro-pore throat system proportion.
- The presence of pore-filling kaolinite booklets reduces micro-pore body system in sandstone samples. Bandera characterized with high kaolinite content shows low micro-pore body proportion of the total pore body system. Nevertheless, the shortage of kaolinite clay in Kentucky and Scioto sandstones preserves the sample's total micro-pore body system revealing strong correlation between kaolinite content and micro-pore body proportion.
- The low contribution of macro-pore system in Kentucky and Scioto samples is attributed to their finer grain size and hence, smaller pore size. In contrast, Bandera shows a clear high proportion of macro-pore due to the absence of quartz overgrowth as a result of clay coating, and relatively coarser grain size.
- MTMR dimensionless number is helpful in selecting the most efficient recovery process. Scioto sandstone showing the highest MTMR indicates the contribution of both macro- and micro-pore systems to fluids flow in this sandstone. Therefore, there is a need to mitigate the oil bypass from micropores pores by using easy to enter fluid such as gas. Conversely, MTMR is quite low indicating the dominance of macropores and hence oil bypass is minimal rendering conventional water flooding as an efficient recovery method.

REFERENCES

1. Cao, Z., Liu, G., Zhan, H., Gao, J., Zhang, J., Li, C. and Xiang, B., 2017. Geological roles of the siltstones in tight oil play. Marine and Petroleum Geology, 83, pp.333-344.
2. Zou, C., Zhu, R., Liu, K., Su, L., Bai, B., Zhang, X., Yuan, X. and Wang, J., 2012. Tight gas sandstone reservoirs in China: characteristics and recognition criteria. Journal of Petroleum Science and Engineering, 88, pp.82-91.
3. National resources Canada. North American tight oil. 2012. http://www.nrcan.gc.ca/energy/sources/crude/2114#oil1.
4. Wang, J., Feng, L., Steve, M., Tang, X., Gail, T.E. and Mikael, H., 2015. China's unconventional oil: A review of its resources and outlook for long-term production. Energy, 82, pp.31-42.
5. Zhang, X.S., Wang, H.J., Ma, F., Sun, X.C., Zhang, Y. and Song, Z.H., 2016. Classification

and characteristics of tight oil plays. Petroleum Science, 13, pp.18-33.

6. Burley, S. and Worden, R., 2003. Sandston diagenesis: Recent and ancient. Reprint Serint Series Volume 4 of the International Association of Sedimentologists.
7. Stroker, T.M., Harris, N.B., Elliott, W.C. and Wampler, J.M., 2013. Diagenesis of a tight gas sand reservoir: upper Cretaceous Mesaverde Group, Piceance Basin, Colorado. Marine and Petroleum Geology, 40, pp.48-68.
8. Alamdari, B.B., Kiani, M. and Kazemi, H., 2012, April. Experimental and numerical simulation of surfactant-assisted oil recovery in tight fractured carbonate reservoir cores. In SPE Improved Oil Recovery Symposium. OnePetro.
9. Zhao, X., Yang, Z., Lin, W., Xiong, S. and Wei, Y., 2018. Characteristics of microscopic pore-throat structure of tight oil reservoirs in Sichuan Basin measured by rate-controlled mercury injection. Open Physics, 16(1), pp.675-684.
10. Sakellariou, A., Sawkins, T.J., Senden, T.J., Arns, C.H., Limaye, A., Sheppard, A.P., Sok, R.M., Knackstedt, M.A., Pinczewski, W.V., Berge, L.I. and Øren, P.E., 2003, October. Micro-CT facility for imaging reservoir rocks at pore scales. In 2003 SEG Annual Meeting. OnePetro.
11. Bultreys, T., De Boever, W. and Cnudde, V., 2016. Imaging and image-based fluid transport modeling at the pore scale in geological materials: A practical introduction to the current state-of-the-art. Earth-Science Reviews, 155, pp.93-128.
12. Peksa, A.E., Wolf, K.H.A. and Zitha, P.L., 2015. Bentheimer sandstone revisited for experimental purposes. Marine and Petroleum Geology, 67, pp.701-719.
13. Giesche, H., 2006. Mercury porosimetry: a general (practical) overview. Particle & particle systems characterization, 23(1), pp.9-19.
14. Rice, K.M., Walker Jr, E.M., Wu, M., Gillette, C. and Blough, E.R., 2014. Environmental mercury and its toxic effects. Journal of preventive medicine and public health, 47(2), p.74.
15. Hinedi, Z.R., Chang, A.C., Anderson, M.A. and Borchardt, D.B., 1997. Quantification of microporosity by nuclear magnetic resonance relaxation of water imbibed in porous media. Water Resources Research, 33(12), pp.2697-2704.
16. Yao, Y., Liu, D., Che, Y., Tang, D., Tang, S. and Huang, W., 2010. Petrophysical characterization of coals by low-field nuclear magnetic resonance (NMR). Fuel, 89(7), pp.1371-1380.
17. Jin, G., Xie, R. and Xiao, L., 2020. Nuclear magnetic resonance characterization of petrophysical properties in tight sandstone reservoirs. Journal of Geophysical Research: Solid Earth, 125(2), p.e2019JB018716.
18. Kenyon, W.E., 1997. Petrophysical principles of applications of NMR logging. The log

analyst, 38(02).

19. Wang, R., Shi, W., Xie, X., Zhang, W., Qin, S., Liu, K. and Busbey, A.B., 2020. Clay mineral content, type, and their effects on pore throat structure and reservoir properties: Insight from the Permian tight sandstones in the Hangjinqi area, north Ordos Basin, China. Marine and Petroleum Geology, 115, p.104281.
20. Karimi, S., Kazemi, H., 2015. Capillary pressure measurement using reservoir fluids in a middle bakken core. In: SPE 174065, SPE Western Regional Meeting. April 27–30, Garden Grove, California, USA.
21. El-Husseiny, A. and Knight, R., 2017. A laboratory study of the link between NMR relaxation data and pore size in carbonate skeletal grains and micrite. Petrophysics, 58(02), pp.116-125.
22. Westphal, H., Surholt, I., Kiesl, C., Thern, H.F. and Kruspe, T., 2005. NMR measurements in carbonate rocks: problems and an approach to a solution. Pure and applied geophysics, 162, pp.549-570.
23. Hu, Y., Guo, Y., Zhang, J., Shangguan, J., Li, M., Quan, F. and Li, G., 2020. A method to determine nuclear magnetic resonance T2 cutoff value of tight sandstone reservoir based on multifractal analysis. Energy Science & Engineering, 8(4), pp.1135-1148.
24. Al Saadi, F., Wolf, K. and Kruijsdijk, C.V., 2017. Characterization of Fontainebleau sandstone: Quartz overgrowth and its impact on pore-throat framework. Journal of Petroleum & Environmental Biotechnology, 7(328), pp.1-12.
25. Zhu, P., Dong, Y., Chen, M., Li, Z., Han, B., Wang, J. and Cui, Y., 2020. Quantitative evaluation of pore structure from mineralogical and diagenetic information extracted from well logs in tight sandstone reservoirs. Journal of Natural Gas Science and Engineering, 80, p.103376.
26. Neasham, J.W., 1977, October. The morphology of dispersed clay in sandstone reservoirs and its effect on sandstone shaliness, pore space and fluid flow properties. In SPE annual fall technical conference and exhibition. OnePetro.
27. Schrader, M.E. and Yariv, S., 1990. Wettability of clay minerals. Journal of colloid and interface science, 136(1), pp.85-94.
28. Yuan, G., Gluyas, J., Cao, Y., Oxtoby, N.H., Jia, Z., Wang, Y., Xi, K. and Li, X., 2015. Diagenesis and reservoir quality evolution of the Eocene sandstones in the northern Dongying Sag, Bohai Bay Basin, East China. Marine and Petroleum Geology, 62, pp.77-89.
29. Rosenbrand, E., Fabricius, I.L., Fisher, Q. and Grattoni, C., 2015. Permeability in Rotliegend gas sandstones to gas and brine as predicted from NMR, mercury injection and image analysis. Marine and Petroleum Geology, 64, pp.189-202.

30. Kuila, U. and Prasad, M., 2013. Specific surface area and pore-size distribution in clays and shales. Geophysical Prospecting, 61(2), pp.341-362.
31. Stueck, H., Koch, R. and Siegesmund, S., 2013. Petrographical and petrophysical properties of sandstones: statistical analysis as an approach to predict material behaviour and construction suitability. Environmental earth sciences, 69, pp.1299-1332.
32. Wang, R., Shi, W., Xie, X., Zhang, W., Qin, S., Liu, K. and Busbey, A.B., 2020. Clay mineral content, type, and their effects on pore throat structure and reservoir properties: Insight from the Permian tight sandstones in the Hangjinqi area, north Ordos Basin, China. Marine and Petroleum Geology, 115, p.104281.
33. Hassan, A., Mahmoud, M., Al-Majed, A. and Al-Nakhli, A., 2019. New chemical treatment for permanent removal of condensate banking from different gas reservoirs. ACS omega, 4(26), pp.22228-22236.
34. El-Din Mahmoud, M.A., 2018. Effect of chlorite clay-mineral dissolution on the improved oil recovery from sandstone rocks during diethylenetriaminepentaacetic acid chelating-agent flooding. SPE Journal, 23(05), pp.1880-1898.
35. Hanafy, A.M., 2018. Investigation of acidizing technologies in high-temperature applications for sandstone and limestone formations (Doctoral dissertation).
36. Tariq, Z., Kamal, M.S., Mahmoud, M., Murtaza, M., Abdulraheem, A. and Zhou, X., 2021. Dicationic surfactants as an additive in fracturing fluids to mitigate clay swelling: A petrophysical and rock mechanical assessment. ACS omega, 6(24), pp.15867-15877.
37. Zimmerman, R.W., Somerton, W.H. and King, M.S., 1986. Compressibility of porous rocks. Journal of Geophysical Research: Solid Earth, 91(B12), pp.12765-12777.
38. Adams, G.I., Girty, G.H. and White, D., 1903. Stratigraphy and paleontology of the Upper Carboniferous rocks of the Kansas section (No. 211). US Government Printing Office.
39. Jewett, J. M., and Abernathy, G. E., 1945, Oil and gas in eastern Kansas: Kansas Geo 1. Survey, Bull. 57, 245 pp.
40. Martino, R.L., 1989. Trace fossils from marginal marine facies of the Kanawha Formation (Middle Pennsylvanian), West Virginia. Journal of Paleontology, 63(4), pp.389-403.
41. Brownfield, R.L., Brenner, R.L. and Pope, J.P., 1998. Distribution of the Bandera shale of the Marmaton Group, Middle Pennsylvanian of southeastern kansas. Current Research in Earth Sciences, pp.29-41.
42. Koch, Z. and Burke, C.D., 2009. Paleoenvironmental interpretation of the Bandera shale formation, marmaton group, desmoinesian stage, middle Pennsylvanian in southeastern Kansas.

43. USGS, 2023. Geological maps of US states, accessed March 29, 2023 at URLhttps://mrdata.usgs.gov/geology/state.
44. Glick, E.E., 1963. Geology of the Clarkson quadrangle, Kentucky: US Geol. Survey Geol. Quad. Map GQ-278.
45. Gildersleeve, B., 1965. Geology of the Brownsville quadrangle, Kentucky (No. 411).
46. Shawe, F.R., 1966. Geologic map of the Reedyville quadrangle, western Kentucky (No. 520).
47. Greb, S.F., Williams, D.A. and Williamson, A.D., 1992. Geology and stratigraphy of the western Kentucky coal field.
48. Harris, D.C., 2007. Kentucky Consortium for Carbon Storage: www. uky. edu. KGS/kyccs/ppt/071207_Harris. pdf.
49. Hull, D.H., Larsen, G.E. and Slucher, E.R., 2004. Generalized columns of bedrock units in Ohio. State of Ohio, Department of Natural Resources, Division of Geological Survey.
50. Hannibal, J.T., Saja, D.B., Thomas, S.F. and Hubbard, D.K., 2006, May. Quarrying history and use of Berea Sandstone in northeastern Ohio. In Proceedings of the 42nd Forum on the Geology of Industrial Minerals (pp. 7-13).
51. Wolfe, M.E. and Stucker, J.D., 2013. 2012 Report on Ohio Mineral Industries: An Annual Summary of the State's Economic Geology. Report to State of Ohio Department of Natural Resources Division of Geological Survey, p.116.
52. Saja, D.B. and Hannibal, J.T., 2017. Quarrying history and use of the Buena Vista freestone, south-central Ohio: understanding the 19th century industrial development of a geological resource. The Ohio Journal of Science, 117(2), pp.35-49.
53. Pepper, J.F., de Witt Jr, W. and Demarest, D.F., 1954. Geology of the Bedford shale and Berea sandstone in the Appalachian basin. Science, 119(3094), pp.512-513.
54. Greb, S.F., Williams, D.A. and Williamson, A.D., 1992. Geology and stratigraphy of the western Kentucky coal field.
55. Hull, D.H., Larsen, G.E. and Slucher, E.R., 2004. Generalized columns of bedrock units in Ohio. State of Ohio, Department of Natural Resources, Division of Geological Survey.
56. Nichols, G., 2009. Sedimentology and stratigraphy. John Wiley & Sons.
57. Ghiasi-Freez, J., Soleimanpour, I., Kadkhodaie-Ilkhchi, A., Ziaii, M., Sedighi, M. and Hatampour, A., 2012. Semi-automated porosity identification from thin section images using image analysis and intelligent discriminant classifiers. Computers & geosciences, 45, pp.36-45.
58. Wardaya, P.D., Khairy, H. and Sum, C.W., 2013, March. Extracting physical properties from thin section: Another neural network contribution in Rock Physics. In International Petroleum

Technology Conference. OnePetro.

59. Asmussen, P., Conrad, O., Günther, A., Kirsch, M. and Riller, U., 2015. Semi-automatic segmentation of petrographic thin section images using a “seeded-region growing algorithm” with an application to characterize weathered subarkose sandstone. Computers & Geosciences, 83, pp.89-99.
60. Varfolomeev, I., Yakimchuk, I., Denisenko, A., Khasanov, I., Osinceva, N. and Rahmattulina, A., 2016, October. Integrated study of thin sections: Optical petrography and electron microscopy. In SPE Russian Petroleum Technology Conference and Exhibition. OnePetro.
61. Doughty, D.A. and Tomutsa, L., 1996. Multinuclear NMR microscopy of two-phase fluid systems in porous rock. Magnetic resonance imaging, 14(7-8), pp.869-873.
62. Ahmed, W., 2008. Contrast in clay mineralogy and their effect on reservoir properties in sandstone formations. Bulletin of the Chemical Society of Ethiopia, 22(1).
63. Buades, A., Coll, B. and Morel, J.M., 2005, June. A non-local algorithm for image denoising. In 2005 IEEE computer society conference on computer vision and pattern recognition (CVPR'05) (Vol. 2, pp. 60-65).
64. Dong, H., Touati, M. and Blunt, M.J., 2007, March. Pore network modeling: analysis of pore size distribution of Arabian core samples. In SPE middle east oil and gas show and conference. OnePetro.
65. Carr, H.Y. and Purcell, E.M., 1954. Effects of diffusion on free precession in nuclear magnetic resonance experiments. Physical review, 94(3), p.630.
66. Green, D.P., Dick, J.R., McAloon, M., Cano-Barrita, P.D.J., Burger, J., Balcom, B. and Oaxaca, C.I.U., 2008, October. Oil/water imbibition and drainage capillary pressure determined by MRI on a wide sampling of rocks. In SCA2008-01 presented at the SCA conference, Abu Dhabi, UAE (Vol. 29).
67. Folk, R.L., 1951. Stages of textural maturity in sedimentary rocks. Journal of Sedimentary Research, 21(3), pp.127-130.
68. Boggs, S., 2012. Principles of sedimentology and stratigraphy.
69. Folk, R.L., 1980. Petrology of sedimentary rocks. Hemphill publishing company.
70. Nelson, P.H., 2009. Pore-throat sizes in sandstones, tight sandstones, and shales. AAPG bulletin, 93(3), pp.329-340.
71. Lai, J., Wang, G., Fan, Z., Zhou, Z., Chen, J. and Wang, S., 2018. Fractal analysis of tight shaly sandstones using nuclear magnetic resonance measurements. AAPG Bulletin, 102(2), pp.175-193.
72. Alotaibi, B., Nasralla, A. and Nasr-El-Din, A., 2011. Wettability studies using low-salinity

water in sandstone reservoirs. SPE Reservoir Evaluation & Engineering, 14(06), pp.713-725.

73. El-Din Mahmoud, M., 2018. Effect of chlorite clay-mineral dissolution on the improved oil recovery from sandstone rocks during diethylenetriaminepentaacetic acid chelating-agent flooding. SPE Journal, 23(05), pp.1880-1898.
74. Wang, R., Shi, W., Xie, X., Zhang, W., Qin, S., Liu, K. and Busbey, A.B., 2020. Clay mineral content, type, and their effects on pore throat structure and reservoir properties: Insight from the Permian tight sandstones in the Hangjinqi area, north Ordos Basin, China. Marine and Petroleum Geology, 115, p.104281.
75. Zhao, H., Ning, Z., Wang, Q., Zhang, R., Zhao, T., Niu, T. and Zeng, Y., 2015. Petrophysical characterization of tight oil reservoirs using pressure-controlled porosimetry combined with rate-controlled porosimetry. Fuel, 154, pp.233-242.
76. Madathil, A., Azrak, O., Pearce, A., Al Amrie, O., Gunasan, E. and Blondeau, C., 2015, November. 24 years of successful EOR through Immiscible Tertiary Gas Injection. In Abu Dhabi International Petroleum Exhibition and Conference. OnePetro.
77. Gao, H., Li, T. and Yang, L., 2016. Quantitative determination of pore and throat parameters in tight oil reservoir using constant rate mercury intrusion technique. Journal of Petroleum Exploration and Production Technology, 6, pp.309-318.
78. Bolandtaba, S.F. and Skauge, A., 2011. Network modeling of EOR processes: a combined invasion percolation and dynamic model for mobilization of trapped oil. Transport in porous media, 89(3), pp.357-382.
79. Lv, P., Wang, Z., Liu, Y., Dong, H., Jiang, L., Song, Y., Wu, B. and Liu, S., 2017. Pore-scale displacement mechanisms investigation in CO_2-brine-glass beads system. Energy Procedia, 105, pp.4122-4127.
80. Nguyen, D., Wang, D., Oladapo, A., Zhang, J., Sickorez, J., Butler, R. and Mueller, B., 2014, April. Evaluation of surfactants for oil recovery potential in shale reservoirs. In SPE Improved Oil Recovery Symposium. OnePetro.
81. Abdelaal, A., Gajbhiye, R. and Al-Shehri, D., 2020. Mixed CO_2/N_2 foam for EOR as a novel solution for supercritical CO_2 foam challenges in sandstone reservoirs. ACS omega, 5(51), pp.33140-33150.

3. PORE FLUID DISTRIBUTION CHARACTERIZATION FOR MICRSOSCOPIC CO_2 INJECTION IN TIGHT SANDSTONES

This chapter utilizes the findings from Chapter 2 to investigate the relationship between clay minerals, pore size distribution and the pore fluids distribution. The aim is to determine the micropore system contribution to pore-fluid distribution (PFD) in tight sandstones. New dimensionless numbers, termed the microscopic confinement index (MCI), a measure of the product of micro-storativity (MSI) and micro-throat modality (MTMR) indices, were developed to select a suitable tight sandstone for CO_2–EOR and CO_2 geo-storage. Routine core analysis, XRD, SEM, MICP, centrifuge displacement and NMR performed on the three tight sandstones from the previous chapter was utilized to achieve this goal. Findings indicate that Scioto sandstone has the highest micropore system capability to store and confine fluids which makes it the most suitable candidate for CO_2–EOR and geo-storage among the tested samples.

The content of this chapter is based on the below publication:
Al-Kharra'a, H.S., Wolf, K.H.A., AlQuraishi, A.A., Mahmoud, M.A., AlDuhailan, M.A., and Zitha, P.L.J., 2023. The Power of Characterizing Pore Fluid Distribution for Microscopic CO_2 Injection Studies in Tight Sandstones. Minerals, 13(7), p.895.

3.1. INTRODUCTION

Chapter 2 demonstrated how various clay minerals affect the pore structures in tight sandstones. PFD, including BVI and FFI, varies in tight reservoirs due to the rock's depositional and diagenetic conditions [1] which can consequently influence fluid flow behavior in these rocks [2]. Hence, understanding these indices and their controlling factors is vital for successful injection of fluid(s). As already discussed in the previous chapter, several primary factors control pore size distribution in sandstones, including mineralogy, diagenetic processes, grain size, and pore size and structure [3–6]. We have argued earlier that primary pores and micropores are the principal components of the pore fluid distribution in sandstones [7]. Primary pores are voids between detrital grains that form during the depositional process, while micropores originate prior to the depositional process and commonly exist between detrital grains and authigenic clay minerals [8]. Micropores are characterized by pore bodies and throats smaller than 10 microns and 1 micron respectively.

Sandstone rocks exhibit a proportional relationship between the primary pore and grain size [9–11] while compaction essentially reduces primary pores and thus decreases sandstone's total porosity [12]. Several studies claim that common long side, concavo-convex, sutured grain contacts correspond to considerable rock compaction, decreasing primary pores [13,14]. Investigation of the effect of grain shape on porosity shows that as grain sphericity increases, the primary pores size decrease because of the tight packing [15]. Furthermore, sorting accounts for the variety in sandstone grain size and correlates well with porosity [16]. Sandstones with good sorting attributes possess substantial primary pores due to grain size homogeneity [17,18]. However, poor sorting leads to complex pore-throat size distribution, leading to a sharp reduction in porosity due to small particles filling the intergranular pores [19–21]. The dissolution of feldspar can cause a remarkable increase in the percentage of the primary pores, leading to better pore connectivity [22].

As discussed in Chapter 2, several studies have investigated the impact of total clay content on the petrophysical properties of tight sandstone [23–25], and they show an inverse relationship between both porosity and permeability and clay content. [26]. In term of clay type, kaolinite booklets can fill rock pores and hence lower sandstone's porosity; however, it has a lesser impact on permeability [27]. Fibrous illite clay on the other hand tends to reduce the effective pore-throat diameter and consequently lower's rock's permeability [28]. Quartz overgrowth affects both porosity and permeability by reducing the primary pore sizes in sandstones [29–31]; however, clay coating can preserve primary pores by coating the detrital quartz grains, thus inhibiting their overgrowth [32].

The impact of pore structure on NMR T_2 distributions for various pore sizes was investigated and sandstone samples with a higher percentage of primary pores exhibit longer NMR T_2 peak values, suggesting the existence of a direct relation between movable water and primary pores [33]. This further supports the idea that a higher movable fluid proportion corresponds to more interconnected pores [34]. Movable and bound fluid volumes can be determined using fluid displacement and NMR measurements [35]. During the displacement process, movable fluid is discharged from interconnected pores leaving bound fluid confined within the micropores due to capillarity effect [36,37]. Several publications investigate the relationship between the proportion of the micropore system and the factors that influence fluid confinement [38–40]. However, they study the proportion of pore size distribution at CT-image resolution, which is different from my objective; to study the CO_2 saturation contribution in an NMR bulk porosity image.

In Chapter 2, we demonstrated the elemental and mineralogical compositions and the petrophysical properties of three tight sandstones. The clay minerals content and type and their

effect on rocks pore and throat size distribution were presented and discussed. In this chapter the relationship between tight sandstone's pore system distribution and PFD are explored. In addition, the contribution of micropore system in overall fluid displacement is investigated by developing new dimensionless number termed MCI to provide novel selection criteria for planning optimal CO_2–EOR and geo-storage.

3.2. RESULTS

In this chapter, we tend to present the MCI results for the investigated sandstone rocks and their interpretation. MCI, a dimensionless number is developed to evaluate sandstone's microscopic fluid storage and confinement (entrapment), is calculated by multiplying the micro-storativity (MSI) defining the storage capacity of the micropore system and micro-throat modality (MTMR) defining the micropore system's entrapment calculated and presented in Chapter 2.

$$MSI = \frac{BVI}{FFI + BVI}$$

Where BVI is the cumulative NMR-porosity after centrifuge test and FFI is fully saturated cumulative NMR-porosity minus BVI.

$$MCI = MTMR \times MSI$$

High MCI value indicates optimum microscopic confinement during CO_2–EOR or CO_2 geo-storage in tight sandstone rocks. Table 3.1 lists the indices calculated for the three tight sandstones investigated.

Table 3.1. Calculated MSI, MTMR, and MCI results of three sandstones.

Sample	**MSI** (v/v)	**MTMR** (v/v)	**MCI** (v/v)
Bandera	0.38	0.56	0.21
Kentucky	0.48	1.03	0.49
Scioto	0.50	1.44	0.72

MSI calculations for the three sandstone samples demonstrates that Scioto sandstone had the highest value of 0.5 MSI, followed by Kentucky sandstone with 0.48 MSI, and Bandera sandstone, which exhibited the lowest value of 0.38 MSI. MTMR calculations presented earlier indicates that Scioto sandstone possessed the highest micropore system confinement with 1.44 MTMR, followed by Kentucky with 1.03 MTMR, and Bandera sandstone, which was characterized by the lowest microporosity entrapment of 0.56 MTMR. MCI values after gas displacement were calculated for the three sandstones investigated. The results confirmed that Scioto sandstone has the highest value of 0.72, followed by Kentucky and Bandera with MCI values of 0.49 and 0.21, respectively. Although the MSI of the Kentucky and Scioto samples showed comparable values, the difference in their calculated MCI values revealed an almost 40%

difference between these two sandstones in favor of the Scioto. As a result, Scioto sandstone is the most suitable candidate for CO_2–EOR due to its high microscopic CO_2 confinement index compared to the other tested sandstones.

3.3. DISCUSSION

As discussed in Chapter 2, Bandera sandstone exhibited the best reservoir quality compared to the other sandstones. Conversely, Kentucky and Scioto sandstones displayed fair porosities and reasonably low permeability values (15% and 0.98 mD for Kentucky and 17.5% and 1.21 mD for Scioto) (Figure 3.1a). We hypothesized that the diagenetic process was accountable for the substantial decrease in the Kentucky and Scioto sandstone's permeability. Relationship of permeability and micro-throat size proportion were found to be inversely related (Figure 3.1b). This confirms that the low permeability values could be ascribed to the small throat size characterizing these sandstones validating the hypothesis of the diagenesis effect. Literature indicates that high porosity values associated with low permeabilities, and vice versa, in tight sandstones are related to the depositional conditions that could reduce the pore structure of the sandstone rocks [41,42].

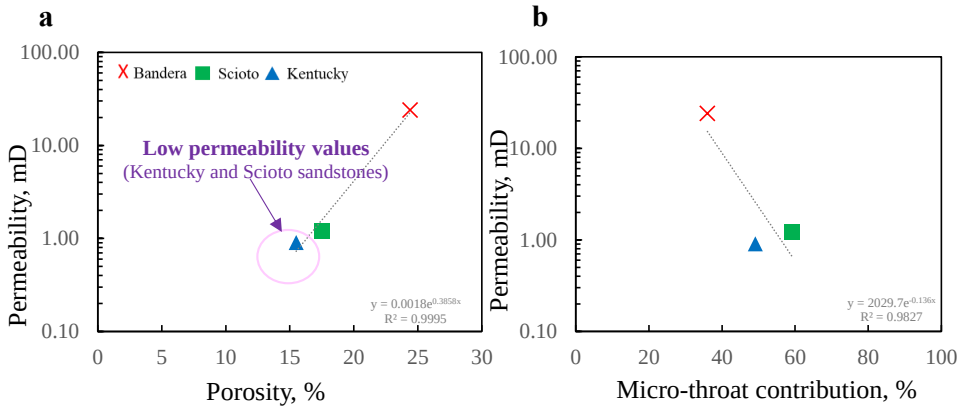

Figure 3.1. Cross-plots demonstrating the relationship of permeability with: **(a)** porosity; **(b)** micro-throat contribution. (*Note the trend lines show the relation between measurements).*

Considering the complexity of the pore system in tight rocks, we advise against the use of permeability as a cut-off parameter to identify tight reservoirs; rather, we recommend including pore-size distribution as an essential characterization parameter in tight reservoir classifications. Note that the micropore system represents a considerable proportion of the tight rock's total porosity [43,44]. This was further confirmed in our study where the following fractions were measured: 38% in the Bandera, 48% in the Kentucky, and 50% in Scioto. These results are consistent with Lai et al. [45], who reported that bound-fluid contribution (micropore system) can account for up to 60% of the total pore system. Thus, it is more convenient to investigate the

relationship between the micropore system and the pore fluid distribution in tight sandstones to enable geologists and petroleum engineers to improve the efficiency of flooding in general and CO_2 injection in specific into tight formations.

Bandera sandstone has a wider pore size distribution than other sandstones, with values ranging from 0.1 ms to 140 ms, as yielded by NMR analyses (Figure 2.8a). Furthermore, the NMR findings show that 62% of the PFD in Bandera sandstone is mobile within the macropore system. This finding agrees well with the MICP results, demonstrating the significant flow contribution of macropore throat system summing up to 64% in Bandera sandstone (Figure 2.7a). SEM images illustrate the visible macropores of the Bandera sandstone (Figure 2.4a) and the presence of clay

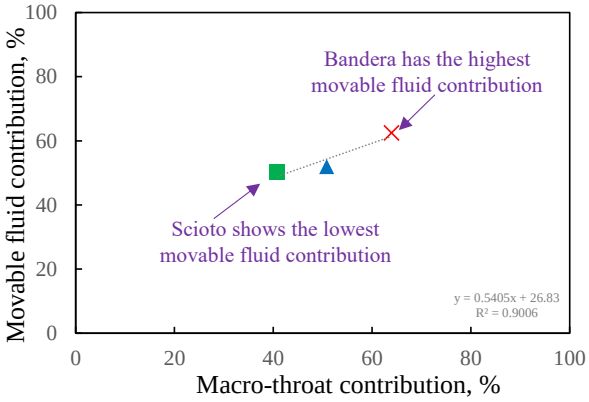

Figure 3.2. Cross-plot of movable fluid contribution versus macro-throat proportion for the three tested sandstones. (*Note the trendlines show the relation between measurements*).

coated grains, which inhibit quartz overgrowth and hence preserve the macropore system [46]. Thus, the above findings demonstrate the high proportion of macropore system of Bandera in comparison with the other investigated sandstones (Figure 3.2). The small contribution of the micropore system in Bandera sandstone (38% to the total pore system) is attributed to the presence of clay minerals, including kaolinite booklets, chlorite, and fibrous illite minerals, which tend to clog throats and fill pores. Negative correlations can be observed between the clay minerals content and the bound fluid contribution represented by the micropore system, as derived from the NMR analyses (Figure 3.3a) and micropore-throat proportion (Figure 3.3b). Low clay content of Scioto (4.1%) and Kentucky (3.6% for) leads to presence of high micropore system proportions, and to higher contribution of the micropore-throat system (59.1% for Scioto and 50.9% for Kentucky). A strong inverse relationship exists between the illite clay mineral and the micro-throat proportion for the tested sandstones, indicating that the contribution of the micropore-throat system decreases as illite content increases (Figure 3.3f). Chlorite and kaolinite clay minerals have less effect on the micropore-throat proportion (Figures 3.3h, d).

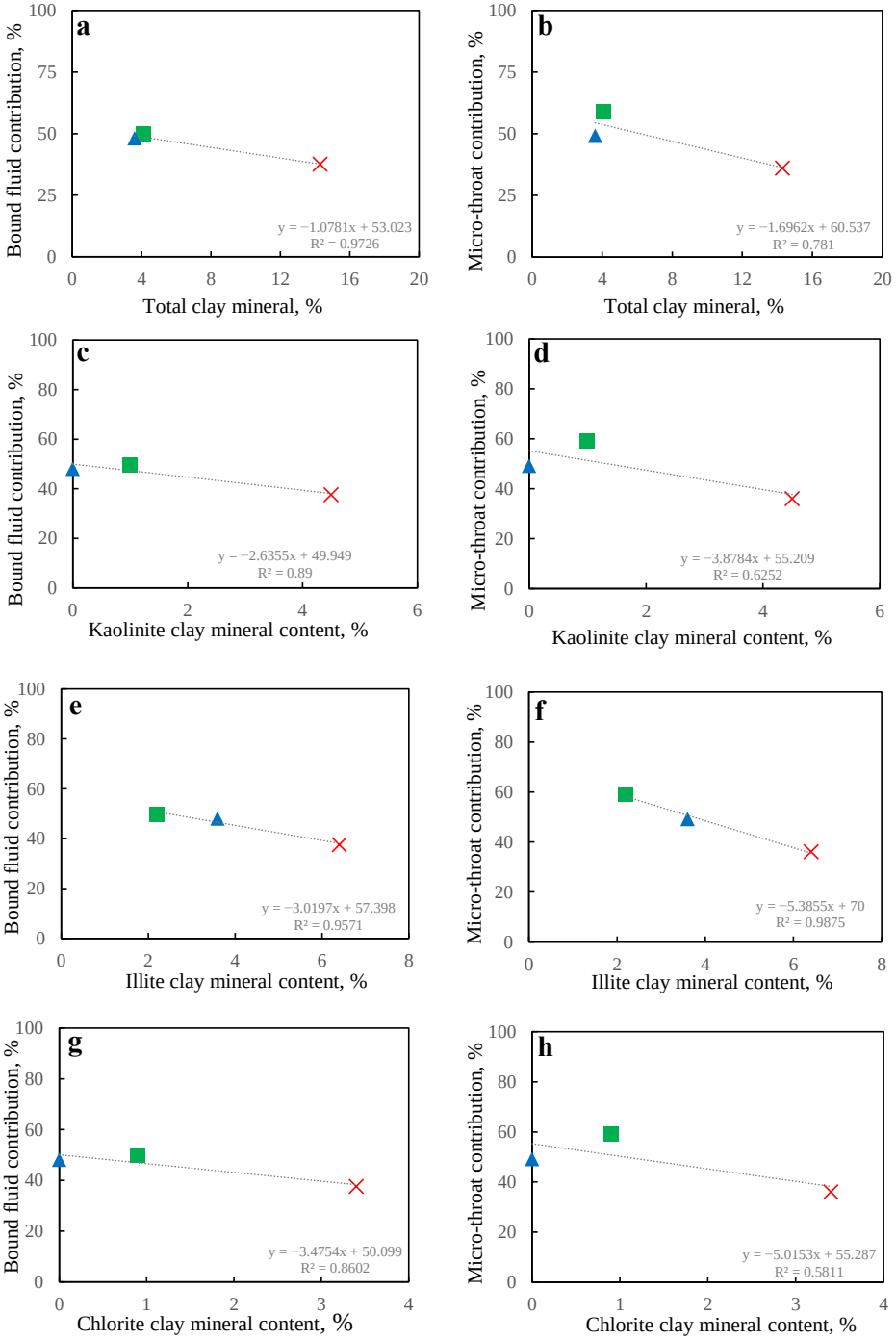

Figure 3.3. Cross-plots of bound-fluid contribution, micro-throat proportion and clay mineral content with: **(a, b)** total clay mineral content; **(c, d)** kaolinite clay content; **(e, f)** illite clay content; **(g, d)** chlorite clay content. (*Note the trendlines show the relation between measurements*).

MCI is a dimensionless number that shows the ability of a micropore system to store and trap the injected fluid. As mentioned earlier, a high MCI value implies that the micropore system in tight rocks is suitable for use in CO_2 injection due to its high storage capacity and well-confined micropore system. On the contrary, a low MCI value demonstrates that the sandstone micropore system exhibits limited capacity and inadequate fluid confinement that makes tight formation unsuitable for microscopic CO_2 injection. The relationships of MCI analyses with the MTMR and MSI of the tested sandstones show a direct relationship with micro-storativity (Figure 3.4a) and micro entrapment (Figure 3.4b).

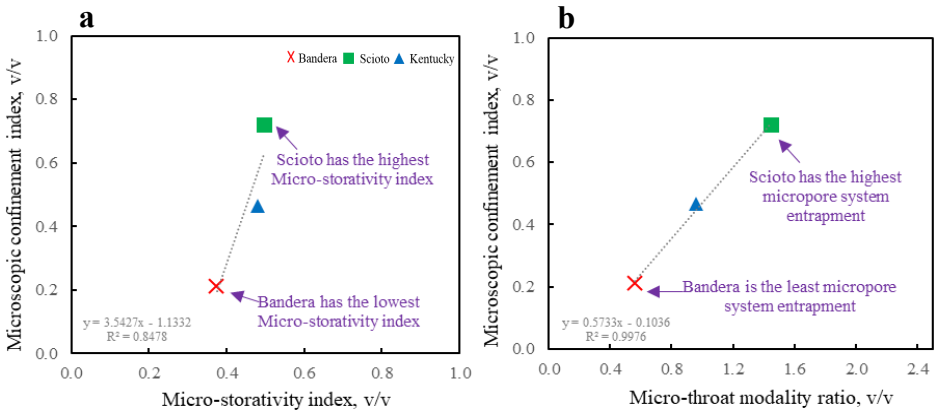

Figure 3.4. Cross-plots showing the relationship of microscopic confinement index of tested sandstones with: **(a)** micro-storativity index; **(b)** micro-confinement index. (*Note the trendlines show the relation between measurements*).

For the tight sandstones analyzed, Scioto sandstone MCI was the highest among the tested sandstones with a value of 0.72. This is attributed to the great capacity of the Scioto sandstone's micropore system of 0.5 MSI and the excellent micropore system entrapment of 1.44 MTMR, suggesting that Scioto sandstone is a suitable candidate for microscopic CO_2 injection. The low contribution of micro-storativity and entrapment of Bandera sandstone (0.38 MSI and 0.56 MTMR) indicate significant reduction in the microscopic confinement index (0.38 MCI) suggesting Bandera as the worse possible candidate for CO_2–EOR or CO_2 geo-storage.

To gain a deeper insight into the relationship of MCI results and MTMR and MSI indices, it is more convenient to focus on the factors impacting these indices. The increase in the micropore-throat proportions results in an increase in the storage capacity of the micropore system of the examined sandstones (Figure 3.5a), a phenomenon which can be related to a strong influence of clay minerals on the micropore system as a result of diagenetic alteration [47]. Furthermore, the reduction in the micropore's storativity proportion is related to the increase in the clay mineral content (Figure 3.5b), and this is in line with the fact that the fibrous illite and booklets of kaolinite

clay minerals can act as pore bridging and pore filling substances, respectively. These processes reduce the existing micropore system and thus affect the bound fluid contribution [48].

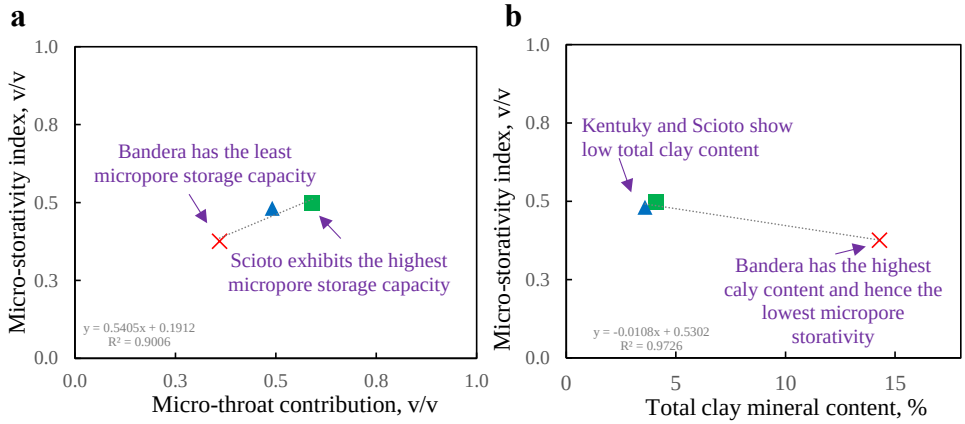

Figure 3.5. Cross-plots showing the relationship of micro-storativity index with: **(a)** micro-throat proportion; **(b)** total mineral content. (*Note the trendlines show the relation between measurements*).

Our analysis further shows that the percentage of micropore throat proportion in the tested sandstones is strongly correlated to the micropore's entrapment (MTMR) (Figure 3.6a). This can be attributed to the fact that smaller throat diameters can lead to greater capillary pressures, preventing fluid mobilization within the tight throats pore system. Comparison of the relationship of the total clay content and the micropore system storativity index (Figure 3.5b) indicates a fair relation between the total clay content and micropore system entrapment (Figure 3.6b). Use of larger dataset would provide a more in-depth understanding of our newly developed dimensionless numbers; however, these outcrops from which the samples were obtained are

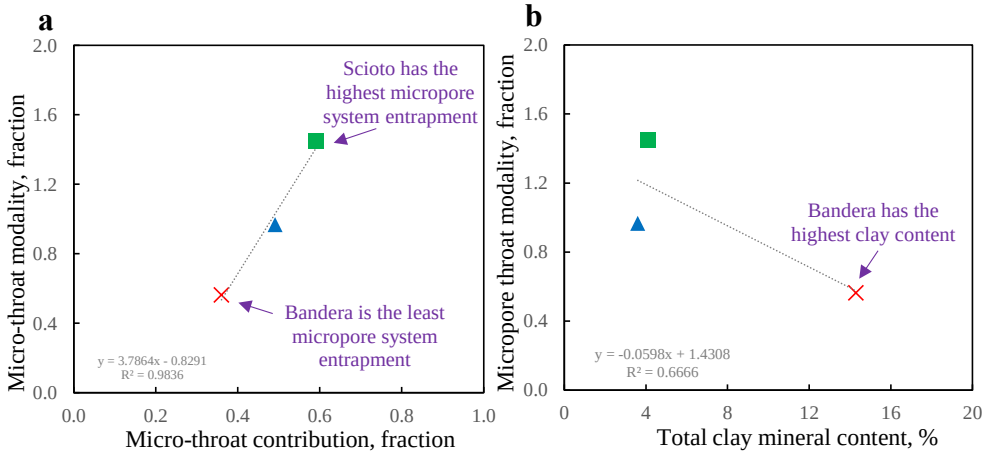

Figure 3.6. Cross-plots showing the relationship of micro- throat modality ratio of tested sandstones with: **(a)** micro-throat proportion; **(b)** total clay mineral content. (*Note the trendlines show the relation between measurements*).

known for their clean and very homogeneous nature and it is believed that the obtained dataset is sufficient.

3.4. CONCLUSIONS

This study focuses on determining the influence of tight sandstones' micropore system on pore fluid distribution. A new dimensionless number, termed MCI, was developed to select a suitable tight sandstone for CO_2 injection and geo-storage. Based on the findings obtained, the following conclusions are derived:

- Bandera micropore system's ability to store and confine fluid was found to be the least among the tested sandstone samples. The low contribution values of storativity and confinement of the micropore system is attributed to the presence of clay minerals content and type. In particular, the presence of pore filling kaolinite booklets can significantly reduce the micropore storativity, and the presence of pore bridging fibrous illite, can reduce the micropore-throat proportion and, hence, reduce the confinement of the micropore system.
- A strong positive relation was obtained between the micro-throat proportion and the micro-confinement contribution in the tested sandstone samples, indicating that the higher the micro-throat contribution, the more confined is the micropore system.
- Higher MCI value indicates better CO_2 injectivity in micropore system of tight sandstones. The calculated MCI values of the three sandstones indicate Scioto as the most suitable candidate for microscopic CO_2 injection and storage due to its high micropore confinement and storativity contributions.

REFERENCES

1. Gao, H., Li, H., 2015. Determination of movable fluid percentage and movable fluid porosity in ultra-low permeability sandstone using nuclear magnetic resonance (NMR) technique. J. Pet. Sci. Eng., 133, 258–267.
2. Worden, R.H., Burley, S.D., 2003. Sandstone diagenesis: The evolution of sand to stone. In sandstone diagenesis: Recent and Ancient. pp. 1–44. International Association of Sedimentologists Special Publication, 4, Blackwell, Oxford, 2003, 3-44.
3. Xiao, D., Lu, Z., Jiang, S., Lu, S., 2016. Comparison and integration of experimental methods to characterize the full-range pore features of tight gas sandstone—A case study in Songliao Basin of China. J. Nat. Gas Sci. Eng. 34, 1412–1421.

4. Yue, D., Wu, S., Xu, Z., Xiong, L., Chen, D., Ji, Y., Zhou, Y., 2018. Reservoir quality, natural fractures, and gas productivity of upper Triassic Xujiahe tight gas sandstones in western Sichuan Basin, China. Mar. Pet. Geol. 89, 370–386.
5. Zhang, L., Lu, S., Xiao, D., Li, B., 2017. Pore structure characteristics of tight sandstones in the northern Songliao Basin, China. Mar. Pet. Geol., 88, 170–180.
6. Cao, Y., Tang, M., Zhang, Q., Tang, J., Lu, S., 2020. Dynamic capillary pressure analysis of tight sandstone based on digital rock model. Capillarity. 3, 28–35.
7. Nabawy, B.S., Khalil, H.M., Fathy, M.S., Ali, F., 2020. Impacts of microfacies type on reservoir quality and pore fabric anisotropy of the Nubia sandstone in the central Eastern Desert, Egypt. Geol. J., 55, 4507–4524.
8. Edwards, A.C., 2001. Grain size and sorting in modern beach sands. J. Coast. Res., 17, 38–52.
9. Worden, R.H., Griffiths, J., Wooldridge, L.J., Utley, J.E.P., Lawan, A.Y., Muhammed, D.D., Simon, N., Armitage, P., 2020. Chlorite in sandstones. Earth-Sci. Rev., 204, 103105.
10. Chang, J., Fan, X., Jiang, Z., Wang, X., Chen, L., Li, J., Zhu, L., Wan, C., Chen, Z., 2022. Differential impact of clay minerals and organic matter on pore structure and its fractal characteristics of marine and continental shales in China. Appl. Clay Sci., 216, 106334.
11. McLean, R.F., Kirk, R.M., 1969. Relationships between grain size, size-sorting, and foreshore slope on mixed sand-shingle beaches. N. Z. J. Geol. Geophys., 12, 138–155.
12. Keelan, D.K., 1982. Core analysis for aid in reservoir description. J. Pet. Technol., 34, 2483–2491. https://doi.org/10.2118/10011-PA.
13. Islam, M.A., 2009. Diagenesis and reservoir quality of Bhuban sandstones (Neogene), Titas gas field, Bengal Basin, Bangladesh. J. Asian Earth Sci., 35, 89–100.
14. Hollis, C., Vahrenkamp, V., Tull, S., Mookerjee, A., Taberner, C., Huang, Y. 2010, Pore system characterisation in heterogeneous carbonates: An alternative approach to widely-used rock-typing methodologies. Mar. Pet. Geol., 27, 772–793.
15. Beard, D.C., Weyl, P.K., 1973. Influence of texture on porosity and permeability of unconsolidated sand. AAPG Bull., 57, 349–369.
16. Li, L., Su, Y., Sheng, J.J., Hao, Y., Wang, W., Lv, Y., Zhao, Q., Wang, H., 2019. Experimental and numerical study on CO2 sweep volume during CO2 huff-n-puff enhanced oil recovery process in shale oil reservoirs. Energy Fuels, 33, 4017–4032.
17. Ajdukiewicz, J.M., Lander, R.H., 2010. Sandstone reservoir quality prediction: The state of the art. AAPG Bull., 94, 1083–1091.

18. Makeen, Y.M., Abdullah, W.H., Ayinla, H.A., Hakimi, M.H., Sia, S.G., 2016. Sedimentology, diagenesis and reservoir quality of the upper Abu Gabra Formation sandstones in the Fula Sub-basin, Muglad Basin, Sudan. Mar. Pet. Geol., 77, 1227–1242.
19. McKinley, J.M., Atkinson, P.M., Lloyd, C.D., Ruffell, A.H., Worden, R.H., 2011. How porosity and permeability vary spatially with grain size, sorting, cement volume, and mineral dissolution in fluvial Triassic sandstones: the value of geostatistics and local regression. J. Sediment. Res., 81, 844–858.
20. Mozley, P.S., Heath, J.E., Dewers, T.A., Bauer, S.J., 2016. Origin and heterogeneity of pore sizes in the Mount Simon Sandstone and Eau Claire Formation: Implications for multiphase fluid flow. Geosphere, 12, 1341–1361.
21. Kashif, M., Cao, Y., Yuan, G., Asif, M., Javed, K., Mendez, J.N., Khan, D., Miruo, L., 2019. Pore size distribution, their geometry and connectivity in deeply buried Paleogene Es1 sandstone reservoir, Nanpu Sag, East China. Pet. Sci., 16, 981–1000.
22. Zhiyong, G., Jiarui, F., Jinggang, C., Xiaoqi, W., Chuanmin, Z., Yuxin, S., 2017. Physical simulation and quantitative calculation of increased feldspar dissolution pores in deep reservoirs. Pet. Explor. Dev., 44, 387–398.
23. Neasham, J.W.,1977. The morphology of dispersed clay in sandstone reservoirs and its effect on sandstone shaliness, pore space and fluid flow properties. In SPE Annual Fall Technical Conference and Exhibition; OnePetro: Richardson, TX, USA.
24. Schrader, M.E., Yariv, S., 1990. Wettability of clay minerals. J. Colloid Interface Sci., 136, 85–94.
25. Schoonheydt, R.A., Johnston, C.T., 2006. Surface and interface chemistry of clay minerals. Dev. Clay Sci., 1, 87–113.
26. Yuan, G., Gluyas, J., Cao, Y., Oxtoby, N.H., Jia, Z., Wang, Y., Xi, K., Li, X., 2015. Diagenesis and reservoir quality evolution of the Eocene sandstones in the northern Dongying Sag, Bohai Bay Basin, East China. Mar. Pet. Geol., 62, 77–89.
27. Kuila, U., Prasad, M., 2013. Specific surface area and pore-size distribution in clays and shales. Geophys. Prospect., 61, 341–362.
28. Wilson, L., Wilson, M.J., Green, J., Patey, I., 2014. The influence of clay mineralogy on formation damage in North Sea reservoir sandstones: A review with illustrative examples. Earth-Sci. Rev., 134, 70–80.
29. Kassab, M.A., Abu Hashish, M.F., Nabawy, B.S., Elnaggar, O.M., 2017. Effect of kaolinite as a key factor controlling the petrophysical properties of the Nubia sandstone in central Eastern Desert, Egypt. J. Afr. Earth Sci., 125, 103–117.

30. Rosenbrand, E., Fabricius, I.L., Fisher, Q., Grattoni, C., 2015. Permeability in Rotliegend gas sandstones to gas and brine as predicted from NMR, mercury injection and image analysis. Mar. Pet. Geol., 64, 189–202.
31. Bjorkum, P.A., 1996. How important is pressure in causing dissolution of quartz in sandstones? J. Sediment. Res., 66, 147–154.
32. Anovitz, L.M., Cole, D.R., 2015. Characterization and analysis of porosity and pore structures. Rev. Miner. Geochem., 80, 61–164.
33. Chima, P., Baiyegunhi, C., Liu, K., Gwavava, O., 2018. Diagenesis and rock properties of sandstones from the Stormberg Group, Karoo Supergroup in the Eastern Cape Province of South Africa. Open Geosci., 10, 740–771.
34. Freiburg, J.T., Ritzi, R.W., Kehoe, K.S., 2016. Depositional and diagenetic controls on anomalously high porosity within a deeply buried CO_2, storage reservoir—The Cambrian Mt. Simon sandstone, Illinois basin, USA. Int. J. Greenh. Gas Control, 55, 42–54.
35. Wu, Y., Tahmasebi, P., Lin, C., Zahid, M.A., Dong, C., Golab, A.N., Ren, L., 2019. A comprehensive study on geometric, topological, and fractal characterizations of pore systems in low-permeability reservoirs based on SEM, MICP, NMR, and X-ray CT experiments. Mar. Pet. Geol., 103, 12–28.
36. Coates, G.R., Xiao, L.Z., Prammer, M.G., 1999. NMR Logging Principles and Applications; Gulf Publishing Company: Houston, TX, USA.
37. Hirasaki, G.J., Huang, C.C., Zhang, G.Q., 2000. Interpretation of wettability in sandstones with NMR analysis. Petrophys.-SPWLA J. Form. Eval. Reserv. Descr., 41, 223–233.
38. Bultreys, T., Van Hoorebeke, L. and Cnudde, V., 2015. Multi-scale, micro-computed tomography-based pore network models to simulate drainage in heterogeneous rocks. Advances in Water resources, 78, pp.36-49.
39. Mehmani, A. and Prodanović, M., 2014. The effect of microporosity on transport properties in porous media. Advances in Water Resources, 63, pp.104-119.
40. Menke, H.P., Maes, J. and Geiger, S., 2021. Upscaling the porosity–permeability relationship of a microporous carbonate for Darcy-scale flow with machine learning. Scientific Reports, 11(1), p.2625.
41. Schmitt, M., Fernandes, C.P., Wolf, F.G., Neto, J.A.B.D.C., Rahner, C.P., dos Santos, V.S.S., 2015. Characterization of Brazilian tight gas sandstones relating permeability and angstrom to micron scale pore structures. J. Nat. Gas Sci. Eng., 27, 785–807.
42. Wang, R., Shi, W., Xie, X., Zhang, W., Qin, S.; Liu, K., Busbey, A.B., 2020. Clay mineral content, type, and their effects on pore throat structure and reservoir properties: Insight

from the Permian tight sandstones in the Hangjinqi area, north Ordos Basin, China. Mar. Pet. Geol., 115, 104281.

43. AlKharraa, H.S., Wolf, K.-H.A., Kwak, H.T., Deshenenkov, I.S., AlDuhailan, M.A., Mahmoud, M.A., Arifi, S.A., AlQahtani, N.B., AlQuraishi, A.A., Zitha, P.L.J., 2023. A Characterization of Tight Sandstone: Effect of Clay Mineralogy on Pore-Framework. In SPE Reservoir Characterisation and Simulation Conference and Exhibition, Abu Dhabi, United Arab Emirates, OnePetro: Tulsa, OK, USA.
44. Bloch, S., Lander, R.H., Bonnell, L.M., 2002. Anomalously high porosity and permeability in deeply buried sandstone reservoirs: Origin and predictability. AAPG Bull., 86, 301–328.
45. Lai, J., Wang, G., Wang, Z., Chen, J., Pang, X., Wang, S., Zhou, Z., He, Z., Qin, Z., Fan, X., 2018. A review on pore structure characterization in tight sandstones. Earth-Sci. Rev., 177, 436–457.
46. Bjørlykke, K., 2014. Relationships between depositional environments, burial history and rock properties. Some principal aspects of diagenetic process in sedimentary basins. Sediment. Geol., 301, 1–14.
47. Bjorlykke, K., Jahren, J., 2012. Open or closed geochemical systems during diagenesis in sedimentary basins: Constraints on mass transfer during diagenesis and the prediction of porosity in sandstone and carbonate reservoirs. AAPG Bull., 96, 2193–2214.
48. Blunt, M.J., Jackson, M.D., Piri, M., Valvatne, P.H., 2002. Detailed physics, predictive capabilities and macroscopic consequences for pore-network models of multiphase flow. Adv. Water Resour., 25, 1069–1089.

4. CO_2 INJECTION INTO TIGHT ROCKS: IMPLICATIONS FOR ENHANCED OIL RECOVERY

In the previous chapter we have shown that, Scioto sandstone has the highest MCI and was selected for further CO_2*–EOR studies. In this chapter the effectiveness of* CO_2 *injection in tight reservoirs is assessed and oil mobilization within the pore system (micro- and macropore) is evaluated. Three core-flood experiments were conducted on core composites of Scioto tight sandstone to evaluate oil recovery by different injection modes and schemes, i.e.; tertiary miscible* CO_2 *injection; secondary immiscible* CO_2 *injection, and; secondary miscible* CO_2 *injection. NMR spectrometry was used to quantify the fluid displacement in pre- and post-flooding schemes. Our results show that secondary miscible* CO_2 *injection provided the highest* E_D *of 88%, with oil mobilized from both micro-and macropores systems, leading to the highest oil recovery of 93% OOIP. Tertiary miscible* CO_2 *injection had* E_D *of 67% providing ultimate oil recovery of 79% OOIP mostly from the macropores system and limited contribution from micropores is attributed to the increased water content because of previously conducted secondary water flooding. Secondary immiscible* CO_2 *injection showed the least oil recovery among the injection schemes of 68% OOIP, believed to be due to the unstable displacement as indicated by* E_D *of 52%. The fluid displacement efficiency was determined through NMR analyses, and the findings are in line with the displacement efficiency values obtained from core-flood experiments. The findings obtained are promising strategy for determining the most efficient* CO_2 *injection scheme in tight rocks during* CO_2*–EOR and storage. In addition, it shows the efficiency of NMR tool in determining the fluid distribution within the rock pore system and the d displacement efficiency.*

The content of this chapter is based on the below publication:

AlKharraa, H., Wolf, K.H., AlQuraishi, A., Al Abdrabalnabi, R., Mahmoud, M. and Zitha, P.L.J., 2023. Microscopic CO_2 Injection in Tight Rocks: Implications for Enhanced Oil Recovery and Carbon Geo-Storage. *Energy & Fuels*.

4.1. INTRODUCTION

Conventional reservoirs are often characterized by high reservoir quality, producing oil by natural drive mechanisms [1]. Over time, the natural drive mechanisms can no longer maintain the reservoirs' energy, resulting in a lower oil recovery. Therefore, secondary methods, i.e. either water or gas injection, are applied to maintain pressure and, increase oil recovery [2]. Further increase in oil recovery is achieved by performing tertiary recovery to improve reservoir sweep (macroscopic) and displacement (microscopic) efficiencies.

Unlike the development plans of conventional reservoirs, tight formations are characterized by low permeability (typically < 1mD) and complex pore system. The low reservoir quality and complexity of pore system can render fluid mobilization in tight rocks; therefore, attention is required for selecting optimal recovery methods to be utilized [3]. MSF is a well completion technique utilized to ease fluid flow in such tight formations; however, fractured reservoirs experience fast pressure drop and hence low oil recovery due to low-pressure connectivity. In addition, the induced fractures might reach nearby water formations, resulting in high water production and/or causing environmental problems such as polluting fresh water reserves [4].

Waterflooding is a widely applied recovery method due to its favorable economics, with oil recovery ranging from 20% to 40% OOIP. however, it is not efficient in tight reservoirs due to its low injectivity and small pore-throat sizes, resulting in low microscopic E_D [5,6]. Waterflooding can also cause clay swelling reducing rock permeability and hence lowering recovery efficiency [7]. In addition, the difference in displacing-displaced fluids viscosity, can cause water channeling and hence, lower the macroscopic volumetric sweep efficiency [8]. Gas flooding, and CO_2–EOR in specific, is one of the tertiary EOR choices of potential due to its environmental benefits. Decades of studies revealed that CO_2 injection is an effective recovery approach in tight formations [9–12]. Nevertheless, a knowledge gap exists on the microscopic performance of CO_2 injection and oil mobilization in micropore systems of tight reservoirs.

Tight rocks have complex pore systems comprising of inter and intra-granular micro-and macro-pores formed during the depositional and diagenetic processes [13]. Understanding these pore systems and their controlling factors are essential for selecting the optimal recovery method to be utilized. Experimental results presented in previous chapters indicate Scioto as the most suitable representative tight sandstone among the three sandstones investigated due to its marginal pore system complexity and its high MCI referring to its pore confinement and storativity. In this chapter, laboratory CO_2 flooding results at different miscible and immiscible injection conditions are presented to determine the recovery and displacement efficiency of different injection process. In addition, NMR measurements were utilized in evaluating microscopic pre flooding pore fluid

distribution and microscopic post flooding assessment including both micro- and macropores fluid displacement efficiencies.

4.2. MATERIALS, EXPERIMENTAL SETUPS, AND PROCEDURES

4.2.1. MATERIALS

Nine Scioto core plugs were selected to form three composite cores made of three plugs each. Plugs were lined up face to face with paper tissue in between for capillary continuity and all were housed in a heated shrinkable Teflon® tape sleeve. Composites used were 3.8 cm in diameter and 15 cm in length with average petrophysical properties listed in Table 4.1.

Table 4.1. Properties of Scioto sandstone composites. The estimated petrophysical properties are the average of the plugs' values.

Composite ID	Core plugs ID	Pore volume (cc)	Porosity (vol%)	Permeability (mD)
1	S18, S17, S21	30.48 ± 0.07%	18.45 ± 0.22%	1.21 ± 0.76%
2	S12, S13, S14	31.04 ± 0.07%	18.53 ± 0.22%	1.24 ± 0.76%
3	S34, S35, S24	30.96 ± 0.07%	18.82 ± 0.22%	1.20 ± 0.76%

Synthetic formation brine and seawater formulated to represent the Arabian Gulf seawater composition and salinity were used to represent the connate water saturation and the displacing phase during waterflooding injection. The compositions and salinity of both brines are presented in Tables 4.2 and 4.3, respectively.

Table 4.2. Constituents of synthetic formation brine (total dissolved solids = 236,840 mg/L).

Component	Formation water (mg/L)
Sodium chloride	148,750
Calcium chloride	69,400
Magnesium chloride	17,910
Sodium sulfate	390
Sodium bicarbonate	390

Table 4.3. Constituents of synthetic seawater (total dissolved solids = 68,602 mg/L).

Total Alkalinity (mg/L)	Bicarbonate (mg/L)	Calcium (mg/L)	Magnesium (mg/L)	Sodium (mg/L)	Potassium (mg/L)	Chloride (mg/L)	Sulfate (mg/L)	Nitrate (mg/L)	Fluoride (mg/L)
174	212	766	2,648	22,353	810	36,585	5,015	37	2.19

N-decane was used to represent the oleic phase in order to minimize rock wettability alteration [14] and pure CO_2 (99.9%) was utilized as a displacing gaseous phase. Several studies have reported that MMP of n-decane and CO_2 is around 85 bar (1,235 psi) at 40°C [15,16]. To ensure good miscibility, miscible flooding runs were conducted at higher injection pressure of 124 bar (1,800 psi). Density and viscosity of liquid phases were measured using Anton Paar-DMA 4500 M density meter and Oswald viscometer, respectively. CO_2 properties were obtained from NIST web-book. These properties are presented at experimental conditions in Table 4.4.

Table 4.4. Fluid physical properties measured at experimental conditions (124 bar and 40°C).

Fluid	Density (g/cc)	Viscosity (cP)
Formation water	1.133	1.21
Seawater	1.025	1.10
Decane	0.730	0.89
sc-CO_2*	0.644	0.05

* CO_2 properties were obtained from the National Institute for Standards and Technology (NIST) Web-book [17].

4.2.2. EXPERIMENTAL SETUPS

Core flooding experiments were conducted using the flooding unit with schematic shown in Figure 4.1. The set-up consists of an injection pump, core holder, and production collection system all connected through 1/8-inch stainless steel tubing equipped with multiple air pneumatic two- and three-way valves to control fluid flow and direction. The core holder is a horizontally laid Hassler-type cell capable of housing samples of 1.5-inch (3.8 cm) diameter with length up to 12 inch (30.5 cm) capable to operate at confining pressures up to 689 bar (10,000 psi).

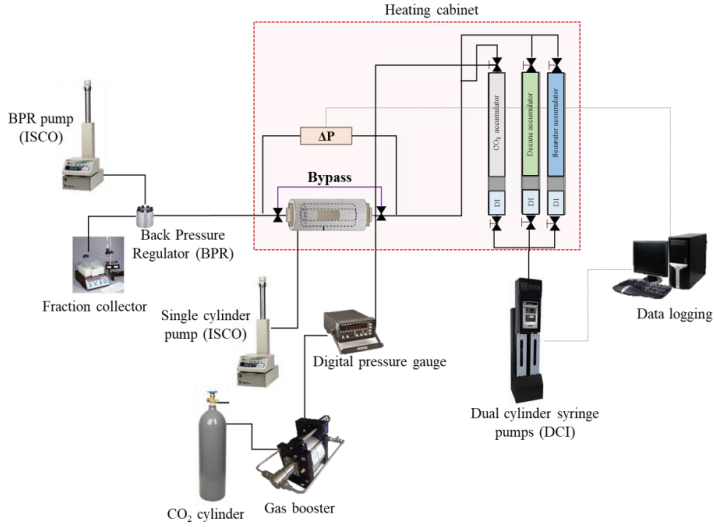

Figure 4.1. Schematic of the flooding unit.

Two inline pressure transducers are utilized to measure the inlet and outlet pressures and aid in calculating pressure drop across the core sample with full-scale pressure accuracy of ±0.05%. DCI dual syringe pump was used to displace distilled water at desired injection rate with a precision of 0.001 cc/min to the bottom of three one-liter Hastelloy floating piston accumulators. The accumulators were used to house the n-decane, CO_2 gas, and seawater. Gas booster was utilized to pressurize the CO_2 within the accumulator.

A dome type back pressure regulator (BPR), placed at the production end of the core-holder, was used to control and maintain the pore pressure up to the desired value. The accumulators and core-holder are housed within an oven of maximum temperature of 150 ± 0.1℃ for temperature control. Produced effluents (water and oil) were collected in glass tubes mounted in a timely set fraction collector while CO_2 gas was vented to atmosphere. All the unit components are linked to control system and data logger connected to a personal computer.

4.2.3. EXPERIMENTAL PROCEDURES

Dry core samples were vacuumed and saturated with formation brine under pressure of 1,379 bar (2,000 psi) utilizing saturation unit. The plugs porosity was redetermined by simple mass balance and NMR T_2 measurements were conducted on the brine-saturated plugs to identify PFD. The brine-saturated plugs were desaturated with n-decane using high speed centrifuge at rotational speed of 18,000 rpm and OOIP and connate water saturation were determined. The desaturated plugs were then subjected to a second round of NMR T_2 measurements to calculate the movable and bound fluid volumes.

Three core-flood experiments were conducted on three composites made of three plugs each and these include tertiary miscible CO_2 injection (Exp.1), secondary miscible CO_2 injection (Exp. 2), and secondary immiscible CO_2 injection (Exp. 3). Composites average connate water saturation and average initial oil saturation were measured at 32% and 68%, respectively. Table 4.5 presents the description and conditions of the core-flood experiments. All experiments were conducted at injection rate as low as 0.2 cc/min to ensure stable displacement. Experiments were conducted at 40°C, the temperature at which minimum miscibility occurs for the fluid pair.

Table 4.5. Core-flood experiments description and conditions.

Exp.	Experiment description	Confining pressure (psi)	Pore pressure (psi)	Pore volume injected (%PV)
1	Waterflooding + miscible CO_2	2,500	1,800	7.3
2	Secondary miscible CO_2 injection	2,500	1,800	3.5
3	Secondary immiscible CO_2 injection	1,700	1,400	7.2

Waterflooding was started in the first composite at connate water saturation and injection continued until oil production ceases after 3.5 PV of seawater injection. Subsequently, tertiary miscible CO_2 injection was started and a total of 3.8 PV of CO_2 was injected. In the second run, secondary miscible CO_2 injection was conducted using the second composite core at connate water saturation with total CO_2 injection of 3.5 PV.

Immiscible CO_2 injection was performed in the third composite core, at connate water saturation and this continues for 7.2 PV of gas injection. The water and n-decane produced were collected and corrected for inlet and outlet dead volumes and differential pressure was continuously measured and recorded throughout the displacement runs. At the end of each experiment, oil recovery, displacement efficiency, and injectivity index were evaluated. NMR T_2 measurements were again performed at the end of each experiment to determine the final pore fluid distribution and verify the calculated resident fluid volumes determined by material balance.

4.3. RESULTS

4.3.1. CORE FLOODING RESULTS

Table 4.6 presents the main results of the performed runs, including the ultimate oil recoveries, injectivity indices, and corresponding displacement efficiency calculations. OOIP of composite cores represent the sum of oil volumes for each core.

Table 4.6. Ultimate oil recovery, displacement efficiency and injectivity index of conducted flooding experiments.

Exp.	Ultimate recovery (%OOIP)	Displacement efficiency (%)	Injectivity index (cc/min/psi)
1	79 ± 3%	67 ± 3%	0.01 ± 0.7%
2	93 ± 3%	88 ± 3%	0.16 ± 0.7%
3	68 ± 3%	52 ± 3%	0.08 ± 0.7%

Figure 4.2 presents the oil recovery and pressure drop profiles for Exp.1. Oil recovery of 35% OOIP was obtained using secondary waterflooding and an incremental 44% OOIP was obtained using tertiary miscible CO_2 injection. The pressure drop increased sharply throughout the experiment to a maximum value of about 11 bar (160 psi) due to the mobility difference between the wetting and nonwetting fluid. Oil recovery of 31% OOIP was attained at water breakthrough of approximately 0.23 PV of seawater injection. Pressure drop decreased slowly after breakthrough to reach a stable value of approximately 8.5 bar (124 psi) due to the dominance of seawater flow and diminishing oil displacement.

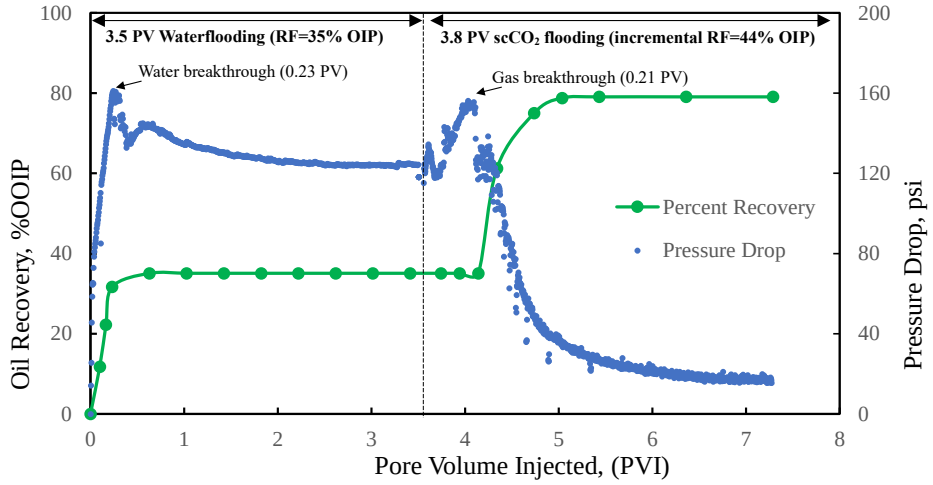

Figure 4.2. Oil recovery and pressure drop profile of secondary water flooding followed by miscible tertiary CO_2 injection conducted on composite #1.

Waterflooding is subjected to mobility difference between injected brine and displaced n-decane, and this can lead to viscosity fingering in addition to the high capillary pressure experienced in tiny pores that prevent their intrusion by displacing fluid. To enhance the oil recovery, tertiary miscible CO_2 injection was started. At this stage pressure drop profile builds up to a peak value of around 10.6 bar (155 psi) because of CO_2 attempting to overcome the water pressure residing within the pores after waterflooding. The gas breakthrough occurred at around 0.21 PV of gas injection, followed by a significant reduction in pressure drop to about 1.1 bar (16 psi and with a circa 89% drop from its maximum value). The experiment was terminated after 7.3 PV of total water and gas injection.

The estimated displacement efficiency and injectivity index at the end of the experiment were calculated and values of 67% and 0.01 cc/min/psi were obtained. The low injectivity of miscible tertiary CO_2 is attributed to excessive water blocking hindering the intrusion of CO_2 gas. This aligns well with previous findings in the literature reporting rocks exhibiting high capillary pressure during tertiary CO_2 injection [18].

Exp.2, performed on composite #2, was secondary miscible CO_2 injection conducted at connate water saturation. Oil recovery and pressure drop profiles are presented in Figure 4.3. In this run, the pressure drop profile increases to around 1.58 bar (23 psi) with oil recovery starting after 0.3 PV of miscible gas injection. The oil recovery continuously increases to maximum value of 93% OOIP after a total CO_2 injection of approximately 3.5 PV. Pressure profile falls gradually after gas breakthrough to around 0.34 bar (5 psi).

Such high oil recovery using miscible CO_2 injection is attributed to the high gas injectivity of 0.16 cc/min/psi and the CO_2-decane phases miscibility yielding comparatively stable higher displacement efficiency of 88% in comparison to the previous injection scheme.

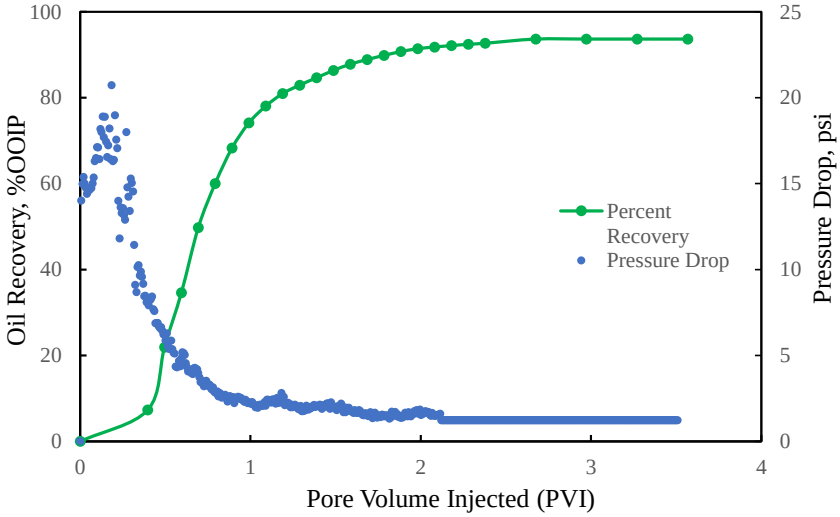

Figure 4.3. Oil recovery and pressure drop profile of miscible secondary CO_2 injection conducted on composite core #2.

Exp.3 was immiscible secondary CO_2 injection conducted in composite #3. The oil recovery and pressure drop profiles are presented in Figure 4.4. In this run, oil recovery started after 0.38 PV of immiscible gas injection. The delay in production is attributed to unfavorable displacement due to the density difference between CO_2 gas and n-decane [19]. Based on the fluctuation in the pressure drop profile marked in red arrows, CO_2 injection appears to be unstable, resulting in a low displacement efficiency of 52% attained after a total immiscible CO_2 injection of 7.2 PV.

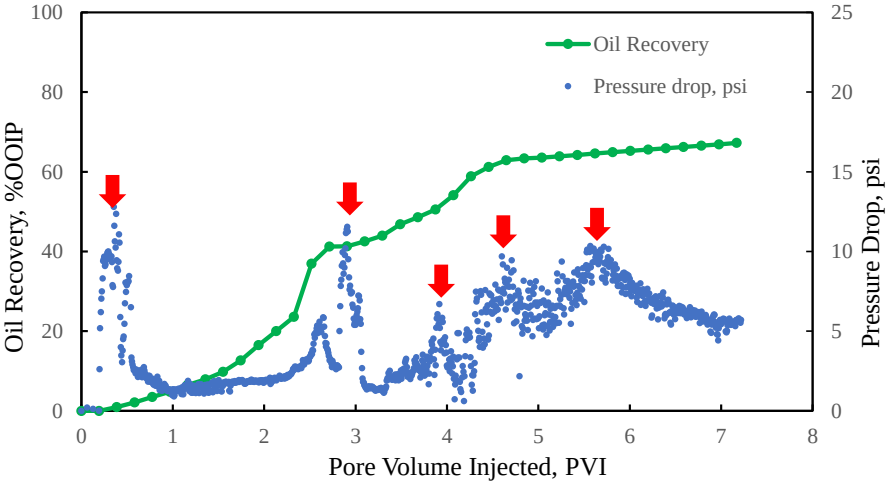

Figure 4.4. Oil recovery and pressure drop profile of immiscible secondary CO_2 injection conducted on composite core #3.

Oil recovery profile continues to increase due to CO_2 injection; however, the recovery process was slow as observed in previous studies [20,21]. The obtained ultimate oil recovery calculated at 68% OOIP was the lowest among the injection schemes tested.

4.3.2. NMR T_2 MEASUREMENTS

NMR was used to verify the flooding runs outcomes and to determine the fluids distribution within the different pores pre and post flooding. As discussed earlier, T_2 relaxation is proportional to pore size where macropores have longer T_2 values, while micropores tend to have shorter T_2 values, hence, rock micro- and macro pores fluid volumes can be analyzed. NMR T_2 measurements were performed before and after the flooding runs conducted to investigate PFD. Figure 4.5 depicts NMR T_2 measurements of the three brine-saturated plugs forming each of three composites. The profiles show identical unimodal characteristics, with T_2 values ranging from 0.1 ms to 177 ms.

Brine-saturated core plugs of the tested composites were desaturated to connate water saturation with n-decan. Figure 4.6 presents the NMR profiles obtained at the end of the desaturation process. Profiles indicate connate water residing in micropores, represented by smaller T_2 values ranging between 0.1 ms to 39 ms while n-decane moves to the macropores corresponding to larger T_2 values ranging from 79 ms to 892 ms.

It is worth noting that desaturated composites signals show extended T_2 values compared to previously presented values of brine-saturated plugs. This can be attributed to the wettability effect that delays T_2 relaxation and causes longer T_2 values [22]. T_2 cut-off value is utilized to determine the fluid residing in the micro-and macropore pores of composite sandstones.

The results demonstrate T_2 cut-off value of 24.6 ± 1.3 ms for Scioto sandstone, which is consistent with the literature findings for the same rock [23,24]. The findings indicate that the prepared composites pore system comprise of an average of 65% macropores and 35% micropores.

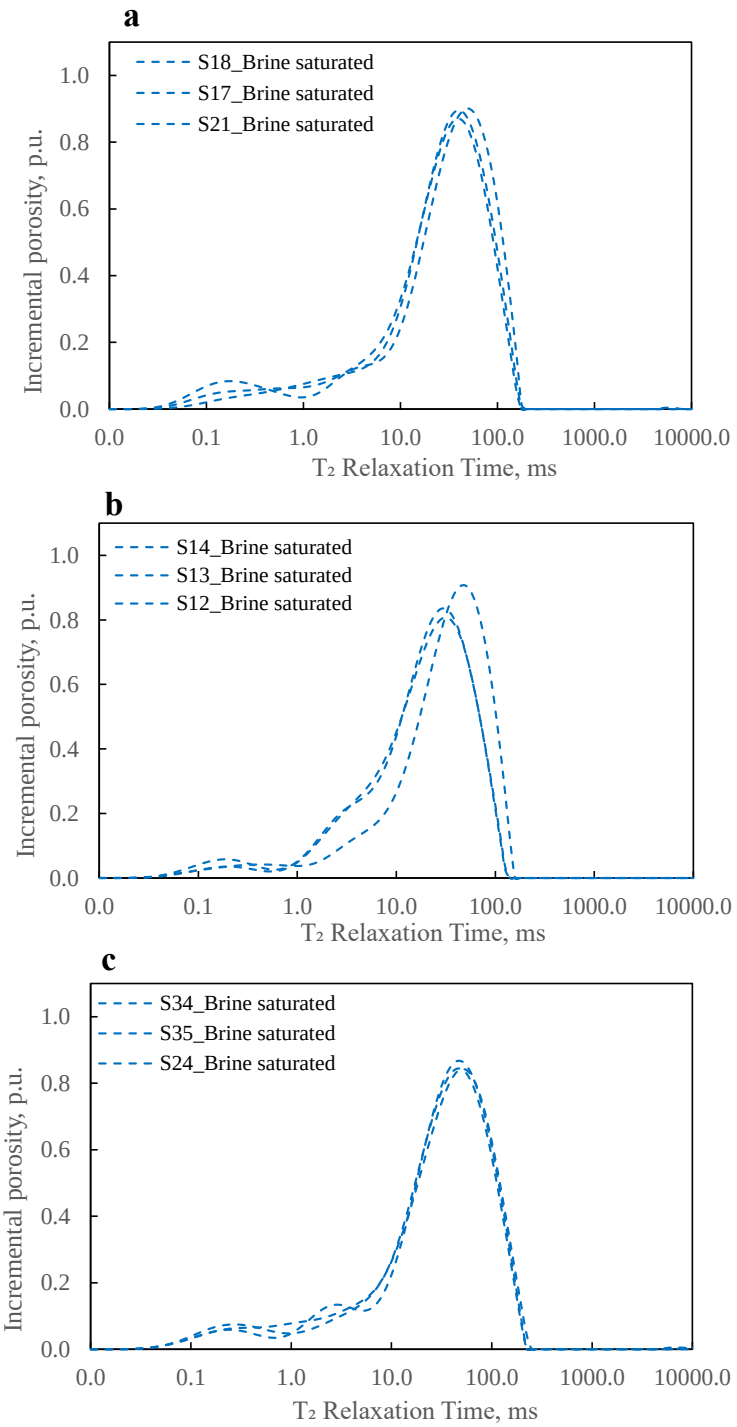

Figure 4.5. NMR T_2 measurements of brine-saturated composites of Scioto sandstone: **(a)** Composite #1; **(b)** Composite #2; and **(c)** Composite #3.

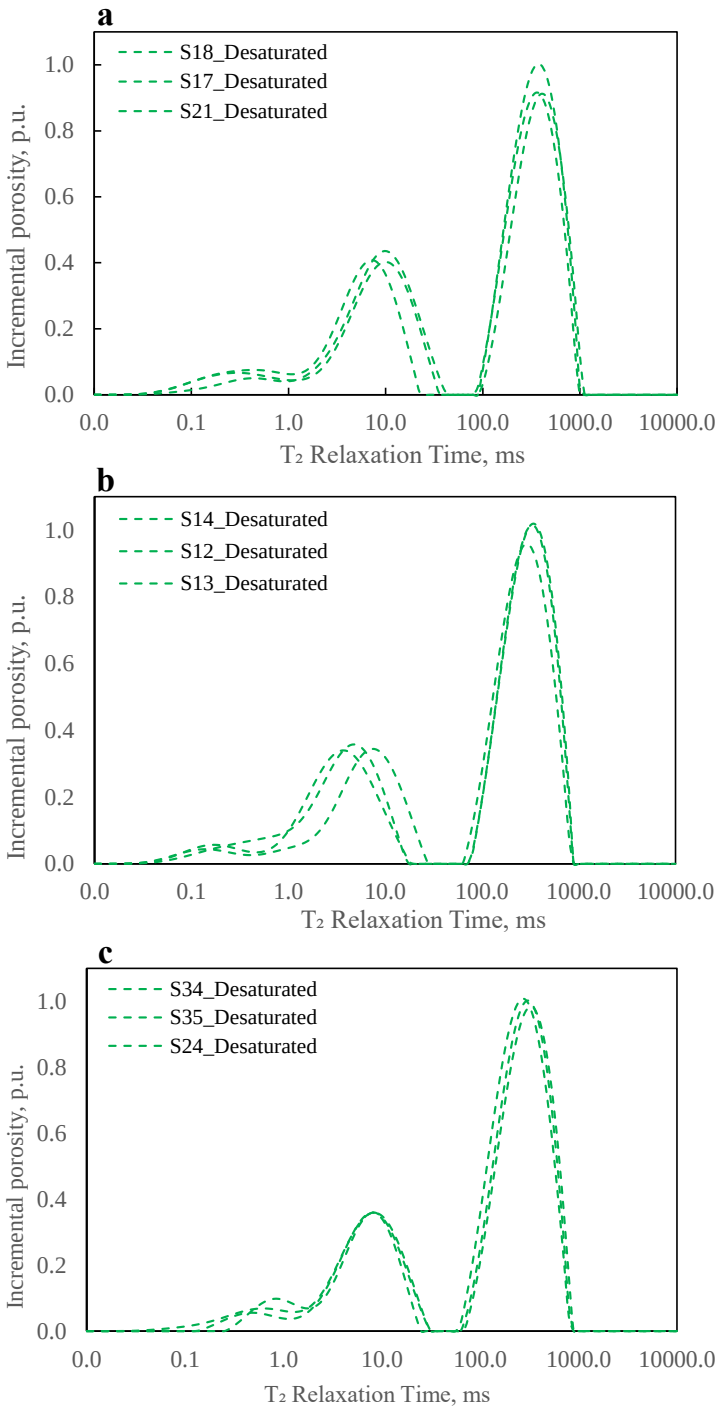

Figure 4.6. NMR T_2 measurements of desaturated composites of Scioto sandstone: **(a)** Composite #1; **(b)** Composite #2; and **(c)** Composite #3.

Figure 4.7 shows the NMR T_2 relaxation times for the composite cores combining both desaturated and post CO_2 injection stages for different flooding schemes to diagnose the performance of fluids displacement by CO_2 injection in tight rocks. As mentioned earlier, the area under the T_2 curve of the desaturated state represents the amount of hydrogen in the pore system. A reduction in this area indicates the removal of hydrogen and the fluid production from the given pores due to CO_2 injection.

For the miscible tertiary CO_2 injection conducted in composite core #1, NMR T_2 curve (Figure 4.7a) shows a unimodal distribution ranging from 0.1 ms to approximately 50 ms. The macropore signal of the desaturated composite core clearly vanished due to CO_2 displacement (marked with blue arrow). No apparent reduction was seen in the micropores denoted by the left signal of the desaturated state, indicating that CO_2 could not intrude the tiny pores (marked with black arrow). The micropore T_2 signal exhibits slight increase of around 9% compared to the original signal measured before CO_2 injection most likely due to the increase of water content after the secondary water injection prior to tertiary CO_2 injection.

The incremental T_2 spectrum at the end of the secondary miscible CO_2 injection, conducted on composite #2, illustrates unimodal signal ranging from 0.1 ms to 22.4 ms (Figure 4.7b). The narrower range of T_2 signal compared to composite #1 (tertiary miscible CO_2 injection) corresponds to more efficient fluid displacement. Similarly, the macro pores vanished (marked with a blue arrow) and micropore signal was reduced by almost 12% compared to the initial desaturated state, indicating that CO_2 injection was able to invade the micropore system (marked with a black arrow).

Figure 4.7c presents the T_2 distributions of the immiscible secondary CO_2 injection performed in composite #3. The profile shows broader T_2 distributions ranging from 0.1 ms to almost 560 ms, illustrating that hydrogen molecules are still within the micro- and macro pores and poor fluid mobilization were attained by immiscible CO_2 injection.

NMR measurements were also used to estimate the displacement efficiency (ED_{NMR}):

$$ED_{NMR} = \frac{Desaturated\ Pore\ Volume - post\ CO_2\ Pore\ Volume}{Deasturated\ Pore\ Volume} \times 100$$

ED_{NMR} for the three injection schemes demonstrated that secondary miscible CO_2 flooding provided the highest value followed by tertiary miscible CO_2 flooding and finally the secondary immiscible CO_2 injection showing the lowest value. Table 4.7 lists the pre and post CO_2 NMR pore volumes and the ED_{NMR} for the three composites.

Table 4.7. NMR pore volumes and the displacement efficiency results for the three core-flood experiments.

Exp.	Fluid pore volume de-saturated state (cc)	Fluid pore volume post CO_2 injection (cc)	Displacement efficiency ED_{NMR} (%)
1	33	15	55
2	33	10	70
3	32	17	47

Table 4.8 and Figure 4.8 present the pre and post CO_2 pore volumes measured using the micro- and macropore NMR signals. The results show that tertiary and secondary miscible CO_2 injection provides macropores ED_{NMR} of 94% and 100%, respectively. Secondary immiscible CO_2 injection shows the least macropores ED_{NMR} displacement efficiency of 67%. It also reveals no clear micropore reduction compared to that observed originally at de-saturated state due to unstable displacement. To the contrary, the micropore signal of secondary miscible CO_2 injection demonstrated a 12% reduction in contrast to tertiary miscible CO_2 injection that showed no significant change in micropores signal.

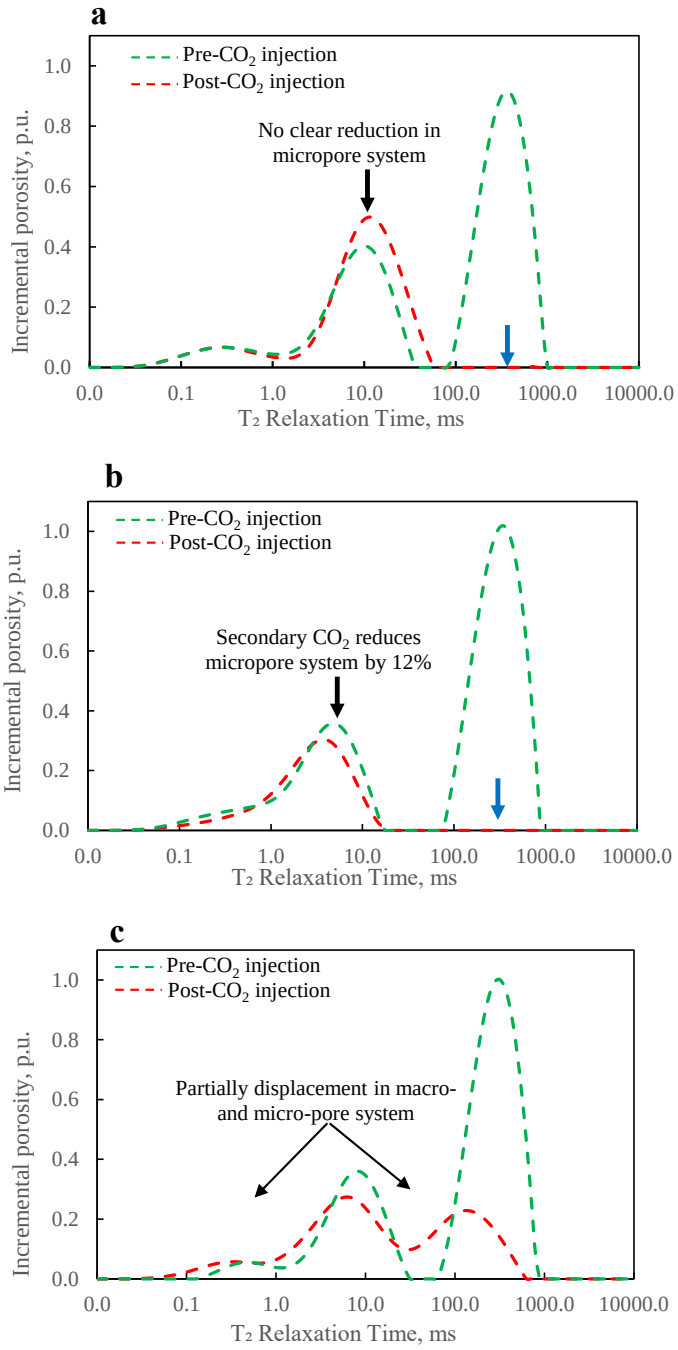

Figure 4.7. Incremental NMR T_2 of desaturated (green dashed line) and post CO_2 injection (red dashed line) for composite cores: **(a)** Tertiary miscible CO_2; **(b)** Secondary miscible CO_2 injection and **(c)** Secondary immiscible CO_2 injection.

Table 4.8. NMR micro-and macropore volumes for the injection schemes.

Exp.	Pore volumes pre-CO_2 injection		Pore volumes post CO_2 injection	
	Micropore (cc)	Macropore (cc)	Micropore (cc)	Macropore (cc)
1	12.5	20.3	13.6	1.3
2	11.1	21.8	9.8	0
3	10.1	21.8	10.1	7.1

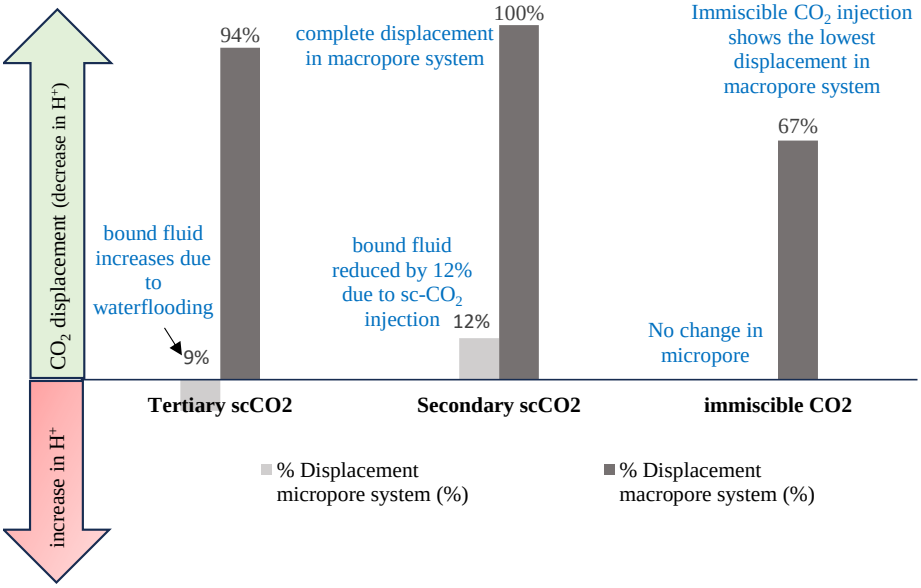

Figure 4.8. Displacement efficiency of micro- and macropores determined by NMR analyses.

4.4. DISCUSSION

Low water injectivity index of 0.002 cc/min/psi and high mobility ratio during water flooding stage resulted in poor displacement efficiency. NMR T_2 measurements shown in Figure 4.9 confirms this as slight reduction was observed in NMR spectra of composite cores (marked with red brace), indicating no intrusion of micropores and limited fluid mobilization in the long T_2 values corresponding to the macropores. In addition, the incremental T_2 profiles exhibit extended T_2 values than those of the initial desaturated core signals (Figure 4.10a). This extended T_2 distribution is due to water imbibition delaying the surface relaxation of the remaining n-decane

(Figure 4.10b). Hydrogen communication between micro- and macropore systems is clearly in line with the observation of Anand and Hirasaki (2007) [25].

Tertiary miscible CO_2 injection provided an incremental recovery of 44% OOIP. We speculate that this low incremental recovery relative to the secondary CO_2 flooding is due to increased water content as a result of previous waterflooding process that has a negative impact on pore fluid displacement and oil recovery due to the water film formed during waterflooding preventing CO_2 from invading small pores [26]. Although CO_2 has a higher injectivity of 0.01 cc/min/psi compared to water, The ultimate recovery of approximately 79% OOIP confirms that tertiary miscible CO_2 injection cannot access micropores efficiently (as marked in black arrow in Figure 4.7b).

Secondary immiscible CO_2 flooding results in an unstable displacement efficiency of 52% as estimated from coreflood results. This is mainly due to the poor displacement as indicated by the observed pressure drop fluctuation during the injection process (Figure 4.4). Poor displacement was also observed by the partial reduction in NMR T_2 spectrum compared to the initial desaturated core signal resulting in estimated low ED_{NMR} of 47% (Figure 4.11). Despite the high injectivity index of approximately 0.1 cc/min/psi, the secondary immiscible CO_2 injection still has relatively low oil recovery of 68% OOIP compared to the secondary miscible CO_2 flooding. Hence, given the low oil recovery and the high gas pore volume injected, we presume immiscible CO_2 injection inefficient EOR method in tight rocks.

Secondary miscible CO_2 injection shows stable displacement compared to other injection schemes as indicated by coreflood displacement efficiency of 88% providing recovery factor of approximately 93% OOIP mobilized from various pore sizes. ED_{NMR} was calculated to be 70% with 100% fluid displacement from macropores and (marked with blue arrow in Figure 4.7b) and 12% from micropores (marked with black arrow in Figure 4.7b) compared to the desaturated core state.

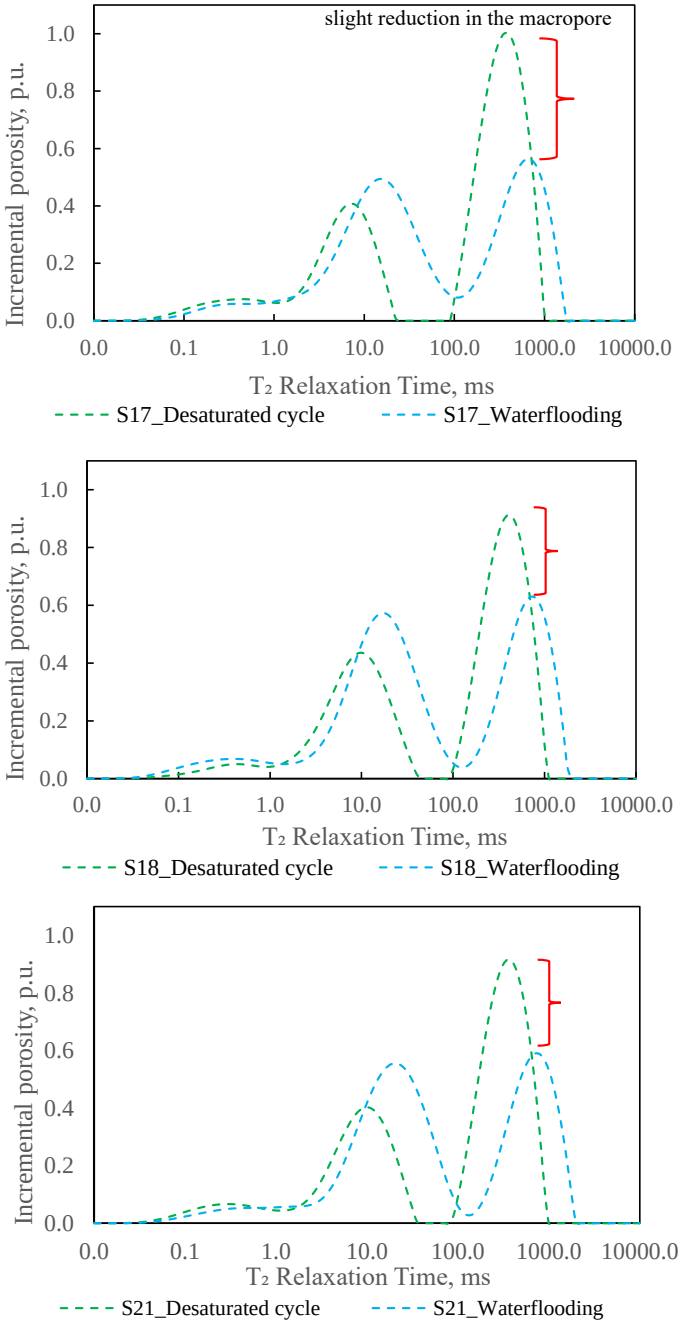

Figure 4.9. NMR T_2 curves of desaturated (green dashed line) and waterflooded (light blue dashed line) of composite core #1. A slight reduction in the macropore indicates poor displacement because of waterflooding (marked in red brace), while the extended NMR T_2 (light blue dashed lines) are due to the delay of surface relaxation caused by the remaining n-decane retained in the rock pore system.

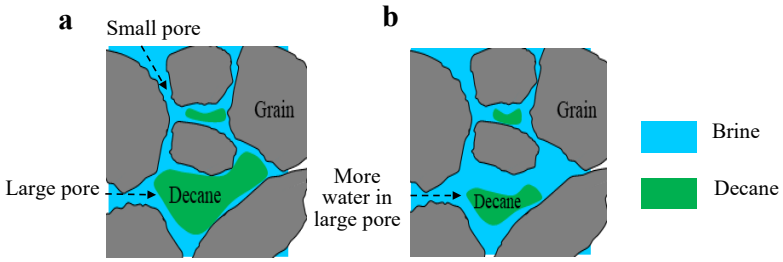

Figure 4.10. Schematic illustrating the drainage and waterflooding covering. **(a)** Decane-desaturated case, where decane resides in big pores and water resides in small pores. **(b)** Waterflooding case showing brine imbibing big pores causing a slight reduction in decane saturation.

In summary, displacement efficiency using material balance and NMR for all runs showed a good relation as indicated in Figure 4.11 and secondary miscible CO_2 injection scheme seems to be the most efficient flooding method for tight formations.

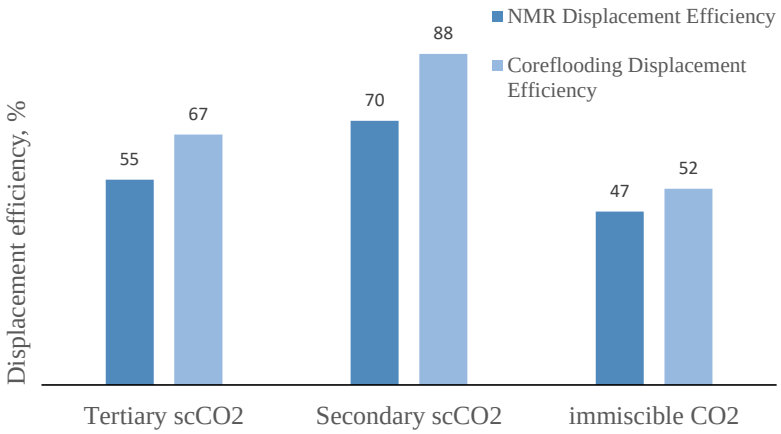

Figure 4.11. Displacement efficiencies obtained from NMR and core-floods.

4.5. CONCLUSIONS

This study evaluates the efficiency of several CO_2 flooding schemes in tight sandstone reservoirs. The flooding runs were analyzed in terms of oil recovery, pressure data, injectivity index, and NMR measurements to discern the microscopic mechanisms responsible for to the observed macroscopic behavior. Based on the findings, the following conclusions are derived:

- Secondary waterflooding provided limited oil recovery and experienced early water breakthrough attributed to multiple factors, including low water injectivity, high capillary forces in small pores that needs to be overcome, and a high MTMR value. NMR T_2 results confirm the experienced poor displacement, as indicated by the extended T_2 spectrum relaxation due to the existence of immobilized n-decane in the pore system.

- The secondary miscible CO_2 injection provides the highest oil recovery, of approximately 93% OOIP. Due to its miscibility with oil, NMR findings revealed that injected CO_2 almost completely displaces the resident fluid in the macropore system and 12% from the micropore system.
- Tertiary miscible CO_2 injection following secondary water flooding depicts an ultimate recovery of around 79% OOIP. Such relatively low recovery performance relative to secondary CO_2 flooding is due to the increase of water content after secondary water flooding stage that retards the micropores CO_2 displacement and hence lowers the injectivity efficiency to 0.01 cc/min/psi. NMR measurements agree with this hypothesis and reveal an increase in hydrogen content in micropores of around 9%, confirming that tiny pores were not accessed by tertiary miscible CO_2 injection.
- Secondary immiscible CO_2 flooding provides the least oil recovery of 68% OOIP relative to the other two flooding schemes investigated. The low oil recovery is attributed to the displacement instability as indicated by the fluctuating pressure drop and low calculated ED_{NMR} of 47%.
- Displacement efficiencies calculated from coreflood results and NMR T_2 measurements are in line with each other proving the effectiveness of NMR tool in observing the different pore systems' contribution in overall hydrocarbon recovery and CO_2 storage efficiency in tight rocks.

REFERENCES

1. Lake, L. W. Enhanced Oil Recovery; Prentice-Hall: Upper Saddle River, NJ, 1989.

2. Dake, L. P. Fundamentals of reservoir engineering; Elsevier, Amsterdam,1983.

3. Holditch, S.A. Tight gas sands. JPT. 2006, 58, 6, 86–93.

4. Economides, M.J.; Nolte, K.G. Reservoir stimulation; Prentice Hall: Englewood Cliffs, NJ, 1989.

5. Chen, M.; Dai, J.; Liu, X.; Kuang, Y.; Wang, Z.; Gou, S.; Qin, M.; Li, M. Effect of displacement rates on fluid distributions and dynamics during water flooding in tight oil sandstone cores from nuclear magnetic resonance. JPSE. 2020, 184, 106588.

6. Yuan, B.; Wood, D.A. A comprehensive review of formation damage during enhanced oil recovery. JPSE. 2018, 167, 287–299.

7. Sheng, J.J. Critical review of low-salinity waterflooding. JPSE. 2014, 120, 216–224.

8. Al Adasani, A.; Bai, B. Analysis of EOR projects and updated screening criteria. JPSE. 2011, 79, 10–24.

9. Bachu, S.; Adams, J.J. Sequestration of CO_2 in geological media in response to climate change:

capacity of deep saline aquifers to sequester CO_2 in solution. Energy Conversion and management. 2003, 44, 20, 3151–3175.

10. Wang, L.; Wang, S.; Zhang, R.; Wang, C.; Xiong, Y.; Zheng, X.; Li, S.; Jin, K.; Rui, Z. Review of multi-scale and multi-physical simulation technologies for shale and tight gas reservoirs. J Nat Gas Sci Eng. 2017, 37, 560-578.

11. Kulkarni, M.M.; Rao, D.N. Experimental investigation of miscible and immiscible Water-Alternating-Gas (WAG) process performance. JPSE. 2005, 48,1–2, 1–20.

12. Song, Z.; Li, Y.; Song, Y.; Bai, B.; Hou, J.; Song, K.; Jiang, A.; Su, S. A critical review of CO_2 enhanced oil recovery in tight oil reservoirs of North America and China. In SPE/IATMI Asia Pacific Oil & gas conference and exhibition, Bali, Indonesia, 2020, October. SPE-196548.

13. Lai, J.; Wang, G.; Wang, Z.; Chen, J.; Pang, X.; Wang, S.; Zhou, Z.; He, Z.; Qin, Z.; Fan, X. A review on pore structure characterization in tight sandstones. Earth-Science Reviews. 2018, 177, 436–457.

14. Elsharkawy, A.M.; Poettmann, F.H. and Christiansen, R.L., 1992, April. Measuring minimum miscibility pressure: slim-tube or rising-bubble method?. In SPE Improved Oil Recovery Conference? (pp. SPE-24114). SPE.

15. Bao, B.; Feng, J.; Qiu, J. and Zhao, S., 2020. Direct measurement of minimum miscibility pressure of decane and CO_2 in nanoconfined channels. ACS omega, 6(1), pp. 943–953.

16. Ahmed, T.H. Prediction of CO_2 minimum miscibility pressures. In SPE Latin America and Caribbean Petroleum Engineering Conference, Buenos Aires, Argentina, 24-27 April, 1994. SPE-27032.

17. Lias, S. G.; Bartmess, J. E. Gas-Phase Ion Thermochemistry. In NIST Chemistry WebBook, NIST Standard Reference Data-base Number 69; Mallard, W. G., Linstrom, P. J., Eds.; National Institute of Standards and Technology: Gaithersburg, MD, Jan 2000 (http://webbook.nist.gov).

18. Blunt, M.; Fayers, F.J.; Orr Jr, F.M. Carbon dioxide in enhanced oil recovery. Energy conversion and management. 1993, 34, 9–11.

19. Andrianov, A.; Farajzadeh, R.; Nick, M.M., Talanana, M.; Zitha, P.L. Immiscible foam for enhancing oil recovery: bulk and porous media experiments. In SPE Asia Pacific Enhanced Oil Recovery Conference, Kuala Lumpur, Malaysia, 19-20 July, 2011. SPE-143578.

20. Rossen, W.R., Van Duijn, C.J., Nguyen, Q.P., Shen, C. and Vikingstad, A.K., 2010. Injection strategies to overcome gravity segregation in simultaneous gas and water injection into homogeneous reservoirs. SPE Journal, 15(01), pp. 76–90.

21. Gbadamosi, A.O., Kiwalabye, J., Junin, R. and Augustine, A., 2018. A review of gas enhanced oil recovery schemes used in the North Sea. Journal of Petroleum Exploration and Production

Technology, 8, pp. 1373–1387.
22. Al-Mahrooqi, S.H., Grattoni, C.A., Moss, A.K. and Jing, X.D., 2003. An investigation of the effect of wettability on NMR characteristics of sandstone rock and fluid systems. Journal of Petroleum Science and Engineering, 39(3–4), pp. 389–398.
23. Hassan, A., Mahmoud, M., Al-Majed, A. and Al-Nakhli, A., 2019. New chemical treatment for permanent removal of condensate banking from different gas reservoirs. ACS Omega, 4(26), pp. 22228–22236.
24. Muqtadir, A., Elkatatny, S.M., Mahmoud, M.A., Abdulraheem, A. and Gomaa, A., 2018, June. Effect of saturating fluid on the geomechanical properties of low permeability Scioto sandstone rocks. In ARMA US Rock Mechanics/Geomechanics Symposium (pp. ARMA-2018). ARMA.
25. Anand, V.; Hirasaki, G.J. Diffusional coupling between micro and macroporosity for NMR relaxation in sandstones and grainstones1. Petrophysics. 2007, 48, 289-307.
26. Campbell, B.T. and Orr, F.M., 1985. Flow visualization for CO_2/crude-oil displacements. Society of Petroleum Engineers Journal, 25(05), pp. 665–678.

5. CONCLUSIONS AND RECOMMENDATIONS

The primary intent of this thesis was to investigate the microscopic displacement of tight sandstone formations during CO_2–EOR. CO_2–EOR is used to help achieve multiple tasks including (1) reducing the atmospheric CO_2 level, and (2) enhancing overall oil recovery by mobilizing the trapped oil. To meet these objectives, experimental work was performed on three representative tight sandstones (Bandera, Kentucky and Scioto) in order to determine the pore fluids displacement and evaluate the impact of clay content on rocks pore system. Routine and special core analyses were implemented to qualify, quantify and compare outcomes of multi-phase displacement characteristics of investigated sandstones. Based on the petrophysical, petrographical and air-water displacement, Scioto sandstone was selected to represent tight sandstone rock used in evaluating the microscopic PFD during CO_2–EOR. Various CO_2 flooding schemes in both miscible and immiscible modes aided by NMR measurements were used to assess the ultimate recovery and the contribution of both micro- and macropore systems. This chapter summarizes the key outcomes of this research and suggests areas for future work.

5.1. CONCLUSIONS

Although tight reservoirs are classified based on a permeability threshold, rocks complex pore system (bodies and throats) is essential for tight reservoirs classification considering that spatial correlations of pore throats and bodies are most relevant parameters affecting tight rock characterization. Chapter 2 presents the impact of clays type and content on pore systems in general and micropore system in specific of three tight sandstone rocks namely, Bandera, Kentucky and Scioto. Experimental investigation was performed using helium porosimeter, gas permeameter, MICP, NMR and Micro-CT imaging to characterize the sandstones investigated and to determine their key petrophysical parameters. Measurements of porosity and permeability indicate better reservoir quality for Bandera and close quality for Scioto and Kentucky. Mineralogical analysis and SEM images indicate the presence of fibrous illite acting as pore bridging in Bandera sandstone that significantly reduces the micro-throat system proportion to 36% of overall pore throat system compared to the other sandstones where pore throat systems are quite high (50.9% for Kentucky and 59.1% for Scioto). On the other hand, observed pore-filling kaolinite booklets in Bandera sandstones is believed to be the reason behind the reduction of its micro-pore body system to 10.6% of total pore body system. However, the shortage of kaolinite clay minerals in Kentucky and Scioto sandstones help to preserve the rocks total micro-pore body systems yielding 29.5% and 23% of total pore body system, respectively. With respect

to macro-pore body, Kentucky and Scioto show low macro-pore body contribution compared to Bandera and this is attributed to their finer grain and smaller pore size. In contrast, Bandera shows a high macro-pore proportion representing 89.4% of total pore system due to the absence of quartz overgrowth because of illite platelet clay coating, and relatively coarser grain size. MTMR, a dimensionless number that relates the proportion of micro-pore throat to macro-pore throat, indicates that Scioto sandstone has the highest value of 1.44 suggesting fluid flow obstruction due to capillarity effect resulting into high proportion of micro-throat system. Hence, precaution should be taken in selecting the efficient recovery process for this tight sandstone and gas flooding seems to be efficient recovery method. Conversely, flow mostly pass through the dominant macro-throat system of Bandera resulting in minimal oil bypass as indicated by MTMR value of 0.56; hence, conventional water flooding is an efficient recovery method in this sandstone.

Chapter 3 utilized the experimental findings discussed in the previous chapter to help in deciding the suitable and most representative lab scale tight sandstone for CO_2–EOR runs conducted and presented in the upcoming chapter. A new dimensionless measure (MCI) was developed to evaluate the estimated microscopic storage and confinement of the tested sandstones. The sandstone sample with the highest MCI value indicates the best candidates for CO_2–EOR. MCI is calculated as a product of calculate MTMR and MSI, a dimensionless number that indicate the fluid storativity of micro- pore system (body and throat) to overall pore system using NMR technique. Results indicate high MCI of 0.72 for Scioto sandstone pointing to its high micropore confinement and storage capacity compared to 0.49 and 0.21 for Bandera and Kentucky sandstone, respectively. Therefore, Scioto sandstone is the most representative tight sandstone for investigating the microscopic CO_2 injection and reservoir fluids displacement among the tested sandstones.

Chapter 4 presents the results of displacement runs conducted on Scioto sandstone chosen based on the findings of previous chapters. Flooding runs in different miscibility modes and injections schemes were conducted and these are, continuous miscible CO_2 injection at connate water saturation, immiscible CO_2 injection at connate water saturation and tertiary miscible CO_2 injection at residual oil saturation subject to waterflooding. Pre and post flooding laboratory NMR measurements were performed to assess the fluid displacement from different rock pore system. Recovery results indicate low oil production of 35% OOIP and early water breakthrough for Secondary waterflooding run. Many factors could have contributed to the low oil recovery at this stage, including the low water injectivity which was insufficient to overcome the high capillary pressure of the existing rock micropore system. We hypothesized in Chapter 2 that waterflooding may not be a suitable recovery method in Scioto due to the high MTMR, which may result in oil

bypass in micropores and minor production from macropores. This is supported by the NMR measurements which show an extended T_2 spectrum resulting from the immobilized n-decane oil encapsulated by water in sandstone pore system. Most of the oil recovered was produced from macropores, and there was no oil displacement from micropores. Tertiary miscible CO_2 injection following secondary waterflooding yielded incremental oil recovery of 44% OOIP. This relatively low recovery is attributed to the increased water content and pore blocking post water flooding stage. NMR measurements confirmed this and revealed an increase in hydrogen content in the micropores of around 9%, confirming that tertiary miscible CO_2 injection could not access the micropores sufficiently.

Secondary immiscible CO_2 injection provided a lower ultimate oil recovery of 68% OOIP. Clearly, unstable displacement and gas channeling occurred due to the density difference between the injected CO_2 gas and n-decan oil. The unfavorable displacement was detected by the pressure drop fluctuation and poor hydrogen reduction as indicated by the NMR T_2 spectrum of around 46% ED_{NMR}. Last flooding run conducted was secondary miscible CO_2 injection and it yielded the highest oil recovery of 93% OOIP. This high recovery is attributed to the high miscible CO_2 injectivity, which led to a stable displacement efficiency of approximately 88%. This was confirmed by the NMR T_2, which showed a high NMR displacement efficiency of 70%. Therefore, it is claimed that the power of miscibility was able to completely displace the oil in the macropore system in addition to yielding a fluid displacement of around 12% from the micropore system. The microscopic displacement efficiency obtained from flooding runs are close to that obtained from the NMR measurements, proving that NMR technique is an effective tool for observing different pore systems' contributions to overall hydrocarbon recovery and CO_2 storage in tight formations.

5.2. RECOMMENDATIONS FOR FUTURE WORK

This work has answered all of the questions posed at the outset of the research; however, several issues still need further attention. Based on the insights provided in this thesis, it is recommended to consider the following in future research efforts:

- Only three tight sandstone rocks were collected and evaluated. It is recommended to extend the dataset by considering the microscopic pore system contribution of other rocks such as tight sands, shales, and tight carbonates of various pore/perm scale types.
- Continuous CO_2 injection was conducted and investigated. As a follow-up, evaluating different CO_2 injection approaches including WAG injection, carbonated water and surfactant alternating gas is recommended.

- N-decane was used to represent the oleic phase. Crude oils of different API are suggested to be used in future work to consider the role of rock wettability and miscibility on enhanced oil recovery. Aging for different rock wettability conditions can also be considered.
- Simulating conducted flooding runs and investigating of different scenarios at core scale are recommended. In addition, upscaling of the current results is important to utilize the findings at field scale.
- Laboratory NMR measurements proved to be an effective tool to assess pore fluids displacement at microscopic level. Considering upscaling; borehole NMR technology exists and it is recommended to be utilized in CO_2 flooded wells to assess the near wellbore performance of CO_2 injection for both EOR and geo-storage purposes.

NOMENCLATURE

ABBREVATION

bbl/d	Barrels of oil daily [-]
BPR	back pressure regulator [-]
BVI	Bound volume index [-]
CO_2–EOR	Carbon dioxide–enhanced oil recovery [-]
CPMG	Carr-Purcell-Meiboom-Gill [-]
CWI	Carbonated water injection [-]
E_D	Microscopic displacement efficiency [%]
EJ	Exajoules [-]
E_R	Recovery efficiency [%]
E_V	Volumetric efficiency [%]
FFI	Free fluid index [-]
GAGD	Gas assisted gravity drainage [-]
GDP	Gross domestic product [-]
GHGs	Global greenhouse gas [-]
Gt	Billion tons [-]
IOR	Improved oil recovery [-]
IPCC	Intergovernmental Panel on Climate Change [-]
k	Permeability [mD]
kg	Kilograms [-]
M	Mobility ratio [v/v]
Ma	Meg-annum [-]
MCI	Microscopic confinement index [-]
mD	Millidarcy [-]
MICP	Mercury injection capillary pressure [-]
Micro-CT	micro-computed tomography [-]
ms	Millisecond [-]
MSF	Multi-stage fracturing [-]
MSI	Micro-storativity index [-]
Mt	Million tons [-]
MTMR	Micro-pore throat modality ratio [-]
N_c	Capillary number [-]

NMR	Nuclear Magnetic Resonance [-]
NRC	National Resources of Canada [-]
OOIP	Original oil in place [-]
PFD	Pore-fluids distribution [-]
ppm	Parts per million [-]
PV	Pore volume [-]
RCPs	Representative concentration pathways [W/m^2]
rpm	Revolutions per minute [-]
SAG	Surfactant alternating gas [-]
SEM	Scanning Electron Microscopy [-]
U.S.	United States [-]
W/m^2	Watts per square meter [-]
WAG	Water alternating gas [-]
XRD	X-ray diffraction [-]
XRF	X-ray fluorescence [-]
ϕ	Porosity [%]
μm	Micron [-]

MINERALS

Al_2O_3	Aluminium oxide [wt%]
CaO	Calcium oxide [wt%]
Fe_2O_3	Iron oxide [wt%]
K_2O	Potassium oxide [wt%]
KCL	Potassium chloride [-]
MgO	Magnesium oxide [wt%]
MnO	Manganese oxide [wt%]
Na_2O	Sodium oxide [wt%]
P_2O_5	phosphorus pentoxide [wt%]
SiO_2	Silicon dioxide [wt%]
SO_3	Sulphur trioxide [wt%]
T_2	Relaxation time [ms]
TiO_2	Titanium dioxide [wt%]

SUMMARY

Oil exploitation of tight reservoirs has gained significant importance lately. Some researchers have defined tight reservoirs as those characterized with permeability lower than 0.1 mD. However, permeability is an absolute value, and tight reservoirs have complex pore systems that require a detailed geological and petrophysical rock characterization for optimal recovery process. Enhanced recovery of tight oil reservoirs is challenging because of possible oil bypass due to high capillary forces. Increasing displacing fluid viscosity will provide stable displacement and preventing any viscous fingering but will lower the displacing fluid injectivity. On the other hand, lowering the displacing fluid viscosity can lead to viscous fingering resulting in increased residual oil. CO_2 injection, a common EOR technique, can positively impacts pore fluid displacement of tight reservoirs, including micropores. However, the main challenge of CO_2–EOR in tight reservoirs is the complex nature of pore systems that can lead to unfavorable displacement.

This work was conducted to experimentally investigate the effectiveness of CO_2–EOR in invading micropores of tight rocks. Three representative tight sandstones (Bandera, Kentucky, and Scioto) were used and detailed set of petrophysical, petrographic, and mineralogical measurements was conducted to characterize the investigated sandstones, assess the pore framework, and investigate the impact of clay minerals on pore systems. Routine core analysis indicates that Bandera shows the best reservoir quality among the investigated sandstones, due to the high percentage of macropore system. Attributed to Pore-filling kaolinite booklets and fibrous illite acting as pore bridging reducing its micro-pore body and micro-throat systems. Scioto and Kentucky show less quality with close porosity and permeability. Shortage of kaolinite booklets in Kentucky and Scioto sandstones reveals higher micro-throat system compared to Bandera sandstone.

New dimensionless numbers, termed as microscopic confinement (MCI) and micro-throat modality (MTMR) indices, were established to screen the tested sandstones for a suitable tight sandstone choice for CO_2–EOR and CO_2 geo-storage. Accordingly, Scioto sandstone is elected as the most appropriate candidate for CO_2–EOR among the tested sandstones due to its high micropore system capacity to store and confine injected CO_2.

Various CO_2 flooding schemes were conducted on Scioto sandstone composite cores. The tested schemes include continuous miscible CO_2 injection at connate water saturation, immiscible CO_2 injection at connate water saturation and tertiary miscible CO_2 injection at residual oil saturation after waterflooding. Laboratory NMR measurements (Pre and post flooding runs) were conducted to confirm the calculated ultimate recovery and assess microscopically the contribution of both micro- and macropore systems.

Results indicate that continuous miscible CO_2 was able to invade micropores providing the highest microscopic displacement compared to the other tested injection schemes. Such microscopic displacement can lead to permanent CO_2 storage in invaded tight pores due to capillarity mechanism. Tertiary miscible CO_2 injection showed a lower ultimate oil recovery compared to the previous run and this is attributed to the increased water content and pore blocking post-water flooding stage. Continuous immiscible CO_2 injection showed the lowest ultimate oil recovery among the investigated runs due to the unstable displacement. NMR measurements showed good agreement with core-flooding results and proved the micropore fluids contribution to overall recovery. Therefore, borehole NMR technology can be utilized to assess the near wellbore performance of CO_2 injection for EOR and geo-storage purposes.

SAMENVATTING

De olie-exploitatie van tight reservoirs heeft de laatste tijd aanzienlijk aan belang gewonnen. Sommige onderzoekers hebben strakke reservoirs gedefinieerd als reservoirs die worden gekenmerkt door een permeabiliteit van minder dan 0,1 mD. Permeabiliteit is echter een absolute waarde, en tight reservoirs hebben complexe poriënsystemen die een gedetailleerde geologische en petrofysische karakterisering van het gesteente vereisen voor een optimaal herstelproces. Verbeterd herstel van tight oliereservoirs is een uitdaging vanwege de mogelijke olie-bypass als gevolg van hoge capillaire krachten. Het verhogen van de viscositeit van de verdringende vloeistof zal zorgen voor een stabiele verplaatsing en het voorkomen van stroperige vingerzetting, maar zal de injectiviteit van de verdringende vloeistof verlagen. Aan de andere kant kan het verlagen van de viscositeit van de verdringende vloeistof leiden tot stroperige vingervorming, wat resulteert in een toename van de resterende olie. CO_2-injectie, een veelgebruikte EOR-techniek, kan een positieve invloed hebben op de verplaatsing van poriënvloeistof in nauwe reservoirs, inclusief microporiën. De belangrijkste uitdaging van CO_2-EOR in tight reservoirs is echter de complexe aard van poriesystemen die tot ongunstige verplaatsingen kunnen leiden.

Dit werk werd uitgevoerd om experimenteel de effectiviteit van CO_2-EOR bij het binnendringen van microporiën in dicht gesteente te onderzoeken. Drie representatieve strakke zandstenen (Bandera, Kentucky en Scioto) werden gebruikt en een gedetailleerde reeks petrofysische, petrografische en mineralogische metingen werd uitgevoerd om de onderzochte zandstenen te karakteriseren, het poriënraamwerk te beoordelen en de impact van kleimineralen op poriënsystemen te onderzoeken. Routinematige kernanalyse geeft aan dat Bandera de beste reservoirkwaliteit vertoont onder de onderzochte zandstenen, vanwege het hoge percentage macroporiënsysteem. Toegeschreven aan porievullende kaolinietboekjes en vezelig illiet dat als porieoverbrugging fungeert en het microporielichaam en microkeelsystemen vermindert. Scioto en Kentucky vertonen minder kwaliteit met nauwe porositeit en permeabiliteit. Een tekort aan kaolinietboekjes in zandsteen uit Kentucky en Scioto laat een hoger micro-keelsysteem zien vergeleken met Bandera-zandsteen.

Nieuwe dimensieloze getallen, microscopische opsluiting (MCI) en micro-throat modality (MTMR) indices genoemd, werden vastgesteld om de geteste zandstenen te screenen op een geschikte strakke zandsteenkeuze voor CO_2-EOR en CO_2-geoopslag. Dienovereenkomstig wordt Scioto-zandsteen gekozen als de meest geschikte kandidaat voor CO_2-EOR onder de geteste zandstenen vanwege de hoge capaciteit van het microporiënsysteem om geïnjecteerd CO_2 op te slaan en op te sluiten. Er zijn verschillende CO_2-overstromingsschema's uitgevoerd op Scioto-zandsteencomposietkernen. De geteste schema's omvatten continue mengbare CO_2-injectie bij

aangeboren waterverzadiging, niet-mengbare CO_2-injectie bij aangeboren waterverzadiging en tertiair mengbare CO_2-injectie bij verzadiging van resterende olie na wateroverstroming. NMR-metingen in het laboratorium (runs vóór en na de overstroming) werden uitgevoerd om het berekende uiteindelijke herstel te bevestigen en microscopisch de bijdrage van zowel micro- als macroporiesystemen te beoordelen.

De resultaten geven aan dat continu mengbaar CO_2 in staat was microporiën binnen te dringen, wat de hoogste microscopische verplaatsing opleverde vergeleken met de andere geteste injectieschema's. Een dergelijke microscopische verplaatsing kan leiden tot permanente CO_2-opslag in binnengedrongen nauwe poriën als gevolg van het capillariteitsmechanisme. Tertiaire mengbare CO_2-injectie liet een lagere uiteindelijke oliewinning zien in vergelijking met de vorige run en dit wordt toegeschreven aan het verhoogde watergehalte en het blokkeren van de poriën na de overstromingsfase. Continue onmengbare CO_2-injectie vertoonde de laagste uiteindelijke oliewinning onder de onderzochte runs vanwege de onstabiele verplaatsing. NMR-metingen lieten een goede overeenkomst zien met de resultaten van kernoverstromingen en bewezen dat de microporiënvloeistoffen bijdragen aan het algehele herstel. Daarom kan NMR-technologie in boorgaten worden gebruikt om de prestaties van CO_2-injectie in de buurt van boorputten te beoordelen voor EOR-en geoopslagdoeleinden.

ملخص الرسالة

اكتسب استغلال النفط في المكامن الصخرية المحكمة ضعيفة النفاذية أهمية كبيرة في الآونة الأخيرة والتي قام البعض بتحديدها بتلك المتميزة بنفاذية أقل من 0.1 ملي دارسي، إلا إن النفاذية قيمة مطلقة وتتميز تلك الصخور بأنظمة مسامية معقدة تتطلب توصيفًا جيولوجيًا وبتروفيزيائيًا دقيقًا حتى تساعد في اختيار وسائل الاستخلاص الأمثل لسوائل هذا النوع من المكامن الصخرية. يعد تعزيز استخلاص النفط من المكامن المحكمة والمتصفة بضعف النفاذية تحديًا بسبب امكانية عدم انتاج موائع المكمن نتيجة القوى الشعرية العالية. يوفر الاستخلاص المحسن باستخدام سوائل الحقن عالية اللزوجة ازاحة مستقرة للزيت ولكن قد يضعف معدل حقن هذه السوائل. من ناحية أخرى، فإن تقليل لزوجة موائع الحقن يمكن أن يؤدي إلى تغلغل هذه الموائع عبر سوائل المكمن الى آبار الإنتاج مما يؤدي إلى بقاء كميات من الزيت في التشكيل المسامي للمكمن دون إنتاج.

تعد تقنية حقن ثاني أكسيد الكربون للاستخلاص المحسن للزيت تقنية شائعة الاستخدام، ويمكن أن يؤثر هذا الحقن بشكل إيجابي على انتاج الزيت من الحقول غير التقليدية المتصفة بالتشكيل المسامي الدقيق والنفاذية الضعيفة. ومع ذلك، فإن التحدي الرئيس لحقن ثاني أكسيد الكربون في هذه المكامن هو نظام المسام المعقد الذي يمكن أن يؤدي إلى انتاج ضعيف.

تم في هذه الدراسة المخبرية التحقق من فعالية ثاني أكسيد الكربون في اختراق المسامات الدقيقة والضيقة لمجموعة من الصخور الرملية المحكمة الممثلة بصخور باندیرا وكنتاكي وسيوتو. وقد أجري في هذه الدراسة مجموعة مفصلة من القياسات الأساسية البتروفيزيائية والبتروغرافية والمعدنية لتوصيف وتقييم الإطار المسامي والتحقيق في تأثير المعادن الطينية على التشكيل المسامي لهذه الصخور. وتشير التحليلات الأساسية إلى أن صخر باندیرا يتميز بأفضل الصفات البتروفيزيائية بين الصخور الرملية المدروسة، حيث يتميز ينسبه عالية من نظام المسام الكبيرة والقليل من المسامات الدقيقة الضيقة نتيجة وجود نسبة عالية من الكاولونايت والإيلايت الليفي. من ناحية أخرى تظهر صخور كنتاكي وسويوتو جودة صخرية أقل مع نسب متقاربة لمعاملات المسامية والنفاذية مع زيادة في نسبة المسامات الدقيقة الضيقة مقارنة بصخر باندیرا ويعزى ذلك لنقص معدن الكاولونايت في التشكيل المعدني لهذه الصخور. كما تم في هذه الدراسة تطوير معاملات جديدة تتمثل بمعدل الاحتجاز المجهري (MCI) ومؤشر النمط الدقيق (MTMR) وذلك لفحص الصخور الرملية المختبرة لتحديد الصخر الأنسب لحقن ثاني أكسيد الكربون. وبناء على هذه المعاملات، تم تحديد صخر سويوتو الرملي كأنسب مرشح لحقن ثاني أكسيد الكربون بين الصخور المختبرة بسبب تشكيلة المسامي الدقيق وقدرته على احتجاز ثاني أوكسيد الكربون المحقون

يناء على ما سبق تم إجراء تجارب حقن متعددة لثاني أكسيد الكربون باستخدام صخر سويوتو وتضمنت حقن ثاني أكسيد الكربون الممتزج والمستمر عند تشبع الماء الأولي، حقن ثاني أوكسيد الكربون غير الممتزج والمستمر عند تشبع الماء الأولي، وحقن ثاني أكسيد الكربون الممتزج الثلاثي عند تشبع الزيت المتبقي بعد غمر المياه. وقد تم إجراء قياسات الرنين المغناطيسي النووي قبل وبعد الغمر بثاني أكسيد الكربون لتأكيد كميات الانتاج وتقييم مساهمة المسامات الدقيقة والواسعة بشكل مجهري. وتشير النتائج إلى أن حقن ثاني أكسيد الكربون الممتزج والمستمر عند تشبع الماء قادر على غزو المسامات الدقيقة وتحقيق أعلى إزاحة مجهرية مقارنة بتجارب الحقن الأخرى بينما أظهر حقن ثاني أكسيد الكربون الممتزج الثلاثي بعد حقن الماء استخلاص أقل للزيت مقارنة بالنوع السابق ويعزى ذلك إلى زيادة محتوى الماء وغلق المسام بعد مرحلة حقن الماء. ويمكن أن تؤدي الإزاحة المجهرية في النوع الأول من الحقن إلى خزن دائم لثاني أكسيد الكربون في المسامات الضيقة بسبب آلية الاحتباس. وقد أثبتت قياسات الرنين المغناطيسي النووي اتفاقًا جيدًا في تحديد كميات الإنتاج الكلي مع تلك المتحصل عليها من نتائج تجارب الغمر كما ساعدت في تحديد مساهمة محتوى المسامات الدقيقة في الاستخلاص الكلي للزيت مما يثبت كفاءة هذه التقنية في تقييم أداء عمليات الحقن لاستخلاص الزيت وتخزين ثاني أكسيد الكربون جيولوجيًا.

ABOUT THE AUTHOR

Name: Hamad Salman Al-Kharra'a
E-mail: hamad.kharaa@aramco.com
Dhahran 31311, P.O. Box 13058
Saudi Aramco
Saudi Arabia

Hamad Salman Alkharra'a was born on March 26, 1987, in Al Khobar, Saudi Arabia. In September 2010 he obtained his BSc degree from King Fahd University of Petroleum and Minerals in Petroleum Engineering with Honors. Since March 2010, he works as a petroleum engineer for Saudi Aramco. In September 2013 he obtained his MSc degree from KFUPM in Petroleum Engineering with Honors. In October 2019 he started his PhD study at Delft University of Technology under the supervision of Prof. Dr. Pacelli Zitha and Dr. Karl-Heinz Wolf. His research was part of a collaboration between Delft University of Technology, Saudi Aramco, King Abdulaziz City for Science and Technology, and King Fahd University of Petroleum and Minerals.

LIST OF PUBLICATIONS

PAPERS PUBLISHED IN PEER-REVIEWED JOURNALS

Al-Kharra'a, H.S., Wolf, K.H.A., AlQuraishi, A.A., Mahmoud, M.A., Deshenenkov, I., AlDuhailan, M.A., Alarifi, S.A., AlQahtani, N.B., Kwak, H.T. and Zitha, P.L.J., 2023. Impact of clay mineralogy on the petrophysical properties of tight sandstones. Geoenergy Science and Engineering, 227, p.211883.

Al-Kharra'a, H.S., Wolf, K.H.A., AlQuraishi, A.A., Mahmoud, M.A., AlDuhailan, M.A., and Zitha, P.L.J., 2023. The Power of Characterizing Pore Fluid Distribution for Microscopic CO_2 Injection Studies in Tight Sandstones. Minerals, 13(7), p.895.

AlKharraa, H.'S., Wolf, K.H., AlQuraishi, A., Al Abdrabalnabi, R., Mahmoud, M. and Zitha, P.L.J., 2023. Microscopic CO_2 Injection in Tight Rocks: Implications for Enhanced Oil Recovery and Carbon Geo-Storage. *Energy & Fuels*.

CONFERENCE PROCEEDINGS

AlKharra'a, H.S., Wolf, K.H.A., Kwak, H.T., Deshenenkov, I.S., AlDuhailan, M.A., Mahmoud, M.A., Arifi, S.A., AlQahtani, N.B., AlQuraishi, A.A. and Zitha, P.L.J., 2023, January. A Characterization of Tight Sandstone: Effect of Clay Mineralogy on Pore-Framework. Paper presented at The SPE Reservoir Characterization and Simulation Conference and Exhibition, Abu Dhabi, UAE.

AlKharra'a, H.S., Wolf, K.H.A., AlQuraishi, A.A., Kwak, H.T., Deshenenkov, I.S., AlDuhailan, M.A., Mahmoud, and Zitha, P.L.J., 2023, February. The Curious Case of Microscopic CO_2 Injection: The Power Of Characterizing Pore Fluid Distribution. Paper presented at Middle East Oil, Gas and Geosciences Show, Bahrain.

AlKharra'a, H.S., Wolf, K.H.A., Kwak, H.T., Deshenenkov, I.S., AlDuhailan, M.A., Mahmoud, M.A., Arifi, S.A., AlQahtani, N.B., AlQuraishi, A.A. and Zitha, P.L.J., 2023, February. Effect Of Clay Mineralogy On the Micropore-System Of Tight Sandstone Reservoirs. Paper presented at Middle East Oil, Gas and Geosciences Show, Bahrain.

ACKNOWLEDGMENTS

First and foremost, thanks to Almighty Allah for making this work possible and giving me the energy to complete this journey during the COVID-19 pandemic. I am indebted to my country, the Kingdom of Saudi Arabia, where I was raised and educated. I am grateful to my employer, Saudi Aramco, for granting me a scholarship to pursue my PhD studies in the Netherlands and to the Netherlands for the great hospitality I have been shown while living here.

I would not have been able to complete this work without the support of my supervisor, **Prof. Dr. Pacelli Zitha**. I have been preparing for the moment when I would defend my thesis in his presence, but sadly, on Sunday, February 18, 2024, Prof. Pacelli left us. He was one of the top experts in the oil & gas and green energy transition fields, and I was honored to have been supervised by him. Prof. Pacelli's passion for green transition inspired me to choose my PhD topic in this vital area. I will always cherish his words of encouragement and inspiration; he reminded me that there was a light at the end of the tunnel and that I needed to focus on the bright side of any challenging situation. Rest in peace, my dear friend and mentor.

I am truly thankful to my PhD co-supervisor, **Dr. Karl-Heinz Wolf**, for his patience when reading my publications, brainstorming the scope of my PhD research, and inspiring me throughout this journey. His door was always open, and he was happy to allocate time to me. Meeting with Dr. Karl and Prof. Pacelli every Tuesday not only enriched my technical abilities but also strengthened my leadership skills.

I highly appreciate **Prof. Dr. Abdulrahman Al-Quraishi** for his limitless support during my PhD research. I am extremely grateful to him for allocating time to fruitful discussions with me, proofreading my thesis, and cheering me up whenever I needed it. His kindness, enthusiasm, guidance, and encouragement are greatly appreciated.

I am grateful to my doctoral committee members for their willingness to evaluate my dissertation.

I wish to thank **Lydia Broekhuijsen-Bentvelzen**, **Marlijn Ammerlaan**, **Ingrid Baidjoe**, **Raf Dabekaussen** and **Ralf Haak** for their administrative assistance and overall support during my PhD studies. Furthermore, I would like to express my gratitude to all my friends and colleagues in the Geoscience and Engineering Department: **Wesam Al Muttawa**, **Dr. Sian Jones**, **Dr. Mohsen Mirzaie Yegane**, **Dr. Martijn Janssen**, **Dr. Kai Li**, **Michiel Wapperom**, and **George Hadjisotiriou**.

This PhD project was a collaboration between Delft University of Technology, Saudi Aramco, King Fahd University of Petroleum and Minerals, and King Abdulaziz City for Science and Technology. I would like to express my appreciation to **Dr. Naif Al-Qahtani**, **Dr. Abdulaziz Al-Qasim**, **Dr. Ivan Deshenenkov**, **Dr. Hyung Kwak**, **Prof. Dr. Mohamed Mahmoud**, **Hamad**

Al-Ghenaim, **Prof. Dr. Khaled Al-Ramadan**, **Dr. Sulaiman Al-Arifi**, **Dr. Saleh Al-Haidary**, **Dr. Yasser Al-Duailej**, **Dr. Abdullah Al-Mansour, Nezar Al-Talhah**, **Dr. Abdulkareem Al-Radwan, Dr. Taha Okasha,** and **Faisal Al-Ghamdi** for their valuable comments and suggestions. I am thankful for the excellent support of all the technical staff, including **Essa Abdullah**, **Ridha Al-Abdrabalnabi, Hamdan Al-Yami**, **Mohammed Al-Qarni**, **Mustafa Al-Satrawi**, **Jun Gao**, **Hussain Al-Ali**, and **Aqeel Furaish**, for assisting with all my experiment runs. Without their enthusiasm and continuous support during the experiments, this project could not have been completed.

In addition, I would like to thank **Dr. Mohammed Al-Duhailan** for his invaluable scientific contributions and for being there for me at every step of my PhD journey. Abo Rayan, I truly appreciate your belief in me, and I am grateful for our technical discussions, which I always enjoyed. I also wish to thank **Hafiz Al-Shammery** for his support and guidance. Abu Saud's direction has been vital, and I am deeply grateful for his belief in my abilities. I also want to take a moment to express my sincere gratitude and heartfelt appreciation to **Khalid Al-Abdulqader** for his unwavering support, limitless assistance, and leadership, which greatly facilitated my PhD journey. I also want to express my sincere gratitude to **Dr. Ghaithan Al-Muntasheri** for his valuable advice during my PhD studies. Abu Ahmed, I value the help you have given me

Finally, I would like to thank my family and my friends for their continuous love, support, and encouragement. To my dear parents, I am immensely thankful for the love and support you have shown me. I have always felt your love and blessings, and I appreciate all you have done for me.